Portland State University
PDXScholar

Winter 3-31-2016

Arsenic Mobilization from Silicic Volcanic Rocks in the Southern Willamette Valley

Gabriela Ribeiro de Sena Ferreira
Portland State University

Let us know how access to this document benefits you.

Follow this and additional works at: http://pdxscholar.library.pdx.edu/open_access_etds

Part of the Geology Commons

Arsenic Mobilization from Silicic Volcanic Rocks in the Southern Willamette Valley

by

Gabriela Ribeiro de Sena Ferreira

A thesis submitted in partial fulfillment of the
requirements for the degree of

Master in Science
in
Geology

Thesis Committee:
Robert Perkins, Chair
Martin Streck
Nancy Price

Portland State University
2016

Abstract

Volcanic tuffs and tuffaceous sediments are frequently associated with elevated As groundwater concentrations even though their bulk As contents ($\sim$ 5 mg kg^{-1}; Savoie, 2013) are only marginally greater than the average crustal abundance of 4.8 μg g^{-1} (Rudnick & Gao, 2003). Thus, As mobilization must be facilitated by conditions particular to these rocks. Alkaline desorption, anionic competition, reactive glass dissolution, and reductive dissolution of iron oxides are proposed processes of As release from volcanic rocks. Geogenic As contamination of groundwater in the southern Willamette Valley in western Oregon has been well-documented since the early 1960s, and previous studies have identified the Little Butte Volcanics Series and Fisher and Eugene Formations as the source of As contamination.

This study examines 19 samples from 10 units of ash flow tuffs and tuffaceous sediments within the Fisher Formation and Little Butte Volcanics Series, representing a range of weathering and devitrification, to determine conditions of mobilization and mineralogical constraints that control As release into solution. Leachate studies were conducted over a range of pH from 7 to 11, phosphate concentrations from 10 μM to 100 mM, and in time series from 4 to 196 hours. Results demonstrate that silicic volcanic tuffs are capable of mobilizing As in concentrations above regulatory limits at pH conditions produced naturally by the tuffs (pH 8-9) or with moderate concentrations of P (10-100 μM). Alteration products, e.g. zeolites and clays, appear to be the primary host phases for mobile As. Samples that do not contain these alteration products tend to produce concentrations of As well below regulatory limits and often below the instrument detection limits of this study. The type of alteration may influence As mobilization: tuffs containing more clays tend to mobilize As through surficial desorption, and tuffs containing more zeolites tend to mobilize As by dissolution or formation of colloids. Additionally, one volcaniclastic sample demonstrates that extremely elevated concentrations of As, up to 1000 μg/L are possible as a result of oxidative dissolution of As-bearing sulfide phases.

Acknowledgements

I am first and foremost grateful to my advisor Ben, for his patience, encouragement, dedication to his students, and passion as an educator. I have benefitted immeasurably from his guidance as a researcher and mentor.

I am also indebted immeasurably to my parents for their example of enormous sacrifice, perseverance, and unconditional love. My brother, Pedro, was a reliable source of relief and confidence in me.

My loved ones, near and far, are invaluable support and were always available for discussion, support, and motivation. I am blessed that they are too many to name individually. Mr. Bun and Dona Flor, my furry companions, always brought me joy and an improved perspective.

I would like to thank my committee members for their availability and review, and Courtney Savoie for her borrowed samples.

Table of Contents

List of Figures

List of Tables

Introduction

Arsenic is a widespread toxin that poses significant risks to human health and the environment. Worldwide, as many as 60-100 million people may be at risk of exposure to excessive levels of As in water (Smedley & Kinniburgh, 2002). Naturally elevated groundwater As levels are frequently attributed to volcanic sources, particularly high silica ash-flow tuffs and tuffaceous sediments (Johannesson & Tang, 2009; Mahlknecht, Steinich, & Navarro de Leon, 2004; Smedley & Kinniburgh, 2002; Vinson, Mcintosh, Dwyer, & Vengosh, 2011; Welch, Westjohn, Helsel, & Wanty, 2000). However, there is little variability in bulk As content within volcanic rocks (generally < 8 μg g^{-1}; Onishi & Sandell, 1955), and their concentrations are equivalent to or only marginally higher than the average concentration in continental crust (4.8 μg g^{-1}; Rudnick & Gao, 2003).

The frequent association of As-contaminated groundwater to silicic volcanic aquifers indicates that processes or host phases specific to silicic volcanism must mobilize As from these source rocks despite their modest As contents (Raymahashay & Khare, 2003; Smedley & Kinniburgh, 2002; Welch et al., 2000). A recent study by Savoie (2013) suggests that the specific route of post-depositional alteration may profoundly influence the mobility of As from high silica ash-flow tuffs.

Arsenic contamination in the southern Willamette Basin in western Oregon has been well-documented since the early 1960s. The most recent study concludes that 21.7% (n=158) of groundwater samples exceeded the current USEPA standard of 0.01 mg/L (Hinkle & Polette, 1999). Eugene, located in Lane County, is estimated to be the second largest city in Oregon, and the county overall experienced an 8.9% population growth

1

from 2000 to 2009 (Population Research Center, 2013). The self-supplied groundwater population is nearly 20% of the total population in Lane County (64,970), which makes Lane County the second-most dependent county on domestic water wells behind Clackamas County (Oregon Water Science Center [OWSC], 2013). The growing population will create further reliance on groundwater supplies as surface water supplies become increasingly depleted, which may in turn increase the risk to human health from As exposure.

All prior studies on As contamination in Lane County indicate the Fisher Formation and Little Butte Volcanics Series as the source of As contamination. The Fisher Formation and Little Butte Volcanics are broadly mapped as non-marine volcaniclastic sedimentary rocks, silicic tuffs, mafic lavas, tuffaceous sandstone, and pebble conglomerates (McClaughry, Wiley, Ferns, & Madin, 2010). Processes of As mobilization into groundwater remain unclear (Goldblatt, Van Denburgh, & Marsland, 1963; Hinkle & Polette, 1999; Whanger, Weswig, & Stoner, 1977).

This study examined ten tuff units of the Fisher Formation and Little Butte Volcanics Series in order to improve understanding of mechanisms governing As mobilization from silicic volcanic rocks. Samples collected from these units were classified in terms of volcanic textures and mineral assemblages, and subjected to a series of aqueous leachate experiments to assess As mobilization under a range of solution conditions. The results were interpreted in terms of potential mechanisms governing As mobilization into solution in an effort to understand how aquifers with near-average bulk As contents result in extensive As contamination.

<center>**Background**</center>

Arsenic geochemistry

Arsenic is highly mobile in a variety of environments, under both reducing and oxidizing conditions, both acidic and alkaline conditions, and both arid and humid climates (Smedley & Kinniburgh, 2002; Wang & Mulligan, 2008). Arsenic in the environment most commonly occurs in trivalent (As(III) or arsenite) and pentavalent (As(V) or arsenate) forms. As(III) is often considered the more mobile of the two species because As(V) forms more extensive inner-sphere complexes (Kocar & Fendorf, 2009), although under high pH conditions, As(III) may be more strongly sorbed than As(V) (Manning & Goldberg, 1997). In natural waters, As dominantly occurs as various oxyanions depending on redox and pH conditions (Figure 1). However, nonequilibrium behavior of the As(V)/As(III) couple is observed, with As(III) found in oxic waters and As(V) in anoxic, which has been explained by slow kinetics or biological interference (Inskeep, McDermott, & Fendorf, 2002; Smedley & Kinniburgh, 2002).

Arsenic host phases

Sources of As are both anthropogenic (e.g. mining, arsenical pesticides, lumber preservatives, fossil fuel processing) and geogenic. Shales, slate, hydrothermal ore deposits, and volcanic rocks are commonly associated with As-contaminated aquifers (Smedley & Kinniburgh, 2002; Wang & Mulligan, 2006; Welch et al., 2000). Host phases include As-bearing minerals (commonly sulfides), metal oxides, clays, and other surface-charged species. Differences in water conditions may affect the type of host phases as well; for example, As may shift from Fe oxides in oxic waters to sulfides in reducing waters (Hering & Kneebone, 2002).
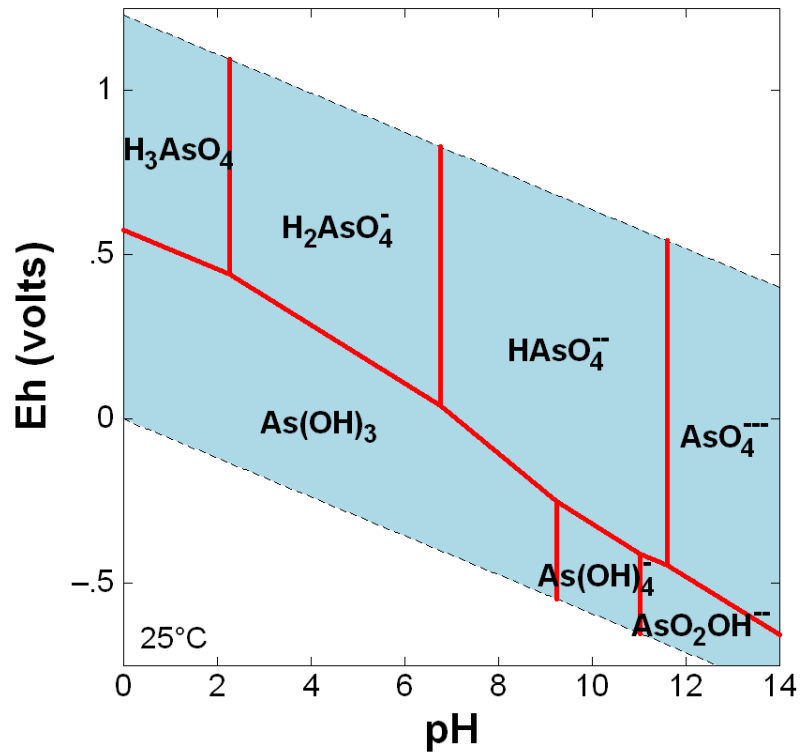
Figure 1: Eh-pH diagram showing dominant species of dissolved arsenic under various environmental conditions (created using Geochemist's Workbench software; SAs = 0.001 m).

As of July 2014, the most recent Mineralogical Society of America publication reported 568 known minerals containing As as a critical component, although many are ore minerals and associated alteration products and are therefore rare in the natural environment (Bowell, Alpers, Jamieson, Nordstrom, & Majzlan, 2014; Smedley & Kinniburgh, 2002). Arsenic frequently substitutes for P(V), Si(IV), Al(III), Fe(III), and Ti(IV) as a trace component within mineral structures. The most common As-bearing minerals are sulfides, in which As occurs as an arsenide or sulfarsenide anion bound to transition metals (e.g. $FeAs_2$; FeAsS) (Bowell et al., 2014; Smedley & Kinniburgh, 2002). The most studied As-producing sulfide is pyrite, which occurs in ore bodies and low-temperature sedimentary environments under reducing conditions around buried and

decomposing organic matter or in the presence of sulfate-reducing bacteria (Bowell et al., 2014; Kreidie et al., 2011; Wang & Mulligan, 2008). Arsenic is also found in association with major gold deposits (Bowell et al., 2014). Precipitation of As minerals occurs within magmatic and metamorphic systems, hydrothermal systems, oxidation zones of ore deposits and mineralization, coal basins, mine wastes and tailings, and former industrial sites (Majzlan, Drahota, & Filippi, 2014). However, under oxic and reducing conditions, many common As minerals are too soluble to precipitate or may still have high dissolved equilibrium concentrations of As if precipitated (Hering & Kneebone, 2002).

Unlike mineral precipitation, sorption of As onto minerals is an important control on As concentrations in most natural waters. As(V) has a strong affinity for most metal (hydr)oxides, commonly Al, Mn, and Fe, as well as clay minerals on which it forms surface complexes. In contrast, As(III) more selectively sorbs to Fe (hydr)oxides (Inskeep et al., 2002). This difference in sorption behavior is attributed to the fact that As(III) forms inner sphere complexes while As(V) may form both inner and outer sphere complexes (Pedersen, Postma, & Jakobsen, 2006).

Among different Fe (hydr)oxides, crystalline structure and speciation determine the strength and amount of As sorption and subsequent mobility (Campbell & Nordstrom, 2014; Kreidie et al., 2011; Wang & Mulligan, 2008). Sorption sites on the surface have relatively rapid kinetics, while slow diffusion into the interior of the aggregate may occur given sufficient time (Campbell & Nordstrom, 2014). Despite crystalline and amorphous Fe oxides (e.g. hydrous ferric oxide vs goethite and magnetite) having similar binding strength and intrinsic surface complexation constants, the crystalline phases of iron

5

oxides typically have lower sorptive capacity for As, owing to a decrease in specific surface area and site density rather than difference in affinity (Dixit & Hering, 2003). As(III) may substitute for Fe(III) on outer layers of sulfides where Fe(II) oxidizes to Fe(III) due to weathering and microbial activity (Kreidie et al., 2011). Goethite has strong sorption of As, such that nearly 80% of goethite must be reductively dissolved before >20% of As is released. Ferrihydrite's sorption is moderate, and lepidocrocite readily releases As into solution (Pedersen et al., 2006). Recrystallization into more stable Fe-oxides results in incorporation of As within the new mineral via occlusion, making it less available to solution (Pedersen et al., 2006). Variations in point of zero charge (ferrihydrite pH = 7.8-7.9; lepidocrocite pH = 6.7-8; goethite pH = 8.9-9.5) and reduction (e.g. ferrihydrite $Eh = 1.394 - 0.177$ volts; hematite $Eh = 1.078 - 0.177$ volts) account for variations in As sorption behavior (Pedersen et al., 2006; Raymahashay & Khare, 2003).

Aluminum oxides are structurally similar to Fe oxides because both can have a +3 valency and have similar radii. On Al oxides, As(III) forms weak outer-sphere complexes from pH 3 to 11 whereas As(V) forms inner-sphere complexes which may be stronger than those on Fe oxides and remain sorbed at higher pH (Campbell & Nordstrom, 2014). Manganese oxides are poorly crystalline and may adsorb As, but their catalyzing effect on redox transformations are more important than potential sorbent capacity (Wang & Mulligan, 2008).

Sorption on clay minerals is highly variable but generally, As(III) is stable from pH 4 - 9 and As(V) adsorbs more strongly above pH~7.5 (Lin & Puls, 2000; Manning & Goldberg, 1997). Aluminosilicate clays are distinct among As host phases in their high

surface charge density and diverse behavior of edge hydroxyl groups (Wang & Mulligan, 2008). Lin & Puls (2000) experimentally demonstrated that the structure of clays influences As adsorption to chlorite, which had stronger sorption of As due to its high iron oxide content, while illite/montmorillonite (2:1 layer) had moderate sorption, and kaolin clays (1:1 layer) had low sorption. Aging of clays led to increased adsorption with increased crystallinity reducing available charged edges (Lin & Puls, 2000). In contrast, Manning & Goldberg (1997) found that illite adsorbed significant As(III) due to the difference in point of zero charge at mineral edges that superseded crystalline effects on charged surfaces. Substantial oxidation for kaolinite and illite occurred above pH 9.2 whereas amorphous $Al(OH)_3$ did not undergo as much oxidation, suggesting reactions with solid phase components on the surface are more significant to oxidation than Al-OH edge sites (Manning & Goldberg, 1997). Several studies have demonstrated the dominating effect of high pH in mobilizing As from a variety of clay minerals (Lin & Puls, 2000; Manning & Goldberg, 1997; Shuichi, Ito, & Hashimoto, 2005).

Due the similar ionic structure of As to P, As may also occur in significant concentrations in phosphate minerals, up to 1000 mg/kg in apatite (Smedley & Kinniburgh, 2002). However, the lower relative abundance of phosphates in most rocks means that these are typically insignificant contributors of As in the environment. Mazziotti-Tagliani et al. (2011) investigated volcanic rocks from the F- and As- contaminated aquifer of Mt. Etna and found that As was exclusively hosted on the rim of apatite crystals and released under reductive dissolution with increased solubility as a result of metasomatism that increased bulk As in the sample. Although As may

preferentially sorb to metal oxides and clays, it also has strong capacity to sorb to different materials as available.

Arsenic mobilization

Dissolved arsenic in natural waters is controlled primarily by dissolution or desorption reactions (Smedley & Kinniburgh, 2002; Wang & Mulligan, 2008; Welch et al., 2000). Common mechanisms of As mobilization include reductive dissolution, sulfide oxidation, interaction with natural organic material, pH desorption, and ionic competition. Precipitation/dissolution reactions are limited by equilibrium with the solid, whereas sorption kinetics allow for greater exchange dependent on sorbent concentration (Hering & Kneebone, 2002).

Reducing conditions mobilize As primarily through dissolution of host phases (commonly Fe(III)-oxyhydroxide on which As is adsorbed). Reduction of As(V) to As(III) may release sorbed As from the surface of Al oxides; however, for Fe-oxyhydroxides, reductive dissolution typically controls mobilization because As(III) may remain sorbed onto Fe oxides (Dixit & Hering, 2003; Inskeep et al., 2002). Amorphous Fe-oxyhydroxides are rapidly dissolved through reduction, with slower reductive kinetics for crystalline phases (Inskeep et al., 2002).

Oxidative dissolution of sulfide minerals is another important source of As (Hering & Kneebone, 2002; Smedley & Kinniburgh, 2002). Pyrite and other iron sulfides are frequent hosts for As, and their instability in aerobic systems results in the formation of Fe oxyhydroxides, the release of dissolved SO_4 and trace elements, including As, and an increased in acidity (Smedley & Kinniburgh, 2002). However, as the system returns to

8

neutral pH, re-precipitation of hydrous ferric oxides typically readsorb As so this only affects highly acidic waters common to acid mine drainage but atypical for natural waters (Smedley & Kinniburgh, 2002). Abiotic oxidation of As(III) by Mn(IV)-oxides may also occur. The oxidized As(V) may remain sorbed or be released into solution depending on surface site availability and solution conditions (Campbell & Nordstrom, 2014).

The presence of natural organic matter (NOM) has several effects on As mobility. NOM may mobilize As through competitive desorption, particularly from iron oxides, and by affecting redox conditions. NOM can also remove dissolved As from solution through direct complexation on solid organic phases or formation of a ternary surface species between As and the oxide surface (Campbell & Nordstrom, 2014; Smedley & Kinniburgh, 2002). However, formation of stable Fe oxide colloids and particles coated with NOM may ultimately result in increased As mobility due to subsequent changes in solution chemistry that drive As remobilization (Campbell & Nordstrom, 2014; Wilkie & Hering, 1996).

Speciation of As, along with the presence and concentration of other ions, determines the effect of pH on As mobility (Dixit & Hering, 2003). Most common oxy-hydroxides that are effective As sorbents have a point of zero charge around 8-9, above which As would be released into solution. High pH can also affect competitive desorption through direct competition by hydroxyls and increased competition of dissociated species (e.g. Si and P; Xu et al., 2012). With regards to iron oxides, at increasing pH, i.e. pH $\geq$ 7, As(V) desorption is greater than As(III) desorption, which remains stable up to pH 9; at low pH, As(V) is more strongly sorbed than As (III) (Dixit & Hering, 2003; Wilkie & Hering,

1996). Typically cited values of As desorption due to increased pH start at 8.5, although ultimately, As mobility is highly sensitive to Eh/pH conditions (Smedley & Kinniburgh, 2002).

Ionic competition can occur between As oxyanions and phosphate, hydroxyl, sulfate, silicate, inorganic carbon, and other species (Campbell & Nordstrom, 2014). Phosphate is frequently cited as the most effective competitor, owing to its similarities in molecular structure and charge, as well as its potential to form inner-sphere complexes on similar surface sites (Campbell & Nordstrom, 2014). The effectiveness of phosphate competition is also demonstrated experimentally (Dixit & Hering, 2003; Neupane, Donahoe, & Arai, 2014; Xu et al., 2012). Xu et al. (2012) found that phosphate desorbed 2-3 orders of magnitude more As than sulfate, silicate, or bicarbonate. Phosphate most effectively desorbs As(V) at high pH (>10) , with limited effects at lower pH and with As(III) (Neupane et al., 2014; Xu et al., 2012).

Other elements may compete with As for sorption sites. Carbonate species, while not effective competitors, are abundant at high pH where carbonate is stable and has greater affinity for surface sites. Sulfate adsorbs to iron oxides but may prefer different surface sites to those preferred by As. Sulfate was observed to competitively desorb As(III) from hydrous ferric oxide within pH 4-7, have decreased competition at higher pH, and have no competitive effect with As(V) (Wilkie & Hering, 1996). Other oxyanion forming metalloids, such as Mo, Se, Cr, and W, may compete with As, but their low concentrations in natural waters makes them poor competitors and unlikely to drive As behavior (Campbell & Nordstrom, 2014). Silica as silicic acid may be an effective

competitor at high pH (>8) when it dissociates to the anionic species, which was experimentally demonstrated by Xu et al. (2012) in As desorption from ferric manganese bearing oxides. Adsorption of divalent cations Ca^{2+} and Mg^{2+} may increase adsorption of As as seen for As(V) on iron oxides perhaps due to the formation of positive surface charges favoring the adsorption of anions. However, the addition of Ca^{2+} decreased As adsorption on kaolinite so effects of cations on As mobility remain unclear (Campbell & Nordstrom, 2014; Wilkie & Hering, 1996).

Volcanic association with arsenic

Volcanic sources of arsenic

Igneous rocks have relatively homogenous As concentrations, slightly increasing with Si content (Onishi, 1955; Smedley & Kinniburgh, 2002; Welch et al., 2000). Concentrations of bulk As in igneous rocks are typically below 5 mg/kg, and volcanic glasses separated from igneous rocks are only marginally enriched (average = 5.9 mg/kg; Figure 2). The frequent association of silicic volcanic rocks with As-contaminated aquifers is commonly attributed to reactive nature of acidic volcanic rocks, particularly fine-grained ash, which tends to produce Na-rich alkaline groundwaters and concentration of As onto weathering products, (e.g. ferric oxyhydroxide; Smedley & Kinniburgh, 2002; Welch, Lico, & Hughes, 1988). Despite relatively low values and variability, many studies attribute As contamination with volcanic rocks, and particularly ash and weathering products (e.g. Smedley & Kinniburgh, 2002; Twarakavi & Kaluarachchi, 2006; Wang & Mulligan, 2006; Welch et al., 1988).

In volcanic processes, As(OH)$_3$ is the dominant form of As. As(OH)$_3$ is enriched in the gas phase by two to three orders of magnitude more than magma at temperatures from 400-900°C; below 350°C, As is preferentially enriched in the liquid phase (Pokrovski et al., 2002; Symonds, Reed, & Rose, 1992). In a study of active fumarolic areas in Japan, Mambo and Yoshida (1993) observed elevated As and the narrow range of As concentrations across all fumarolic ejections, regardless of composition, which suggests direct vaporization from magma with little modification, consistent with fumarole temperature correlating with As content (Mambo & Yoshida, 1993).
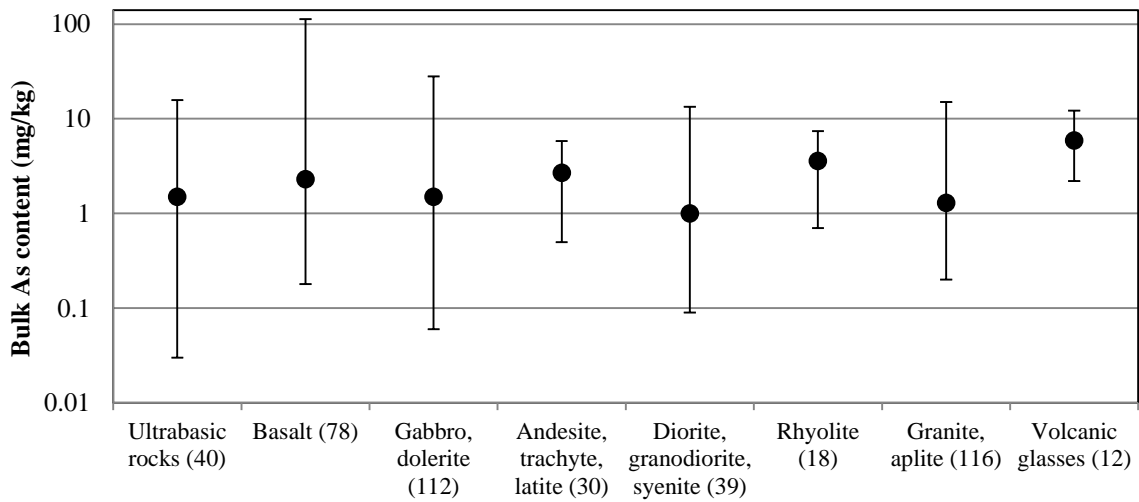
Figure 2: Average bulk As content (mg/kg) in igneous rocks and associated deposits; number in parenthesis indicates number of analyses. Data modified from Smedley & Kinniburgh (2002) and Onishi & Sandell (1955).

Pyroclastic deposits

Ross and Smith (1960) define an ash-flow tuff as "consolidated deposits of volcanic ash resulting from an ash flow." Ash flow tuffs are distinct from ash fall tuffs in that ash fall tuffs are sorted and may display bedding, whereas ash flow tuffs may preserve flow features due to emplacement processes. Pyroclastic material can then be crystallized

through devitrification, which takes place within glass fragments or masses, or vapor-phase crystallization, wherein vapor phases crystallize within open pores. Devitrification produces radial or needly intergrowths of microcrystalline cristobalite and feldspar (spherulites and axiolites). In contrast, vapor phase crystallization is typically coarser grained and results in a more variable mineral assemblage due to the variation in vapor composition (Breitkreuz, 2013; Ross & Smith, 1960; Vaniman, Chipera, Bish, Carey, & Levy, 2001). Typically, both devitrification and vapor phase crystallization refer to crystallization that occurs during or synchronous with cooling, and any subsequent crystallization is commonly considered secondary, low-grade alteration although it can be difficult to determine the timing of crystallization (Ross & Smith, 1960; Smith, 1980). Welding is the deformation of glass particles that begins immediately after emplacement and continues until the tuff is either completely welded or cooling/crystallization of glass prohibits further welding. Welding and crystallization are interrelated in that the densely welded zone of tuffs has no pore space and only devitrification may occur. Conversely, crystalline porous zones in ash flows are dominated by vapor phase crystallization (Ross & Smith, 1960; Smith, 1980). The type of pyroclastic deposition also determines the form of crystallization: ash fall pyroclastic deposits allow for separation of the gas phase, while pyroclastic flows and surges retain gas in the deposit, allowing for vapor phase crystallization if pore space is retained (De' Gennaro, Incoronato, Mastrolorenzo, Adabbo, & Spina, 1999).

Alteration of pyroclastic deposits

Volcanic glass is unstable at surface conditions and will alter to more stable crystalline phases, such as smectite and zeolite, given sufficient time or elevated

13

temperatures (De' Gennaro et al., 1999; Vaniman et al., 2001). The alteration product depends primarily on eruptive and depositional conditions, and secondarily on composition, grain size, and age. The presence of condensing water vapor is essential to zeolitization and therefore is contingent upon depositional mechanism; ash flow tuffs and surges retain water vapor, whereas there is immediate separation of water vapor in ash fall tuffs (De' Gennaro et al., 1999). Finer grain size allows for more contact between permeating solutions and glass, reducing reaction time (De' Gennaro et al., 1999). In terms of composition, the Si/Al ratio and Na/K ratio are the most important tools in determining which alteration minerals form; for example, zeolites such as phillipsite and chabazite form in K- and Na-rich, Si-poor environments, whereas smectites form in Si-rich, alkaline conditions (De' Gennaro et al., 1999; Fuente, Cuadros, Fiore, & Linares, 2000). Illite and illite-smectite were thought to form from glass with smectite as an intermediary, but direct alteration of glass to illite and illite-smectite was observed on the surface and rims of glass while preserving the original form particle morphology (Fuente et al., 2000). Given the tectonic regimes in which tuffs occur, subsequent hydrothermal alteration or metamorphism is also common (Vaniman et al., 2001).

Extensive chemical modification may also occur at the time of emplacement and subsequent alteration. During initial cooling, devitrification, and hydration, volatiles (potentially including As) may be lost and alkalis locally mobilized. Subsequent leaching of Na, K, and Si, oxidation of metal oxides, enrichment of Ca and Mg, and changes accompanying formation of clay minerals and zeolites may occur (Noble, 1970; Scott, 1971; Vaniman et al., 2001). Aluminum remains relatively immobile during devitrification and zeolitization and alkali to alumina ratios are commonly used as an

14

indicator of geochemical alterations (Vaniman et al., 2001). While lava flows may be considered a relatively closed system upon emplacement, pyroclastic deposits, particularly tuffs, have significant glass-shard surface area allowing significant fluid migration, constrained by the degree of welding (Scott, 1971). The thickness of the tuff deposit, and in turn its degree of welding and zonation, strongly controls potential for alkali exchange and other modification; thicker units (typically >100 m) display extensive alkali exchange through water-glass interactions in addition to modification made possible by devitrification (Scott, 1971). However, not all studies report geochemical changes accompanying devitrification: Rowe, Ellis, & Lindeberg (2012) in their study of the Tuff of Knob within the Snake River Plain did not observe any difference in bulk geochemical analysis between the vitrophyre and devitrified portion. However, differences in alkali content were observed between the groundmass of each suggesting alteration only affected the tuff on a very local scale.

Considering volcanism's substantial contribution of environmentally hazardous trace elements, alteration of volcanic units which may make these contaminants available to the environment remains remarkably unstudied. Several studies have focused on the potential of fresh, unaltered volcanic glass and ash for sorption, particularly with regard to nuclear waste disposal. Wolfsberg et al. (1979) examined sorption capacity of several tuffs from Jackass Flats, NV, and found that differences in mineralogy indeed effected sorption capacity: the zeolitized and fresh glassy tuffs have high to intermediate sorption while the partially welded, devitrifed tuff had low to intermediate sorption and greater total desorption for all elements studied. Glass was particularly associated with high sorption for Sr, Cs, and Ba, while zeolites had high sorption for Sr, Cs, Ba, Eu, and Am.

15

Anionic or soluble complex-forming elements (I, Sb, Mo, and U) had low or zero

sorption under the conditions of the experiment (Wolfsberg et al., 1979).

Stimac et al. (1996) in their study of the Bandelier Tuff observed increased Pb

content within and potentially on the surface of fine-grained replacement products (e.g.

smectite and hematite), formed during post-emplacement vapor-phase crystallization and

devitrification. Most of the Pb distribution within the unit was dependent on original

magma chamber distribution, with only local redistribution by vapor transport and

devitrification. Elements enriched in high-temperature magmatic vapors are also more

abundant in sublimate assemblages (e.g. vapor-phase crystallization), suggesting that they

formed directly from magma vapor and continued to form during the earliest stages of

cooling. Stimac et al. (1996) suggest that similar to Pb, other metals that partition into the

vapor-phase (such as As, Ag, Bi, Cu, Re, and Sb) are incorporated into or deposited onto

micron-scale minerals upon eruption and through processes of vapor-phase crystallization

and devitrification are more readily available to the environment.

Volcanic aquifers contaminated with arsenic

Volcanic ash and tuffs are responsible for As-contaminated aquifers around the

world, e.g. Italy, Mexico, Argentina, and the western United States (Smedley &

Kinniburgh, 2002; Welch et al., 2000). Common attributes include Na-HCO$_3^-$ type,

oxidizing, alkaline ground waters, elevated concentrations of B, Cr, F, Mo, Sb, U, and V

(Aiuppa, D'Alessandro, Federico, Palumbo, & Valenza, 2003; Casentini, Pettine, &

Millero, 2010; Mahlknecht et al., 2004; H. B. Nicolli, Suriano, Gomez Peral, Ferpozzi, &

Baleani, 1989; Rango, Vengosh, Dwyer, & Bianchini, 2013; Tang & Johannesson, 2010;

Vinson et al., 2011). Mobilization of As from silicic volcanic products is commonly attributed to primary glass dissolution followed by secondary sorption onto Fe, Mn, and Al oxyhydroxides and clays, which is subsequently readily mobilized by pH desorption (Aiuppa et al., 2003; Johannesson & Tang, 2009; H. Nicolli, Bundschuh, & García, 2010; Rango et al., 2013; Tabelin, Hashimoto, Igarashi, & Yoneda, 2014; Welch et al., 2000). In regions of higher geothermal activity, sulfide oxidation is considered the dominant mechanism mobilizing As (Aiuppa et al., 2003; Mahlknecht et al., 2004).

Arsenic contamination in the Southern Willamette Valley

Arsenic contamination in Lane County, located in western Oregon, has been a well-documented problem since the early 1960s. Goldblatt, Van Denburgh, & Marsland (1963) published the first data on groundwater As, finding 30.5% (n=53) of well samples exceeded 0.02 mg/L. They determined that the As-enriched water was principally dominated by dissolved Na^+ and HCO_3^- with low concentrations of Ca^{2+} and Mg^{2+}, as well as pH greater than 8.0. A second water type with As values mostly less than 0.01 mg/L has high TDS values (>500 mg/L), dominated by dissolved Na, Cl, and Ca, and high B. The third water type reported by Goldblatt et al. (1963) is dilute, with TDS less than 100 mg/L, and negligible values of As. Although well depth did not correlate with As concentration, most water samples in excess of 0.05 mg/L of As came from depths greater than 100 ft. and most samples from depths shallower than 50 ft. contained less than 0.01 mg/L of As. Goldblatt et al. (1963) attribute the elevated As to the Fisher formation, consisting of tuffaceous sediments, conglomerates, vitric and crystalline tuffs, breccias, and andesitic lava flows, with possible influence from the Eugene formation. They note that As is not uniformly distributed within the Fisher formation, but tends to

concentrate in the central and eastern areas of the formation, which typically contain younger units. Goldblatt et al. (1963) hypothesize that As and B were contained within the pyroclastic rocks deposited in the Fisher formation, then percolating surface water chemically altered the groundwater by replacing Ca and Mg with Na ("softening" the water) concurrently releasing As and increasing pH.

Whanger, Weswig, & Stoner (1977) studied As contamination throughout all of Oregon. They reiterate the common characteristics of high As waters in Oregon of low Ca^{2+} and Mg^{2+} relative to Na^+, high B, high pH, high orthophosphate, with variable TDS, sulfate, and chloride. Their speciation data also showed that the vast majority (>95%) of As is present as As(V), although their specific methodology of As speciation were not reported.

Nadakavukaren, Ingermann, Jeddeloh, and Falkowski's (1984) study of fourteen wells in Lane County did not find any correlation with As and pH, although eight of the fourteen wells had lower As concentrations in winter compared to summer. They suggested that deeper wells may have higher As contamination, and rainfall may also play a role although they were unable to make any definitive statements with such a limited study.

Hinkle and Polette (1999) reviewed historical data and conducted additional sample analysis for a combined 728 spatially distinct groundwater samples within the Willamette Valley to further understanding of As sources and mobility within the valley. They reported that 8.0% (n=58) of samples exceeded the EPA As standard at the time of their study (0.05 mg/L), and 21.7% (n=158) exceeded the WHO guideline of 0.01 mg/L,

18

which is the current EPA standard for As as of 2002 (USEPA, 2014). Similar to Goldblatt et al. (1963), they did not find a correlation of As with depth; they also found that most of the high As groundwater occurred within areas of exposed or thinly-covered bedrock in south-central and eastern Lane and Linn counties. They concluded that elevated As occurs within the Fisher and Eugene Formations, and within undifferentiated tuffaceous sedimentary rocks, tuffs, and basalt. They suggest that volcanic glass – still abundant in the Willamette Basin - is the primary source of As and, further, given that much of the glass in regional volcanic units has been devitrified, As is likely to have become associated with devitrification alteration products (e.g. clays and metal oxides) or to have been released into solution and subsequently precipitated or adsorbed elsewhere or flushed out. However, no direct measurement of As host phases was conducted in their study. Although redox potential was not measured by Hinkle and Polette (1999), field observations frequently noted sulfide odors, which indicate reducing conditions in the groundwater. Previous studies also found low dissolved oxygen, which further supports their hypothesis of reducing conditions. Because their study did not find especially alkaline waters, they believe some combination of reducing conditions, anionic competition, and elevated pH to be the most important factors in As contamination within the Willamette Basin.

These previous studies agree that the source of elevated As in groundwater are the Fisher and Eugene Formations and mostly agree that As-rich groundwater is characterized by low Ca^{2+} and Mg^{2+} relative to Na^+, high B, high pH, and high phosphate, with variable TDS, sulfate, and chloride. However, precise processes of As liberation into groundwater remain unclear. Goldblatt et al. (1963) argued that the percolation of surface

water promoted weathering of volcanic glasses and minerals and the release of Na^+ which, in conjunction with ion exchange of Ca^{2+} and Mg^{2+} for Na^+ on clay surfaces, increased groundwater pH and mobilized As. Hinkle and Polette (1999) likewise agree that volcanic glass is the primary source of As. However, because their study did not find especially alkaline waters, they conclude that reducing conditions and anionic competition are the most important factors in As contamination within the Willamette Basin.

Although population exposure to As has historically been minimal because alternate water supplies have been used, increasing population and water demands in the future may increase human health risk (Morton, Starr, Pohl, & Stoner, 1976; OWSC, 2013). The self-supplied ground water population is nearly 20% of total population in Lane County (64,970), which makes Lane County the second-most dependent county on domestic water wells behind Clackamas County by both population served and self-supply ground water withdrawals (6.50 Mgal/day). Total water use, including surface and ground water has increased 500% from 1995 to 2005, and 167% from 2000 to 2005. Growing population indicates further reliance on ground water supplies as surface water supplies become increasingly depleted.

Sample collection and preparation

For this study, 24 samples were collected from 14 distinct outcrops within the Fisher Formation and Little Butte Volcanics Series in the southern Willamette Valley (Figure 3; Table 1). Samples were identified and located using reference maps from McClaughry et al. (2010) and Retallack et al (2004). Every effort was made to collect representative samples of each tuff unit within the formations. However, the region is largely vegetated and exposed outcrops are scarce. Where significant, observable differences were noted at an outcrop, multiple samples were collected. Eight additional samples from a previous study (Savoie, 2013) were included to better represent area tuff units identified by previous workers.

Collected hand samples were first trimmed with a water-cooled rock saw to remove any obviously weathered surfaces. A portion of each sample (~30 g) was then crushed to a fine gravel size with a Braun jaw-crusher and powdered with a tungsten carbide ring mill vibratory pulverizer for 2-3 minutes. The powdered samples were split using a Jones riffle splitter, with a subsample sent to Washington State University (WSU) Geoanalytical Lab, in Pullman, WA for bulk geochemical analysis and the rest retained for mineralogical analyses and leachate studies. Additional portions of the sample were either used for preparation of thin sections or retained for reference.
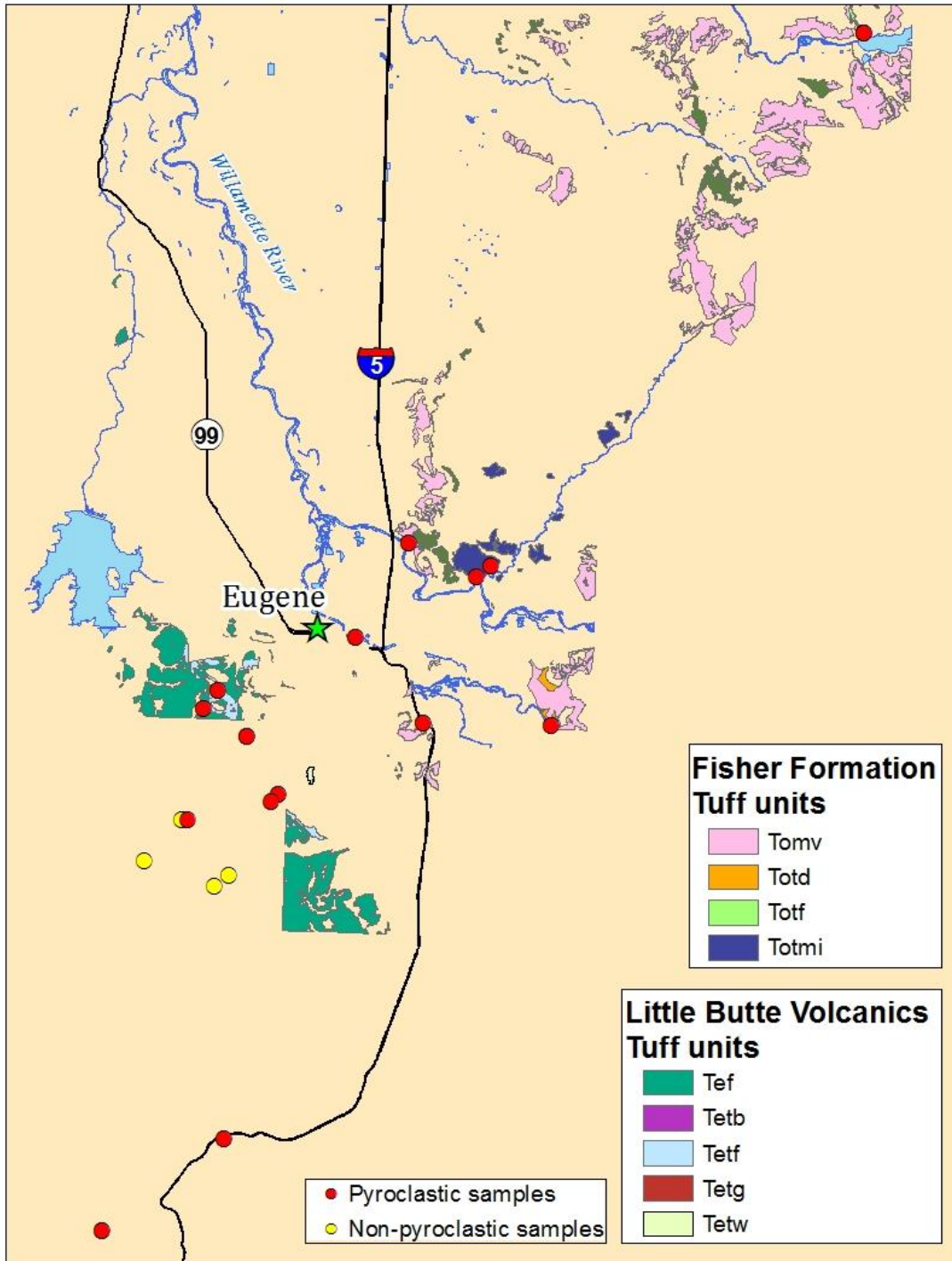
Figure 3: Sample locations referenced in this study

Table 1: Sample locations and units sampled in this study

Formation	Unit	Age (Ma)	Sample ID	Latitude	Longitude
	Tuff of Dexter (Totd)	25.9	DX	44.002109	-122.908858
	Tuff of Foster Dam (Totf)	26.3	FD1-4*	44.419917	-122.665317
	Mehama (Tomv) "Tuff above Willamette Flora"	30.6[1]	WF, WFw	44.001258	-123.014311
	Tuff of Mohawk, intracaldera facies (Totmi)	30.9[2]	MK1*	44.095583	-122.962883
			MK2*	44.089033	-122.974017
Little Butte Volcanics Series	Mehama (Tomv) Tuff of Spores Point	31.3[1]	SP	44.107890	-123.031594
			FineSS, Upper Cong	44.002109	-122.908858
			OCshale, Basal SS	44.001258	-123.014311
	Mehama (Tomv)	25.9-34.8	SporesPtSS	44.107890	-123.031594
			WS2*	43.939033	-123.206820
			WS3	43.955445	-123.132974
	Undivided (Tef)	38[1]	LDNTuff	43.749120	-123.167949
	Fox Hollow Tuff (Tetf)	41.0[1]	FHr, FHb	43.989685	-123.160442
	Tuff of Gimpl Hill (Tetg)	41.8[2]	GHg	44.005758	-123.197287
			GHw	44.016537	-123.185691
Fisher Formation			CongSSWeat	43.906797	-123.171772
	Undivided (Tef)	34.8-41.8	CongSS, WeatBasalt	43.899833	-123.182794
			MicaSS	43.913169	-123.241703
			PebCong	43.938822	-123.211908
			LDNTuffSS, MicaSS	43.692377	-123.266201

[1]Retallack, 2004; [2]McClaughry et al., 2010   *Samples from Savoie, 2013

Bulk chemistry

Samples submitted to WSU were analyzed for major elements and trace elements (As, Ba, Ce, Cr, Cu, Ga, La, Ni, Nb, Nd, Pb, Rb, Sc, Sc, Sr, Th, U, V, Y, Zn, Zr) by x-ray fluorescence (XRF). Additional trace element analysis (Pr, Sm, Eu, Gd, Tb, Dy, Ho, Er, Tm, Yb, Lu, Hf, Ta, Cs) was performed by inductively coupled plasma mass spectrometry (ICP-MS).

Five samples were analyzed for bulk As at Portland State University. Acid digests were prepared following US EPA Method 3052 (US EPA, 1996). Powdered samples were weighed to 0.250 ± 0.001 g and added to Teflon containers along with 1.5 mL trace-metal grade HF, 4.5 mL trace-metal grade HNO_3^-, and 1 mL trace-metal grade HCl. Samples were digested in a Milestone Ethos EZ Microwaves digester for 40 minutes, reaching a final temperature of 240°C for 20 minutes. Following digestions, samples were poured into 50 mL plastic centrifuges tubes. The digest solutions were diluted to 50 mL with rinsate from the digest tubes and 18.2 MΩ-cm deionized water. Samples were further diluted ten and fifty times for analysis by Agilent 700 Series ICP-OES.

Optical mineralogy

Cut samples were sent to Spectrum Petrographics in Vancouver, WA, for preparation of covered thin sections which were examined to determine volcanic textures, pyroclastic materials, and primary mineral assembly.

X-Ray diffraction

Sample mineral assemblages were determined via X-ray diffraction (XRD) analyses using a Phillips (now PANalytical) Theta-Theta PW3040 X-ray diffractometer equipped with a standard scintillation counter and copper anode X-ray lamp. For these analyses, powdered samples were further crushed with an agate mortar and pestle until passing a 65-μm sieve and prepared as random powder mounts in a side-pack aluminum sample holder. Diffraction patterns were obtained in continuous mode using a step size of 0.020 degrees two theta (º2θ) and scan step times of 1.00 second from 3 to 70 º2θ. Sample diffraction patterns were analyzed with the PANalytical X'Pert Highscore Plus software package.

Scanning electron microscopy

Billets that remained after thin section preparation for select samples (FHr, FHb, and BCw) were analyzed by scanning electron microscopy. The billets were polished down to a 1-μm finish by diamond polish and coated with carbon to reduce charging during the SEM examination.

Due to instrument repairs, the FHr and FHb samples were analyzed on an FEI Sirion SEM equipped with Oxford EDS detector at 20 kV. Compositional images were generated by the secondary-electron detector with negative bias turned off to create a pseudo-compositional mode. The BCw sample was analyzed on a Zeiss SIGMA SEM equipped with Oxford WDS/EDS detector at 20 kV. Mineral chemistry was determined using the WDS/EDS detector for in situ point analysis and element abundance maps.

25

Spectra and mineral phase identification was completed using Oxford AZTEC software package.

Leachate experiments

Powdered samples were evaluated for aqueous As mobility under a variety of pH conditions and P concentrations (Table 2). These experiments utilized 1:20 solid:solution ratios, usually 0.5-1.0 g to 10-20 mL of solution depending on subsequent analyses. All solutions were prepared using 18.2 MΩ-cm deionized water and reagent-grade or trace-metal-grade chemical reagents. Samples were mixed in 50 mL centrifuge bottles at 20 rpm then centrifuged at 3000 rpm for 15 minutes. Except for a set of time-series experiments, samples were mixed for 24 hours. Following centrifugation, 8 mL of supernatant were pipetted from the top of the solution column and acidified with 0.200 mL (2.5%) trace-element-grade HNO_3^- for elemental analysis, while the remainder was decanted for pH measurement and anion analysis if applicable.

Time series were conducted by weighing samples to 2.500 g ± 0.002 g and mixing with 50 mL of solution, either deionized water or 0.1 mM phosphate as P in centrifuge tubes. At five time points (4, 10, 24 or 50, 72, and 194), samples were centrifuged at 3000 rpm for 15 minutes, and 8 mL were pipetted into clean aliquots and acidified with 0.200 mL of trace metal grade nitric acid for analysis. Because a 24 hour analysis had already been performed for water only leachate in prior experiments, samples were additionally separated at 50 h while 0.1 mM phosphate solutions were removed at 24 h.

Elemental analyses were performed using an Agilent 720 axial inductively coupled plasma – optical emission spectrometer (ICP-OES); operating conditions and elemental wavelengths used are included in Appendix A.

Quality assurance

Quality assurance and control procedures were maintained throughout this study to ensure data accuracy and precision. Sample bottles and vials were cleaned by soaking in a 5% (by volume) nitric acid bath for 24+ hours and triple rinsing with 18.2 MΩ-cm deionized water. All leachate experiments were run in duplicate.

For elemental analyses via ICP-OES, a calibration was performed prior to each sample run using a minimum of five external standards prepared from commercial NIST-certified multi-element stock solutions. Most elements were analyzed via multiple wavelengths in case of unexpected spectral interferences and, where interferences were negligible, to provide verification of resulting concentrations.

Table 2: Composition of leachate solutions

Solution name	Composition	pH of Solution
Water	Deionized water (18.2μS/L)	--
MOPS7	$[C_7H_{15}NO_4S]$ + 0.1 M HCl (10 mM)	7.0
pH 7 + P	KPO_4 monobasic + $NaPO_4$ dibasic	7
Tris8, Tris9	Trizma base $[(HOCH_2)_3]$ + Trizma HCl $[(HOCH_2)_3CNH_2 \cdot HCl]$ (10 mM)	8.09, 8.71
pH 9	Boric acid + NaOH +KCl	9
CAPS 10	$C_9H_{19}NO_3S$ + 0.1 M NaOH	10.0
pH 10	0.05 M $NaHCO_3$ + 0.1 M NaOH	10.4
pH 11+P	$NaPO_4$ tribasic + $NaHCO_3$	11

| 10 μM P, 0.1 mM P | Diluted from 1 ppm P solution | 6-7 |
| 1 mM P, 100 mM P | K_2HPO_4 | 7.25, 8.8 |

Quality control standards, prepared from different NIST-certified multi-element stock solutions, were run at a minimum after every 20 samples. Instrument detection limits and method reporting limits (IDLs and MRLs) were determined twice during the course of this study by analyses of seven to ten near-blank (~ 5 ug/L) standards. The IDLs were calculated to be three times the standard deviation of the resulting measured concentrations for each element and the MRLs ten times the standard deviation. Because results from multiple analyses are combined for comparative purposes, the most conservative limit is used. Since multiple wavelengths are analyzed for each element, wavelength selection was based on the degree of precision (determined by difference from known standards) and detection limits. Quality control/assurance data for elements discussed are included in Appendix C.

Geospatial distribution of groundwater As

Data for groundwater As concentrations were downloaded through the Pacific Northwest Water Quality Data Exchange Network (Department of Environmental Quality, 2015), which provides latitude/longitude of wells sampled and As concentration. The point data were spatially joined to surficial geologic maps in the region created by McClaughry et al. (2010). Geologic units were broadly grouped on the basis of lithologic type. Complete units for each group are provided in Appendix E.

Bulk geochemistry

Bulk chemistry data were examined from analyses of eight tuff and tuffaceous sediment units within the Willamette Valley (BC, DX, FD, FH, MK, SP, WF, and WS; see Table 1 for unit definitions). Interpretation and visualization of bulk chemistry to characterize volcanic rocks and compare samples within units was performed with Geochemical Data Toolkit (Janoušek, Farrow, & Erban, 2006). Complete geochemical results for samples analyzed in this study are included in Appendix B. Additional geochemical data were obtained from McClaughry et al. (2010) and Savoie (2013). A total alkali versus silica plot of tuff samples indicates that most samples plot as rhyolite or dacite (Figure 4).
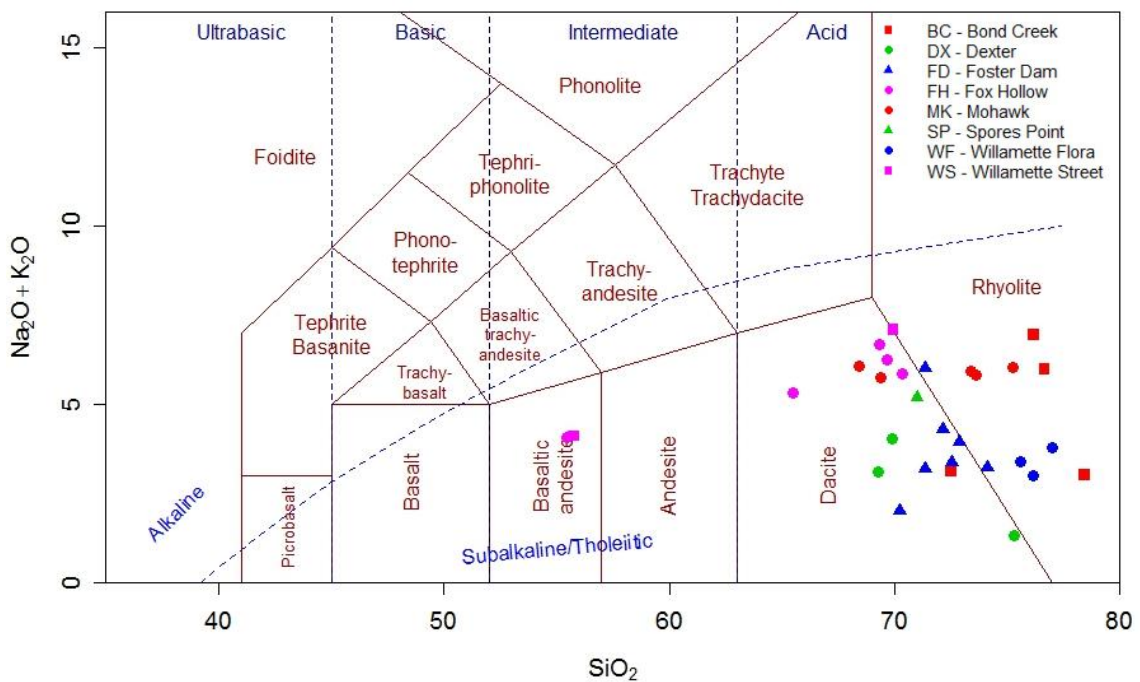
Figure 4: Total alkali silica diagram of samples in the study based on Le Bas et al., 1986.

It is very likely that significant loss of Na_2O and K_2O has occurred in the time since deposition, since samples are 25-42 Ma and any alteration or weathering is likely to result in loss of alkalis (De' Gennaro et al., 1999; Vaniman et al., 2001). Two samples plot as basaltic andesites: a Fox Hollow (FH) sample from DOGAMI's database and sample of Willamette Street (WS) unconsolidated sediment. The Ishikawa alteration index (AI), which quantifies the loss of sodium associated with plagioclase and volcanic glass breakdown, is defined below (Ishikawa, Sawahuchi, Iwaya, & Horiuchi, 1976):

$$AI = \frac{100 \ (K_2O + MgO)}{(K_2O + MgO + \ Na_2O + CaO)}$$

The Ishikawa alteration index was originally developed to identify volcanically hosted massive sulfide deposits, but is also applied to glassy volcanic rocks to determine degree of alteration (e.g. Gifkins & Allen, 2001; Large, Gemmell, Paulick, & Huston, 2001). Ishikawa alteration indices for samples in this study range from 17 to 43 (Table 3). Values ranging from 20 to 60 are interpreted as weak or diagenetic alteration, and values from 50 to 100 are interpreted as hydrothermal alteration (Gifkins & Allen, 2001; Large et al., 2001).

Table 3: Ishikawa (1976) alteration indices for tuff samples in this study

Sample ID	BCg	BCw	DX	FD1	FD2	FD3	FD4	
Alteration Index	32.8	32.5	23.4	26.7	20.8	17.3	43.3	
Sample ID	**FHb**	**FHr**	**MK1**	**MK2**	**WF**	**WFw**	**WS1**	**WS2**
Alteration Index	31.0	23.9	22.6	23.7	16.2	17.3	21.2	26.5

Spider diagrams were constructed for available trace elements to examine differences among samples within the same tuff unit and to confirm that samples collected for this study were associated with the correct unit. Data source for bulk chemistry is indicated by prefix (D: McClaughry et al., 2010; CS: Savoie, 2013; GF: this study). For comparative purposes, samples were normalized to the average composition of three Foster Dam samples analyzed by McClaughry et al. (2010) because they are likely the least altered as evidenced by their glassy groundmass. Trace elements are generally arranged from the left to right by decreasing mobility based on ionic potential, following Pearce (1983).
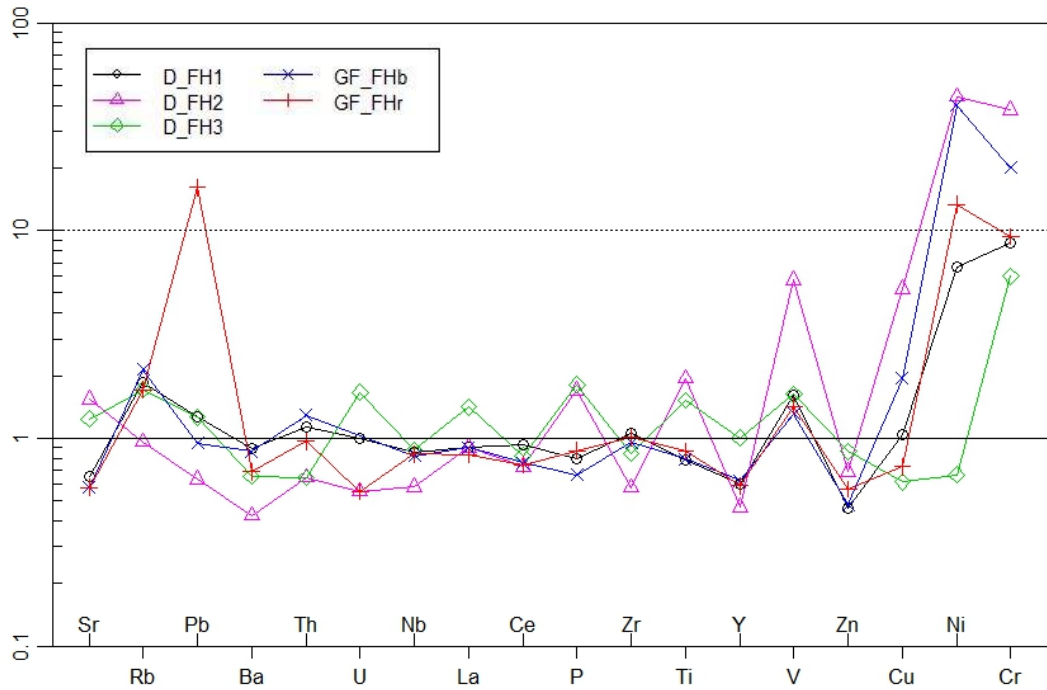
Figure 5: Trace element geochemistry of Fox Hollow tuff samples normalized to average of Foster Dam tuff samples.

D_FH1 corresponds with the location sampled for this study (GF_FHr and GF_FHb) and all three follow similar patterns, with greater deviation occurring for Pb, U, and transition metals Cu and Ni (Figure 5). FHr is enriched in Pb significantly as well as P and depleted in U. FHb has elevated Cu, Ni, Cr, Ba, and Th relative to both D_FH1 and GF_FHr.
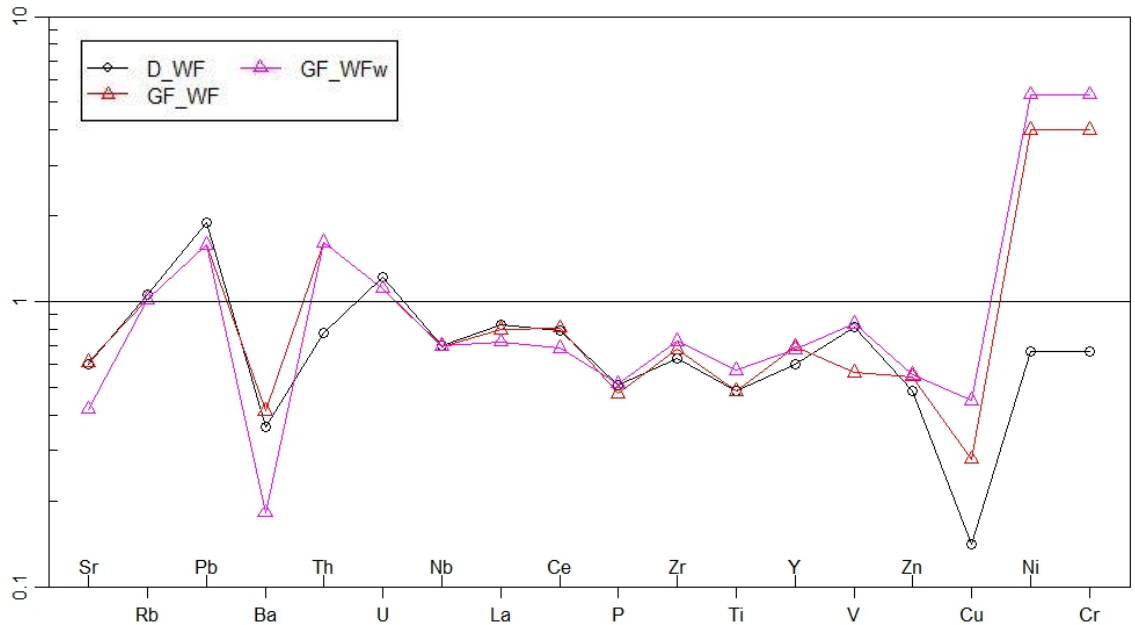
Figure 6: Trace element geochemistry of Tuff above Willamette Flora samples normalized to average of Foster Dam tuff samples.

All three samples of Willamette Flora are from the same outcrop and follow a similar pattern with greater variation occurring for transition metals Cu, Ni, and Cr (Figure 6). GF_WFw is depleted in Sr and Ba, and enriched in Cu, Ni, and Cr relative to GF_WF and D_WF. GF_WF is depleted in V and somewhat enriched in Cu, Ni, and Cr relative to D_WF.

All four samples of Mohawk tuff are from distinct outcrops and display greater variation with the transition metals, Ti, Zn, Cu, Ni, Cr, and V and P (Figure 7). CS_MK1

32

is enriched in Ni and Cr compared to other MK samples examined. CS_MK2 is depleted in P, Zn, Cu, and Cr relative to other MK samples examined.
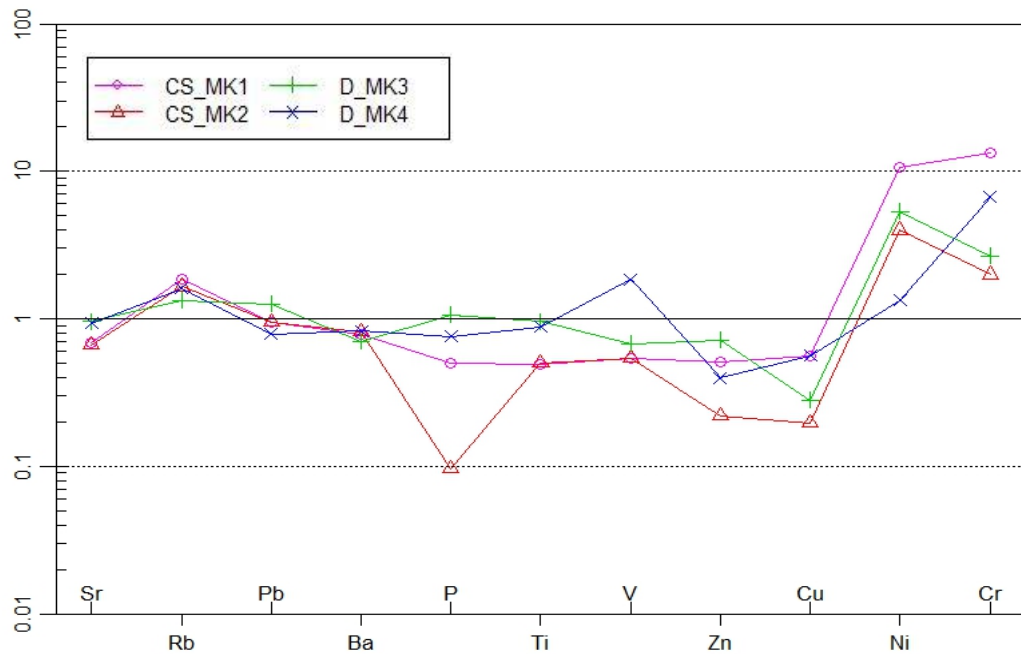
Figure 7: Trace element geochemistry of Mohawk tuff samples normalized to average of Foster Dam tuff samples.

Crystallization and welding classification

Tuffs are classified (Table 4) based on the form of crystallization and welding following Streck (1994) as determined by optical mineralogy. Crystallization is broadly categorized as either glassy or devitrified. Incipiently devitrified tuffs are defined as retaining glass shards with a devitrified fine-grained matrix, often altered to sericite, which occurs post-emplacement (Camp, 2004; Figure 8). Entirely axiolitic shards that retain glass morphology are classified as cryptocrystalline, which Streck (1994) describes as vapor phase crystallization.

Table 4 : Crystallization and welding classification of samples (following Streck, 1994).

	Unit (Ma)	Sample ID	Crystallization	Welding	Tuff classification
Little Butte Volcanics Series	Totf (26.3)	FD1	glassy	partially welded	vitric-pumice-lithic ash tuff
		FD2	glassy	partially welded	vitric-pumice-lithic ash tuff
		FD3	glassy	partially welded	vitric-pumice-lithic ash tuff
		FD4	glassy	partially welded	vitric-pumice-lithic ash tuff
	Tomv (30.6)	WF	axiolitic rims[1]	nonwelded	incipiently devitrified ash fall tuff
		WFw	axiolitic rims	nonwelded	incipiently devitrified ash fall tuff
	Totmi (30.9)	MK1	pervasively devitrified (felsitic)	densely welded	devitrified crystal-rich ash flow tuff
		MK2	pervasively devitrified (felsitic)	densely welded	devitrified crystal-pumice ash flow tuff
	Tomv (31.3)	SP	pervasively devitrified (felsitic)	partially welded	devitrified crystal-rich ash flow tuff
	Tetb (34.8)	BCg	axiolitic rims, few spherulites	incipiently welded	incipiently devitried ash flow tuff
		BCw	Volcaniclastic sandstone		
Fisher Formation	Tetw (35-36)	WS1	pervasively devitrified (felsitic)	densely welded	devitrified pumice-lithic ash flow tuff
		WS2	pervasively devitrified (felsitic)	densely welded	devitrified crystal-ash tuff
		WS3	Unconsolidated sediment		
	Tef (38)	LDN	lithophysae	partially welded	crystal-lithic lapilli tuff
	Tetf (40.8)	FHr	devitrified (cryptocrystalline)	incipiently welded	devitrified ash-flow tuff
		FHb	devitrified (cryptocrystalline, spherulites)	incipiently welded	devitrified ash-flow tuff
	Tetg (41.8)	GHg	lithophysae	partially welded	lapilli-pumice-lithic tuff
		GHw	pervasively devitrified (felsitic)	densely welded	devitrified lithic-tuff

[1] *Incipiently devitrified* defined by Camp, 2004

Pervasively devitrified with no glass retained is described as felsitic, which Streck (1994) called pervasively devitrified (Figure 8b). Spherulites, radial intergrowths of quartz and plagioclase feldspar, are found in isolation within vugs or completely intergrown forming groundmass (Figure 8c, 8e). Sericite alteration commonly accompanies devitrification products, sometimes entirely replacing spherulites or axiolitic rims. Lithophysae are defined as recrystallization phenomena where a crystallization rind grows outward to form crystal-filled voids, and then may become partially or completely hollow (Figure 8g; Streck, 1994). Lithophysae and spherulites, both considered high temperature crystallization domains, are distinct from vapor phase crystallization and vesicles formed by the exsolution of volatiles (Breitkreuz, 2013).

Nonwelded tuffs completely retain cuspoid and Y-junction glass shards. Incipiently welded tuffs indicate preservation of glass shard shape with some adhesion of glass shards. Partially welded with pumice or fiamme (flattened pumice) has deformed or flattened glass shards. Densely welded tuffs are identified on the basis of pervasive devitrification, although most pervasively devitrified tuffs are dominantly felsitic which overprints welding degree. Densely welded obsidian-like black vitrophyre was not found within the sample area as the base of most units within the study are not exposed (McClaughry et al., 2010).
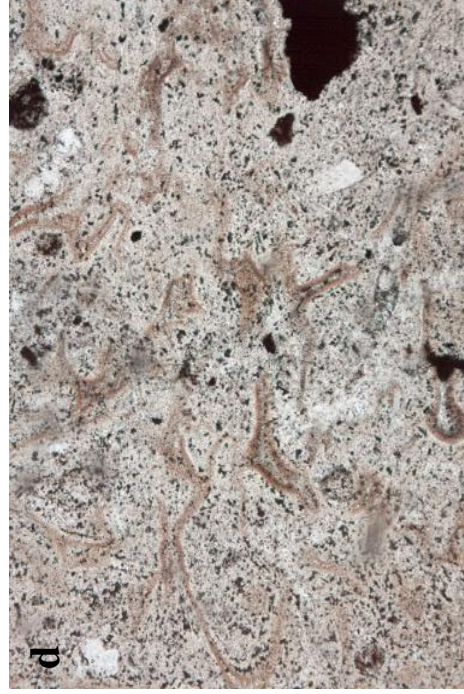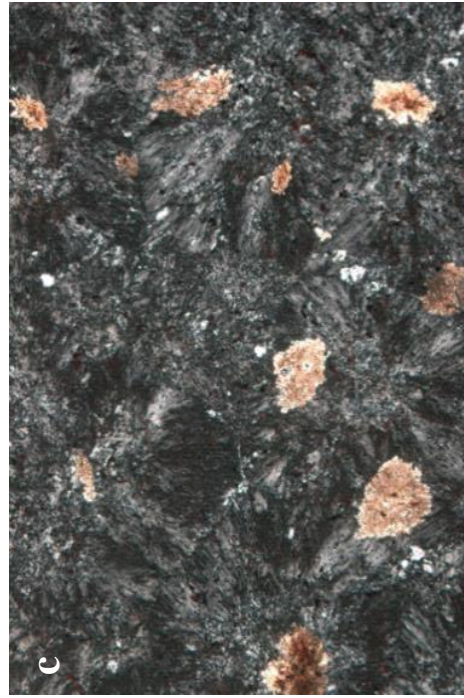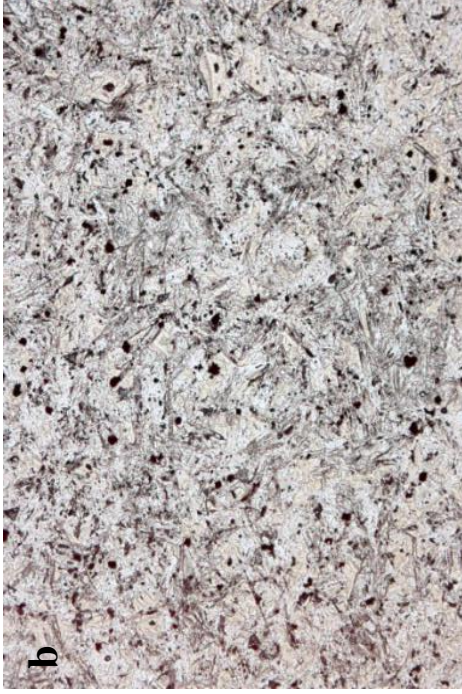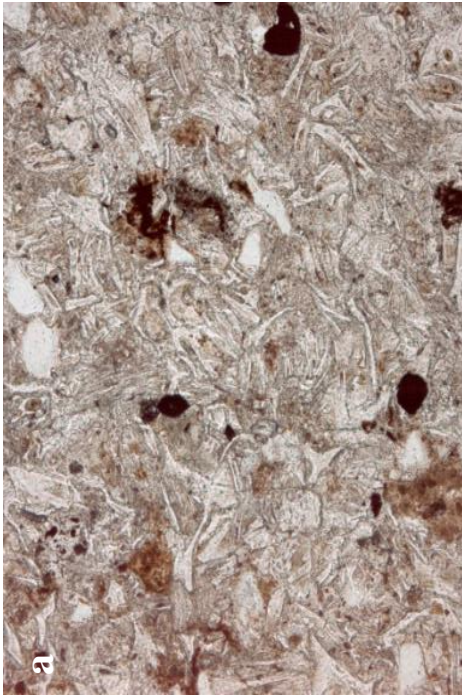
Figure 8a-d: (a) WF: PL incipiently devitrified groundmass with large oxides FOV = 16μm; (b) SP: PL felsitic groundmass texture, small oxides, FOV = 16μm; (c) FHb: XP, intergrown spherulites and sericite, FOV = 16μm; (d) FHr: devit/ox glass gm, FOV = 8μm
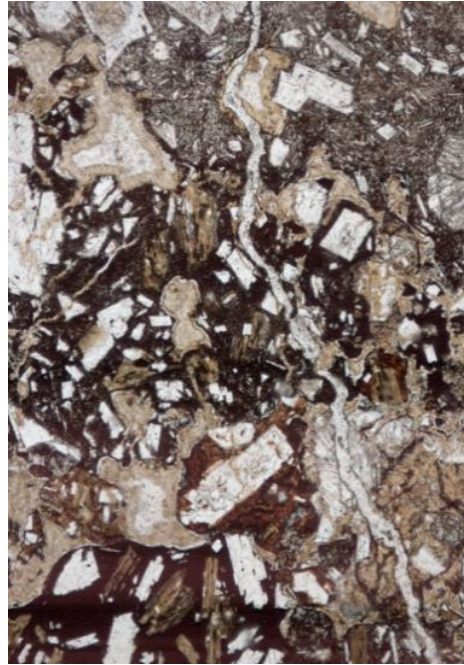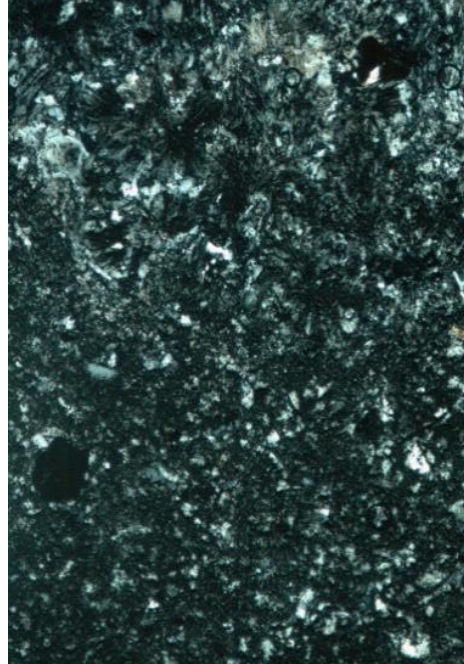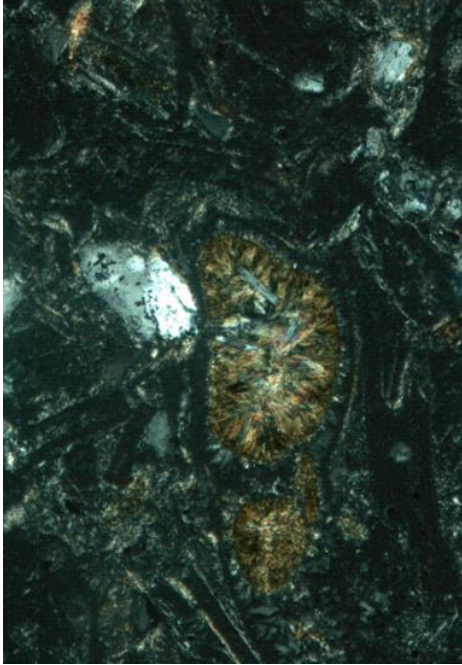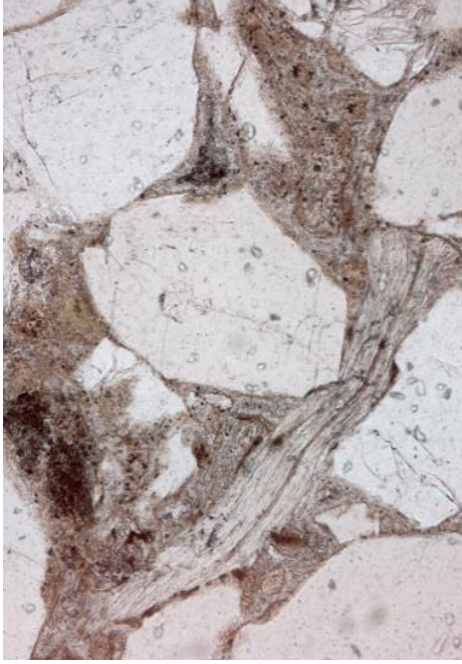
Figure 8e-h: (e) BCg: XP, spherulite altered to sericite, FOV = 8μm; (f) BCw: PL, flattened pumice in volcaniclastic ss, FOV = 16μm; (g) LD: PL, oxidized gm with lath plag lithics and recrystallized pores, FOV = 64μm; (h) GHw: PL, boundary between spherulitic and cryptocrystalline textures, FOV = 32μm

Mineral Assemblage

The mineral assemblage was determined by optical microscopy and x-ray diffractometry. Major mineral phases identified in samples are summarized in Table 5. Most common minerals include feldspars, silica phases, clay alteration products, and trace ferromagnesian minerals and oxides. Several feldspar diffraction patterns have similar peaks so the closest pattern match was selected, typically andesine and albite. Alteration products identified by XRD include zeolite minerals, most commonly heulandite, and clay minerals, most commonly montmorillonite and sericite. Ferromagnesian minerals commonly occur as large glomerocrysts, most commonly pyroxenes. Large amorphous oxides, the specific compositions of which were not determined, were identified in several tuffs.

SEM-EDS Compositional Analysis

Mineral phases were identified in BCw through chemical composition element maps and in-situ analyses. Phases were identified by characteristic element spectra to produce mineral phase maps. Mineral phases were identified in FHb and FHr using selected in-situ analyses based on SEM-SE imaging. Individual spectra represent single point data, since phase mapping was not available. Phases identified in FHb and FHr, along with the corresponding count of points, are listed in Table 6.

Table 5: Mineral assemblage and volcanic texture of samples discussed in the study as determined by XRD and optical microscopy. Major mineralogy is >30%, minor is <30% and accessory is <10%.

	Unit (Ma)	Sample ID	Crystallization	Major	Minor (accessory)
Little Butte Volcanics Series	Totd (25.9)	DX	NA	Quartz, andesine, heulandite	(Stellerite)
	Totf (26.3)	FD1	Glassy	Heulandite, glass	Mordenite, quartz, albite (smectite, sericite)
		FD2	Glassy	Heulandite, glass	Mordenite, quartz, sericite, albite (smectite)
		FD3	Glassy	Heulandite, glass	Mordenite, quartz, sericite, albite (smectite)
		FD4	Glassy	Heulandite, glass	Mordenite, quartz, sericite, albite (smectite)
	Tomv (30.6)	WF	Axiolitic rims	Mordenite	Quartz, clinoptilolite, albite, am oxides
		WFw	Axiolitic rims	Mordenite	Sanidine, am oxides (qtz, zeolite)
	Totmi (30.9)	MK1	Pervasively devitrified (felsitic)	Albite	Quartz, smectite, clinopyroxene, (oxides)
		MK2	Pervasively devitrified (felsitic)	Albite, quartz	Oxides (smectite, sericite)
	Tomv (31.3)	SP	Pervasively devitrified (felsitic)	Albite	Microcline, tridymite, oxides (sericite, zeolite, ferrobustamite)
	Tetb (34.8)	BCg	Axiolitic rims, few spherulites	Clinoptilolite quartz, albite	Orthopyroxene, sericite (zeolite, smectite)
		BCw	Sediment	Quartz, albite, orthoclase, volcanic lithics	Clinoptilolite (augite, pyrite)
Fisher Formation	Tetw (35-36)	WS1	Pervasively devitrified (felsitic)	Albite	Quartz, Cristobalite, illite, smectite
		WS2	Pervasively devitrified (felsitic)	Heulandite	Albite, stilbite, (illite, chlorite)
		WS3	Sediment	Quartz	Orthoclase, albite, kaolinite
	Tef (38)	LDN	Lithophysae	Anorthite	Orthopyroxene, albite, oxides, qtz (smectite)
	Tetf (40.8)	FHr	Devitrified (cryptocrystalline)	Quartz, albite	Anorthite, sanidine, oxides (sericite)
		FHb	Devitrified (cryptocrystalline, spherulites)	Quartz, albite	Sericite, oxides (smectite)
	Tetg (41.8)	GHg	Lithophysae	Andesine, heulandite, quartz	Magnetite (smectite)
		GHw	Pervasively devitrified (felsitic)	Quartz, albite, sanidine	Orthopyroxene, orthoclase

Table 6: Individual spectra count of phases identified in FHb and FHr. Phases are assigned on the basis of chemical composition from SEM-EDS analysis.

Phase	Total Spectra Counts	
	FHb (n = 83)	FHr (n = 35)
Glass	23	12
(Fe|Ti) oxides	35	14
Aluminosilicates	10	3
Ferrous lime	4	2
Ferrosilicate	0	1
Amphibole	2	0
Apatite	5	0
Lime	0	2
Illite	1	0
Pyrite	1	0
Zircon	2	0

BCw was examined using electron dispersal spectroscopy on a total six phase maps. As was identified as a trace component in several phases, most commonly sulfides, although As was also detected in TiO* and three groundmass phases. The sulfide phase contained Fe at a ratio of Fe:S > 2. Although quantification is very approximate, SEM-EDS analysis indicated that As concentration in the sulfide phases was ~0.1-0.4%. The As-bearing sulfide commonly occurs within the groundmass and in mineral grain cracks (Figure 9).
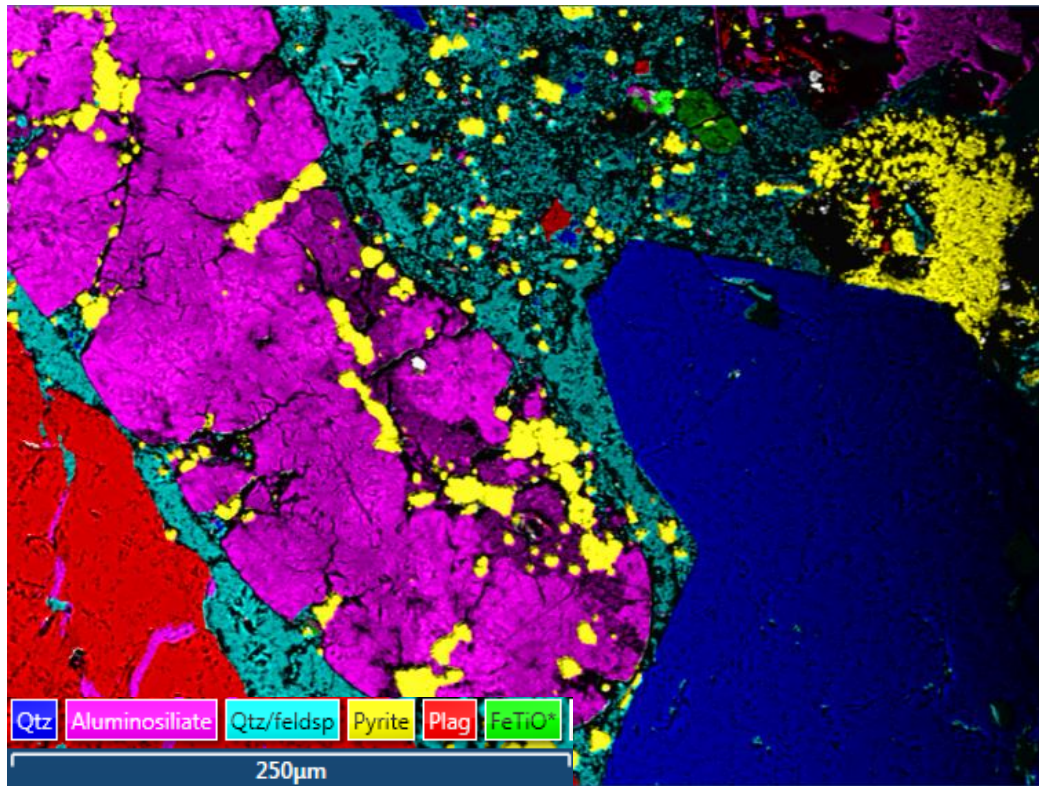
Figure 9: False-colored scanning electron micrograph identifying major phases within BCw. The Sulfide phase and aluminosilicate contain measurable As.

Water leachate

Leachate experiments were performed in order to measure the potential mobility of As from tuff and tuffaceous sediment samples and to try and elucidate modes of occurrence and processes controlling the release of As into solution. Results of quality control standards indicate most elements achieved a 15% recovery; major elements Al, Ca, K, Na, Si exceed 15% recovery in low standards (20-50 µg/L) which is acceptable considering these elements tend to occur in solution at higher concentrations. Transition metals, Cu, Fe, and Zn, and metalloid, As, exceed 15% in a few (3-7) check standards but are still within industry-accepted recovery of 20%. Mobility of As was tested under a range of pHs (7 to 11), concentrations of anionic competition (10 µM to 100 mM phosphate as P), and through time (4 to 192 hours). Complete results of leachate

41

experiments are included in Appendix D. A summary of percent of As mobilized with

different solutions is presented in Table 7.

Table 7: Percent of total bulk As mobilized under various pH buffers and phosphate solutions. Darker shaded values percent indicate highest percent mobilized for that sample.

		Total As (ppm)	Water	pH 7	pH 9	pH 10	10 μM P	0.1 mM P	1 mM P	100 mM P
Devitrified	FHr	21.0	0.2%	<0.004%	0.2%	0.3%	0.1%	0.2%	0.3%	0.8%
	FHb	20.0	1.3%	<0.004%	<0.004%	3.2%	0.2%	0.4%	0.4%	0.8%
	MK1	4.7	2.1%	>0.02%	>0.02%	4.6%	1.9%		3.0%	5.0%
	MK2	9.2	2.3%	0.3%	0.9%	6.3%	2.6%	2.9%	3.3%	4.1%
	SP	16.8	0.7%	0.2%	0.6%	1.3%				
	GHg	11.2	2.1%	0.3%	2.7%	4.8%				
Incipiently devitrified	WF	6.5	3.3%	1.5%	3.1%	5.6%	7.8%		6.0%	3.9%
	WFw	8.0	4.5%	0.8%	3.8%	6.2%	6.4%		6.9%	5.5%
	BCg	9.4	1.4%	0.3%	2.9%	5.0%	1.3%	1.2%	5.3%	7.1%
Glassy	FD1	5.4	0.5%	<0.02%	<0.02%	2.6%	0.4%		2.2%	5.0%
	FD2	5.5	0.9%	<0.02%	0.4%	2.2%				
	FD3	9.0	0.7%	<0.01%	0.6%	2.9%				
	FD4	13.1	1.3%	0.1%	1.7%	3.9%	1.6%	1.3%	3.7%	5.3%
Litho-physae	GHw	4.9	1.2%	0.03%	1.1%	2.4%				
	LDN	8.0	1.5%	0.1%	1.2%	3.3%				
Sed	BCw	57.2	3.7%	5.7%	26%	37%				
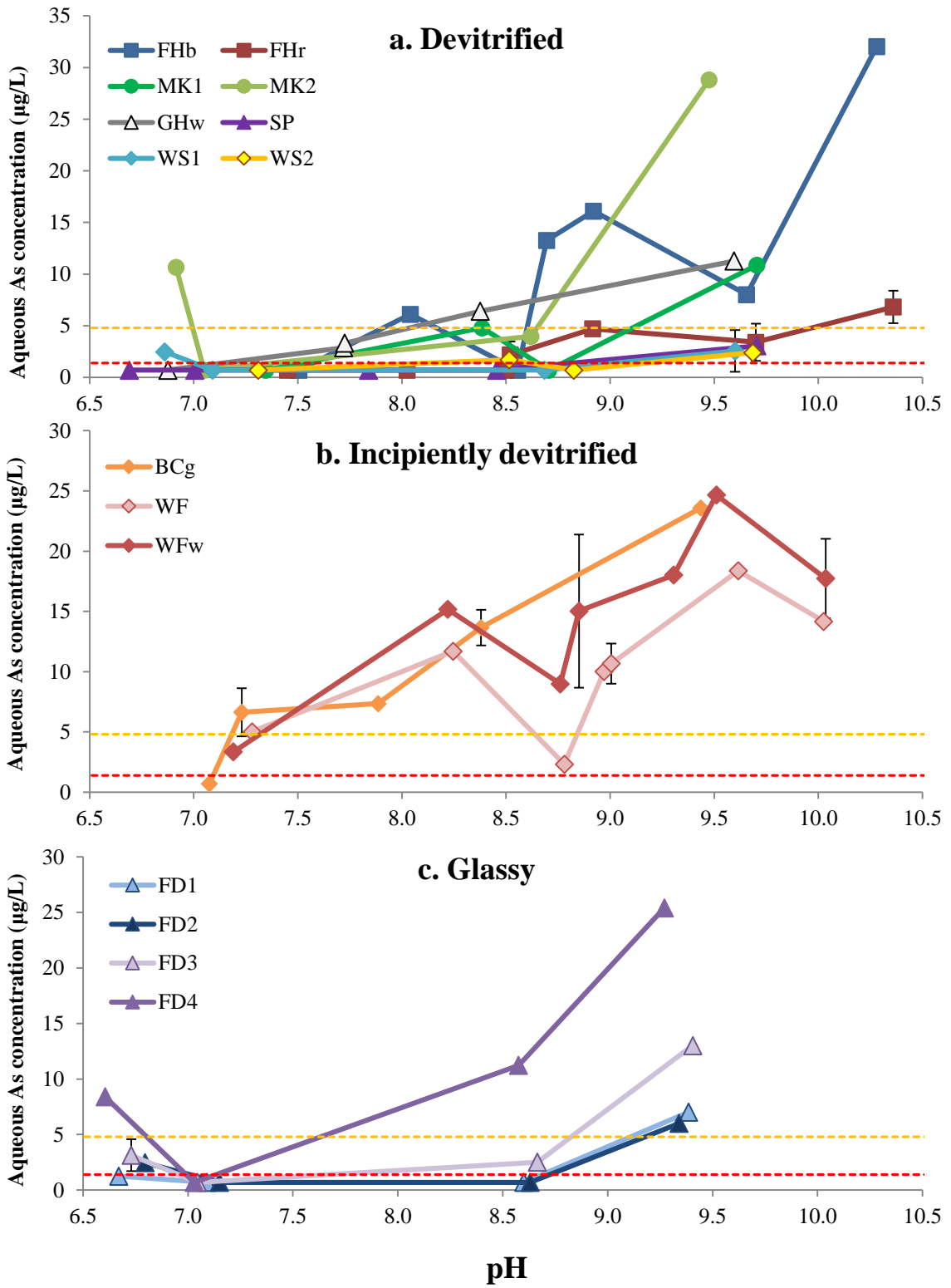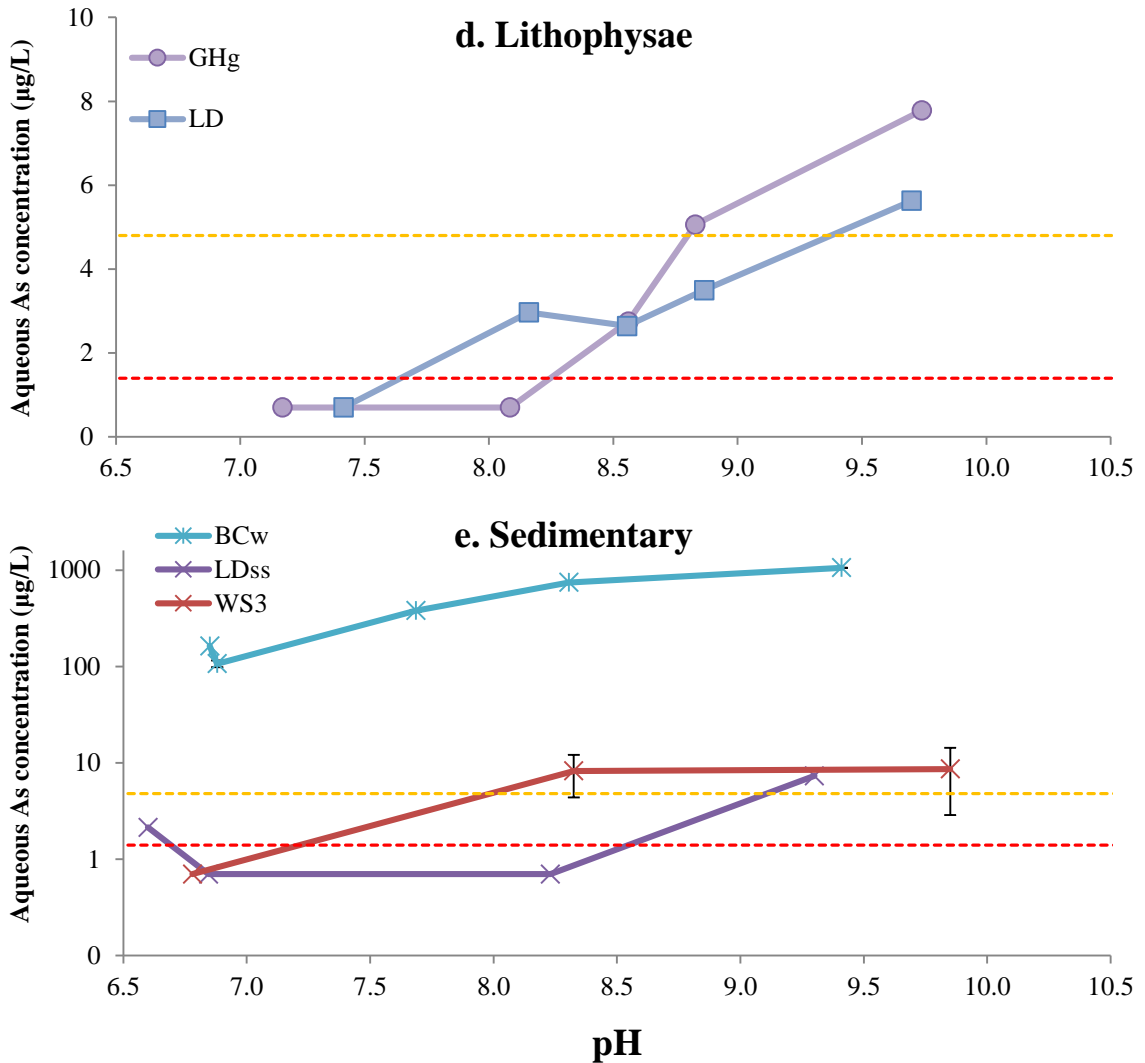
Figure 10a-e: Average aqueous As concentrations resulting from leaching of different classifications of tuffs by various pH buffers. Method detection limit (1.4 µg/L) and method reporting limit (4.8 µg/L) indicated by red and orange dotted lines, respectively. Samples below detection limit are represented by half the detection limit (0.7 µg/L) Difference between duplicates exceeding the method detection level (1.4 ppb) are indicated by error bars.

Samples display a variety of As mobilization behavior, between and within crystallization types (Figure 10a-e). There is an overall trend of increasing aqueous As with elevated pH, although in many cases, pH must be well above 9.0 before exceeding regulatory limits (10.0 µg/L). Leachate solutions vary in final pH because the samples

themselves buffer the solutions to varying extents. The largest sample group, devitrified tuffs, contains samples which produce experimental leachate concentrations of As that do not exceed 5 µg/L, even at pH > 9 (SP, WS1, WS2). Leachate solution produced by samples from the same outcrop, FHb and FHr, under the same buffer solution (pH 10) have substantially different maximum As concentrations, 7 µg/L from FHr and 32 µg/L from FHb. Similarly, MK1 and MK2, both from the same unit although different outcrops, produce different maximum As concentrations under the same buffer solution (pH 10), 10 µg/L from MK1 and 29 µg/L from MK2. Incipiently devitrified samples BCg, WF, and WFw produce consistently elevated As concentrations in solution, with relatively steadily increasing As with increasing pH. Lithophysae samples GHg and LD do not produce significant As concentrations in solution, only exceeding the MRL above pH~9. Among sedimentary samples, LDss and WS3 produce at most ~8 µg/L of As in buffer solutions above pH~9, while BCw produces the highest aqueous As concentrations of any sample in the study, ranging from 110 µg/L to >1000 µg/L at pH 9.4.

Kendall tau rank statistics were applied to samples which for which there were sufficient treatments (n≥5) to determine which elements behaved similarly to As in solution (Table 8). Kendall tau was selected due to the small number of sample treatments and nonparametric distribution. The Mann-Whitney test was performed to determine statistical significance for α=0.05.

Table 8: Correlation of As with other elements in pH experiment conditions. Degree of correlation is calculated by Kendall correlation coefficient. Number of buffer solutions included in correlation test indicated in parentheses. Negative sign indicates the correlation is negative. Italicized values are not significant at α=0.05.

	Devitrified		Incipiently devitrified		
	FHr (7)	**FHb (7)**	**BCg (5)**	**WF (7)**	**WFw (7)**
No correlation (τ < 0.3)	Si, Fe, K, Ni *Zn*	*Zn,* Fe,	Si, Al, *Cu, Cr,* Ni, Pb, *Zn,* Fe, -K	Ca, Sr, K	Sr, Ca, K
Weak correlation (0.3 ≤ τ < 0.5)	Al, -Mg, *Cr,* Cu	Si, Al, K, Ni, -Mg, -Mn, -Cu	-Sr,	Al, Mg, Cu	Cu
Moderate correlation (0.5 ≤ τ < 0.7)	-Mn, -Ca, *V, -Pb,* -Sr	-Ca, Cr, -Sr, *V*	-Ca	Si, Fe, Mn, *Cr, Ni,* Pb,	*Ni, Cr,* Zn, Si, Al, Pb, V
Strong correlation (τ ≥ 0.7)		-Pb	-Mn, -Mg, *V*	V, Zn	Mg, Mn, Fe

For most leachate solutions, As concentration in solution correlates with V. Leachate solutions produced by FHr, FHb, and BCg show no correlation for As with Si nor Al. Concentrations of As in solutions produced by WF and WFw correlate with Si and Al, along with several transition metals (Mn, Fe, Ni, Cr).

Phosphate experiments

Samples exhibiting a variety of devitrification textures which produced solutions with elevated As were tested for mobilization by anionic competition through introduction of phosphate at increasing concentrations, from 10 µM to 100 mM as P (Figure 11).
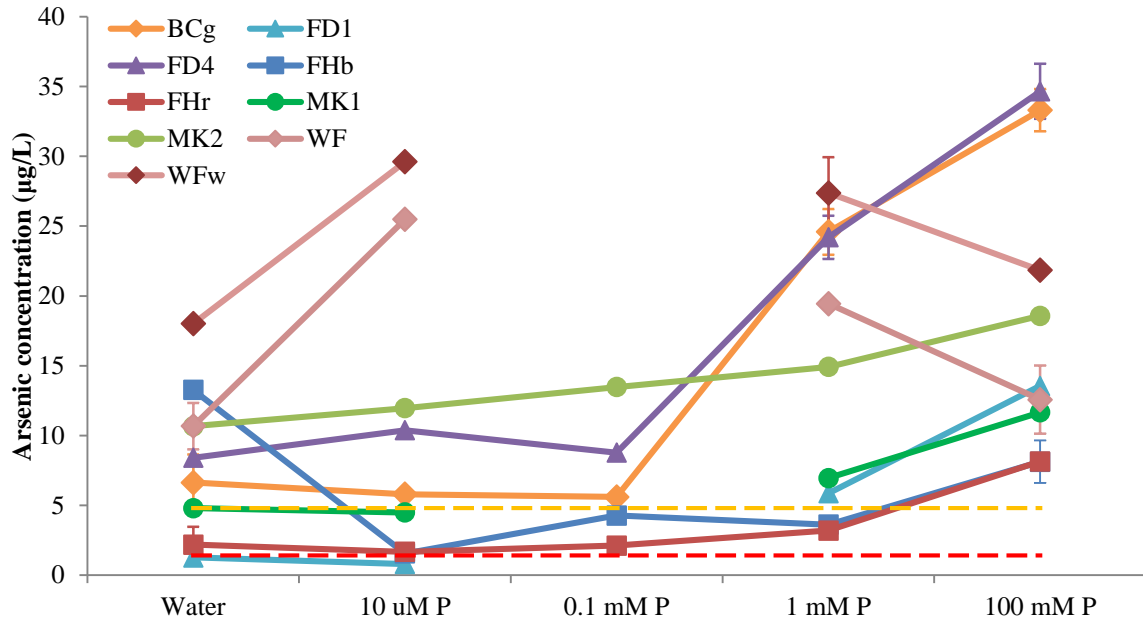
Figure 11: Concentration of arsenic in solution with varying concentrations of phosphate. Method detection limit (1.4 μg/L) and method reporting limit (4.8 μg/L) indicated by red and orange dotted lines, respectively. Samples below detection limit are represented by half the detection limit (0.7 μg/L) Difference between duplicates exceeding the method detection level (1.4 ppb) are indicated by error bars.

Leachate solutions produced by BCg and FD4 exhibit rapidly increased As concentrations above 1 mM P. Concentrations of As in leachate solutions produced by WF and WFw increase slightly with 10 uM P, but then experience a decrease with additional phosphate, suggesting secondary precipitation. Leachate solutions produced by MK1, MK2, FD1, and FHr experience slight but relatively insignificant increases in As and only with very high concentrations of P (100 mM). Aqueous concentrations of As in solutions produced by FHb decreases markedly with the introduction of phosphate, from 13.3 ug/L with water to less than 5 ug/L for all phosphate concentrations examined.

Aqueous leachate concentrations of As were compared with other elements by Kendall tau rank statistical test for individual samples (Table 9). Higher values of τ

indicate greater correlation. The Kendall tau rank statistical test was applied to samples

for which there were sufficient treatments (n≥5). Kendall tau was selected due to the

small number of samples and nonparametric distribution. The Mann-Whitney test was

performed to determine statistical significance for α=0.05.

Table 9: Kendall tau rank correlation of As to other elements in solution with varying concentrations of phosphate. N=5 for all samples included. Negative sign indicates the correlation is negative. Italicized values are not significant at α=0.05.

	Devitrified			Incipiently Devitrified	Glassy
	FHr	**FHb**	**MK2**	**BCg**	**FD4**
No correlation (τ < 0.3)	*Cr*	Si, *Al,* Fe, Mn, Mg, *Ca, Cr,* Pb	Si, Al, Fe, Mn, Cu, *Mn, V, Zn,* Ni	*Ca, Cr,* Mg, Pb, *Sr, V*	Si, Cu
Weak correlation (0.3 ≤ τ < 0.5)	-Ni, -V, Pb -Ca, -Sr, Mg, *Na*	*-V,* Cu, Na	-Cu, Ni		Ni, Pb, -Al, -Fe, *-Mn, -Zn*
Moderate correlation (0.5 ≤ τ < 0.7)	-Zn, -Mn	-Ni, *-Zn*	*Sr*	-Cu	Ca, *Na*
Strong correlation (τ ≥ 0.7)	-Fe, *-Al,* -Si, *-Cu*		Na, Ca, Mg, Pb, *Cr*	*Na, -Al,* -Fe, -Mn, -Ni, -Si, *-Zn*	Mg, Sr, *V, Cr*

Leachate solutions produced by FHb, MK2, and FD4 display no or weak correlation

for As in solution with Si and Al. Solutions produced by FHr and BCg display negative

correlation for As in solution with Si and Al. Solutions produced by MK2 and FD4 have

positive moderate to strong correlations for As with Sr, Na, Ca, and Mg. As in solutions

produced by FHr and BCg correlates negatively with Fe, Al, Si, and other metals.

Time series

Time series experiments were performed on five tuff samples with varied alteration and secondary mineralogy and which produced leachate solutions with As concentrations above the regulatory limit (10 µg/L).
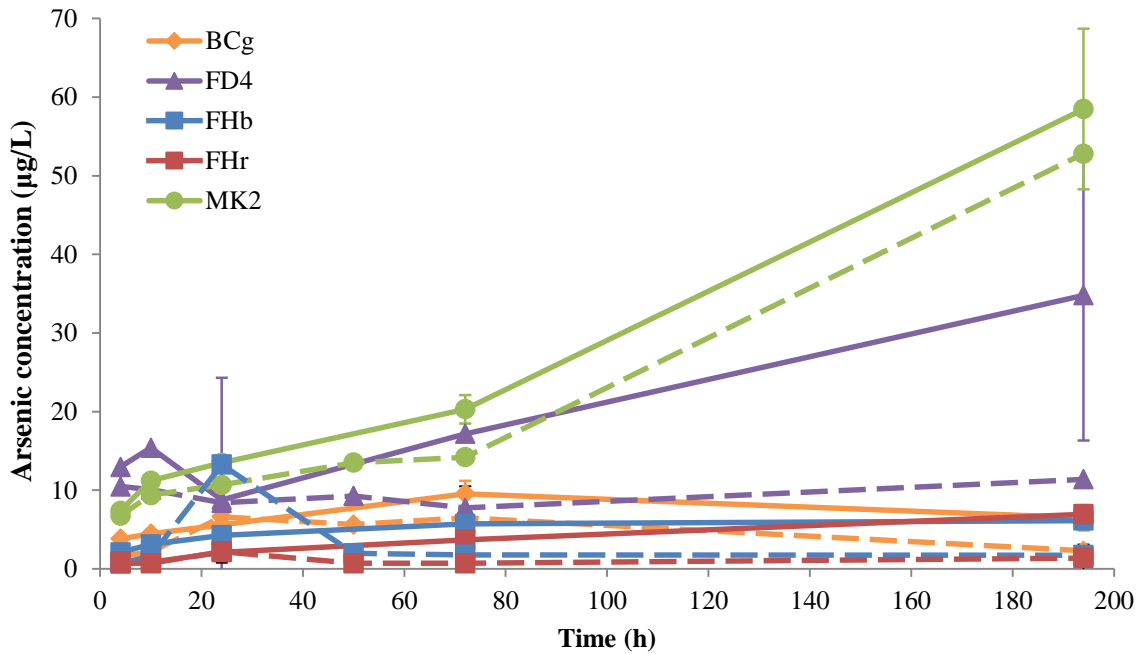
Figure 12: Aqueous arsenic concentrations in leachates over time for select samples. Solid lines indicate 0.1 mM phosphate and dotted lines indicate water solution, including 24h analysis from previous experiment. Samples below detection limit are represented by half the detection limit (0.7 µg/L) Difference between duplicates exceeding the method detection level (1.4 ppb) are indicated by error bars.

Examination of As in leachate over time indicates that As either increases continually (FD4 and MK2) or does not increase significantly (BCg, FHb, FHr; Figures 12-13). Cumulative percent is calculated based on a liquid:solid ratio of 1:20 and dividing by bulk As concentration. Concentrations of As in leachate produced by FD4 and MK2 continue increasing during the time series, reaching 14% and 24% respectively of total As mobilized by 0.1 mM P and 7% and 21% with water only solutions. Leachate solutions produced by BCg increase slightly in As, but flatline at 72h. Concentrations of

As in leachate produced by FHr and FHb remain relatively low, under 1% and 2% of

total As, respectively.
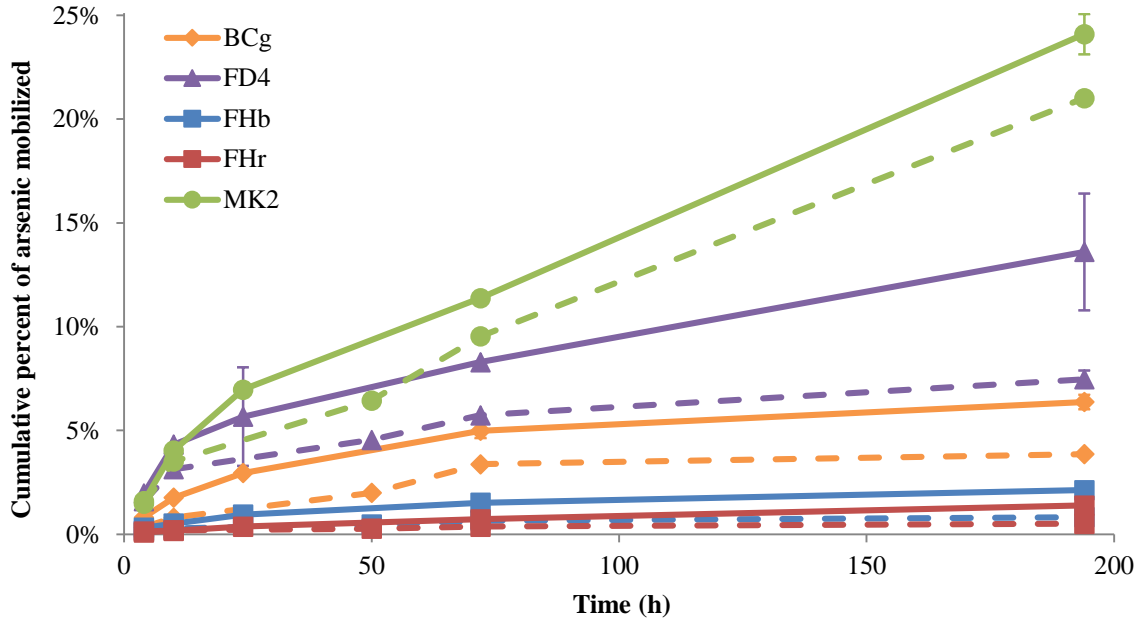
Figure 13: Cumulative percent of total arsenic mobilized during time series. Dotted line indicates water solution, solid line indicates presence of 0.1 mM phosphate. Samples below detection limit are represented by half the detection limit (0.7 μg/L) Difference between duplicates exceeding the method detection level (1.4 ppb) are indicated by error bars.

Aqueous leachate concentrations of As were compared with other elements by

Kendall tau rank statistical test for individual samples (Table 10). Higher values of τ

indicate greater correlation. The Kendall tau rank statistical test was applied to samples

which had sufficient experimental conditions (n>5). Kendall tau was selected due to the

small number of samples and nonparametric distribution.

Leachate solutions produced by MK2 and BCg display high correlation between As

and most elements, which increase substantially in concentration with time along with

As. Leachate solutions produced by FD4 also display increased As concentrations over

time but As does not correlate with other elements. FHb and FHr produce leachate

solutions with low release of As through the time series; there is no correlation between

As concentrations and most other elements.

Table 10: Kendall tau rank correlation of As to other elements in time series for both water and 0.1 mM P solutions. N=10 for all samples included. Negative sign indicates the correlation is negative. Italicized values are not significant at α=0.05.

	Devitrified			Incipiently devitrified	Glassy
	FHb	FHr	MK2	BCg	FD4
No correlation ($\tau < 0.3$)	Ca, Cu, Mn, Na, Ni, V, Zn	Cr, Fe, K, Mg, Mn, Ni, *Pb,* Si, Al, V, Zn, Cu			Ca, Cr, Cu, Fe, Mg, Mn, Ni, Pb, Si, Al, *Sr,* Zn
Weak correlation ($0.3 \leq \tau < 0.5$)	-Cr, -Fe, Mg, -Al, -Si	Na, K		K, Si	K, Na, *V*
Moderate correlation ($0.5 \leq \tau < 0.7$)	K	Ca		Cr, Na, V, Al	
Strong correlation ($\tau \geq 0.7$)	-Pb		Ca, Cr, Cu, Fe, K, Mg, *Mn,* Na, Ni, Pb, Si, Al, V, Zn	Ca, *Cu,* Fe, Mg, Mn, *Ni,* Pb, Zn	

Geospatial distribution of groundwater As in relation to mapped surface lithologies

Arsenic concentrations in groundwater reported by the USGS and ODEQ were

obtained through the Pacific Northwest Water Quality Exchange (2015). The geospatial

distribution of As concentrations in the study area was then analyzed with respect to

surface lithologies as mapped by McClaughry et al. (2010). Of 1,481 distinct data points

included in the resulting As distribution map (Figure 14), 101 (7%) exceeded the EPA

MCL. The locations of these 101 wells define localized "hotspots" of elevated As

concentration.
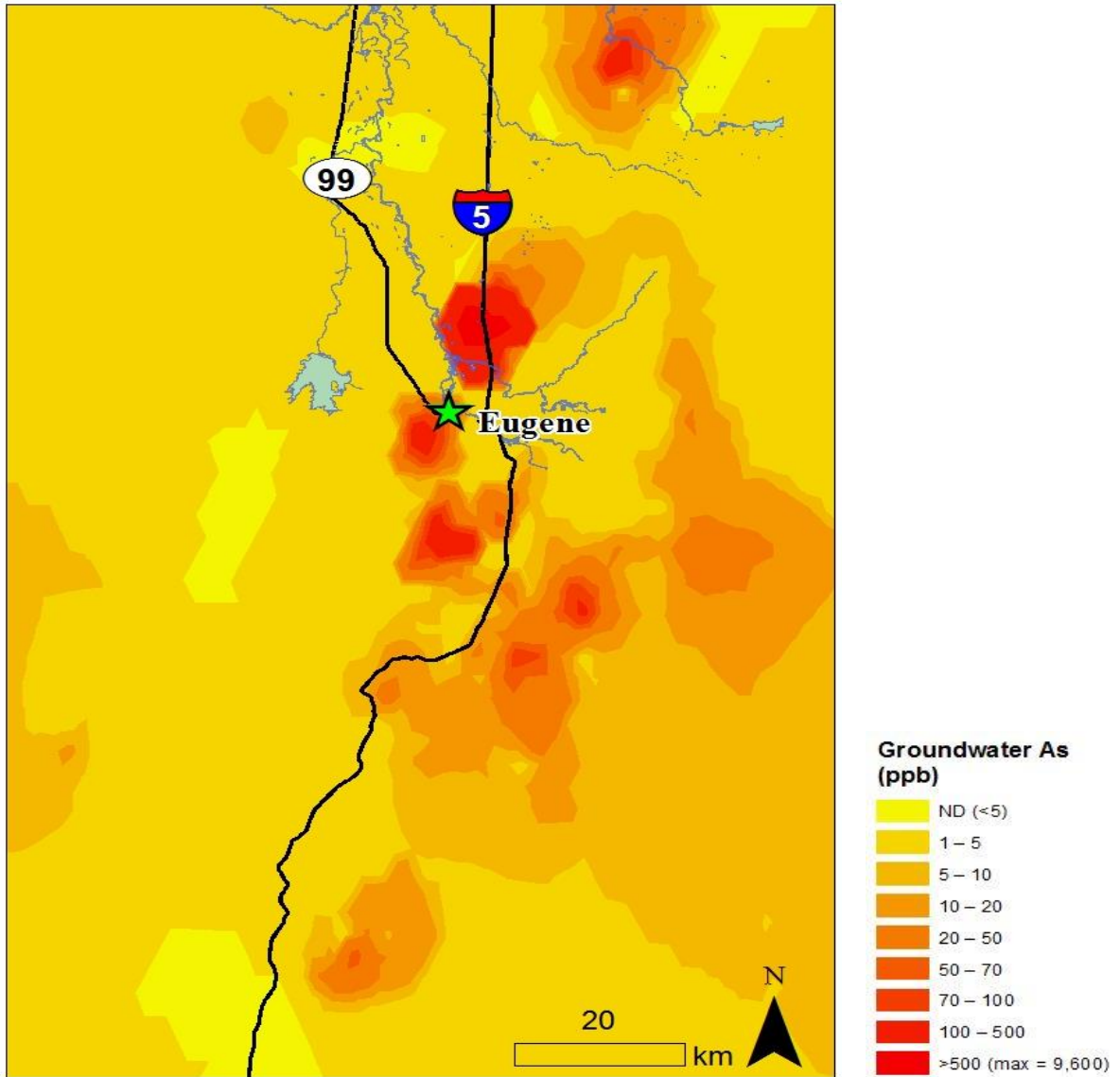
Figure 14: Inverse distance weighted distribution of groundwater As concentrations (in parts per billion) from USGS and ODEQ water databases, available through Pacific Northwest Exchange (2015).

Point data of As measurements in groundwater were spatially joined to lithologies to

determine which, if any, units are associated with high As. This was done with the

realization that the surficial units may not correspond with geologic units at the depths

that wells are screened. Geologic units mapped by McClaughry et al. (2010) were

grouped according to major lithologies present in the Willamette Valley. Fisher and Little

Butte Volcanics, undifferentiated, were named as their own group to determine if they presented distinct As distributions. Three potential outliers at the 1% significance level were identified by Rosner's outlier test, and were consequentially removed from the dataset.
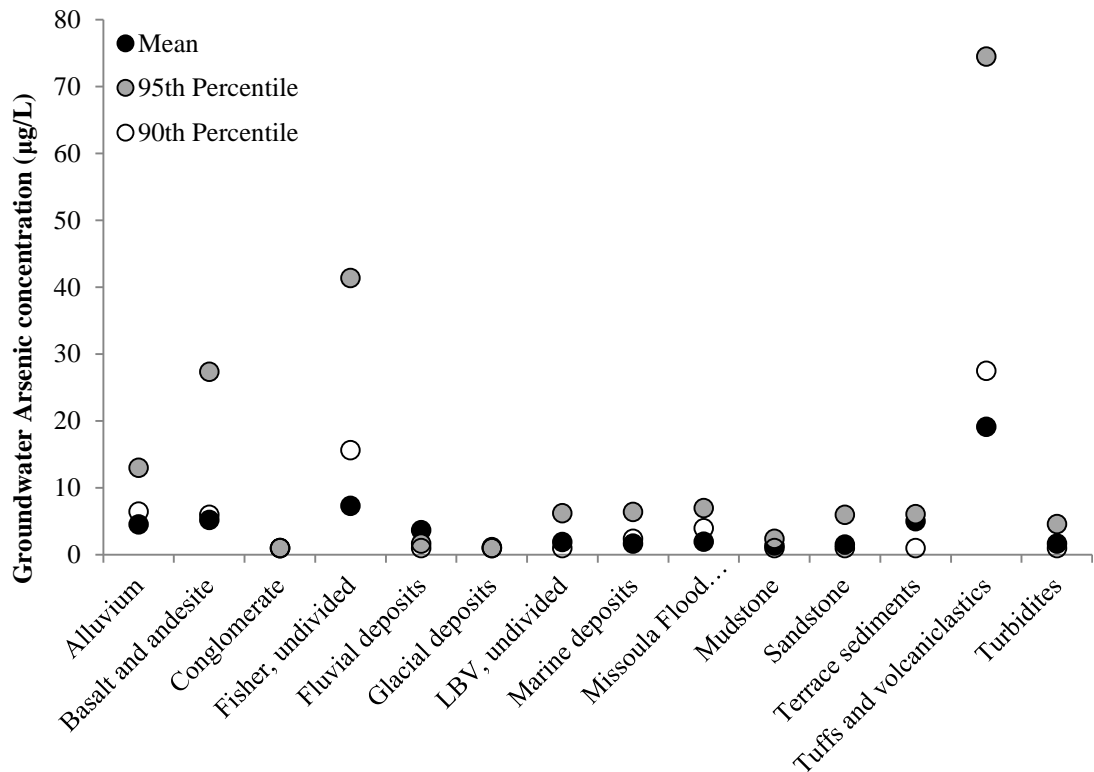
Figure 15: Groundwater arsenic concentration associated with major lithologies combined from geologic units mapped in the Willamette Valley. Data modified from Department of Environmental Quality, 2015; McClaughry et al., 2010.

Measurements of As in groundwater overlain by surficial units of tuffs and volcaniclastic lithology average 19 ppb, which is far greater than the other lithologies, which all average less than 10 ppb (Figure 15). Discrete points included in the tuff lithology group total 5% (n = 62) of examined data. The distribution of As groundwater

concentrations associated with surficial tuff lithologies are the highest included in the dataset, followed by Fisher, undivided lithologies.

Discussion

This study demonstrates that silicic volcanic tuffs are capable of producing leachate solutions with concentrations of arsenic above regulatory limits, at alkaline pH conditions produced naturally by the tuffs (pH 8-9) and with typical concentrations of P (10-100 μM P). Different alteration products, e.g. zeolites and clays, are potential host phases for As, which form as a result of devitrification and diagenetic alteration. Dissolution and/or desorption of As from these host phases results in concentrations of As significantly above the regulatory limit, which has significant implications for human health. Additionally, one volcaniclastic sample (BCw) demonstrates how weathering of pyroclastic deposits to sediment and subsequent sulfide alteration produces leachate solutions with highly toxic concentrations of As, up to 1000 μg/L.

Alteration Products

Tuffs display a variety of alteration products developed in the time since deposition. Glass is unstable at the surface and will devitrify during or post-emplacement (De' Gennaro et al., 1999; Vaniman et al., 2001). Devitrification textures identified include spherulites, axiolitic textures, and entirely felsitic groundmass (Table 4; Figure 8). Many of the devitrification textures were mostly or entirely replaced by sericite, which also occurs in veins and groundmass.

Alteration products identified by XRD analysis are primarily zeolites and clays. Formation of zeolites within these tuffs likely results from the hydrolysis of glass, which produces elevated pH, and/or the dissolution of glasses, as is the case for tuff units in the John Day formation, which correlate temporally with the Fisher Formation tuffs (Cotton, 2008; Retallack et al., 2004; Sheppard & Hay, 2001). Formation of clays may occur directly on glass surfaces and coat glass particles syn- or post-depositionally (De' Gennaro et al., 1999; Fuente et al., 2000; Gifkins & Allen, 2001). Location within a flow has been observed to influence alteration, such that lower portions of the flow tend to completely alter due to percolation of water (Sheppard & Hay, 2001). However, tuff units examined in this study do not typically have exposed contacts. Groundwater composition and primary tephra characteristics, i.e. crystallinity, zonation, original porosity and permeability, exert first-order controls on which zeolite or clay forms (Gifkins & Allen, 2001; Sheppard & Hay, 2001). Significant variation can occur in the composition of alteration products as a result of cation to hydrogen ion ration and high ionic activity (Sheppard & Hay, 2001).

Alteration products were identified in devitrified and glassy samples (Foster Dam). Some tuffs, despite being >30 Ma and containing substantial alteration products, retain preserved glassy components (e.g. Bond Creek and Willamette Flora tuffs). Given the extensive alteration of samples examined in this study and lack of multiple exposed outcrops within the same ash flow a unit, conclusions regarding the specific factors controlling composition of alteration product formation are beyond the scope of this study. The range of alteration indices (Table 3) indicates observed alteration is weak and regionally extensive, which suggests it is diagenetic in origin. Based on the observed

proximity of alteration products to glass shards, the partial or complete dissolution of glass is likely a precursor to formation of alteration products, and the constituents of the alteration products are likely entirely derived from original glass composition, as observed in other studies (e.g. de la Fuente, Cuadros, & Linares, 2002; Hawkins, 1981).

Solution chemistry and mobilization

Tuff samples examined in this study produce leachate solutions in response to increased pH and phosphate concentrations according to a variety of mobilization behaviors. Individual tuff units and their specific mobilization processes are discussed in more detail below.

Fox Hollow Tuff

Fox Hollow tuff samples examined in this study (FHb_1, FHb_2, and FHr) are devitrified, displaying a cryptocrystalline texture, although glass morphology is still apparent. FHb contains frequent spherulites replaced by sericite. Both samples contain sericite and FHb contains smectite.

FHb_1 produces solutions which increase in As along with other oxyanion forming elements, e.g. Cr and V, with increasing pH (Figure10a)

Solutions produced by FHr and FHb_1 under pH leachate conditions do not demonstrate correlation between As with Si nor Al, which indicates As is not released by dissolution of aluminosilicates (Table 8). FHb_1 releases up to six times more As than FHr under the same buffer conditions, possibly as a result of FHb_1 containing increased spherulites altered to sericite. During the phosphate mobilization and time series experiments, FHb_2 and FHr produce As in solutions at concentrations typically below 5

56

ppb. Release of other elements is not significantly elevated in those experiments, suggesting stability of host phases under the conditions tested.

The results of the pH experiments suggest FHb$_1$ releases As through desorption from a charged surface as a result of increased pH. Locally, the Fox Hollow outcrop sampled in this study displays significant differences among examined samples. Though both FHb$_1$ and FHr are devitrified, FHb$_1$ has more spherulites which are altered to sericite, quantified by a higher alteration index (Table 3). The spherulites may provide a nucleus for alteration of feldspar and quartz to sericite. Sericite, a fine-grained clay alteration product, may host As on positively charged corners and broken edges in contrast to negatively charged clay surfaces, primarily due to isomorphous substitution (Lin & Puls, 2000; Manning & Goldberg, 1997). These positively charged corners then subsequently release As with increasing pH due to deprotonation of charged surfaces or increased hydroxyl competition.

Tuff of Mohawk, Intracaldera Facies

The Mohawk tuffs (MK1, MK2) are pervasively devitrified, demonstrating a felsitic texture. In MK1, smectite and clinopyroxene occur as primary minerals, with amorphous oxides as a trace component. MK2 contains oxides as a secondary mineral with smectite and sericite as a trace mineral (Table 5).

Under increasing pH conditions, MK1 and MK2 produce solutions with increased As above pH 9 (Figure 10a). Although there are not sufficient data points for correlation, As in solutions produced by MK2 follow a pattern similar to that of Fe, Si, Al, Mn, V, and Zn with increasing pH. The values of these elements are substantially elevated and

increase more than fivefold fold with increased pH, which may indicate dissolution of aluminosilicates phases, e.g. sericite and smectite, and/or Fe oxhydroxides. Greatest increases occur for Fe and Al, which increase 14 and 12 times respectively. MK1 contains less than half the bulk As compared to MK2 and typically mobilizes less As by percent although it also mobilizes increased As into solution with increased pH. MK2 appears to release As as a result of colloidal transport, and MK1 does not release significant concentrations of As into solution. The higher alteration index of MK2 (Table 3) suggests more alteration products are present, which may host As on surficial species, making As more available to solution.

Both MK1 and MK2 release increased concentrations of As with increased addition of phosphate. MK1 increases from 4.8 ppb to 11.7 ppb, and MK2 increases from 10.7 ppb to 18.6 ppb. Correlation statistics demonstrate significant increases of Mg and Ca along with As in solutions produced by MK2 with increased P concentrations. Solutions produced by MK2 present positive correlation between concentrations of As with Na, Ca, Mg, and Pb.

MK2 was further examined in the time series, during which concentrations of As increased from 7 ppb to 52 and 58 ppb in the water only leachate and 0.1 mM phosphate. Other elements, most significantly Si, Al, Cr, Cu, Fe, Mg, Mn, Ni, Sr, V, and Zn, also increased by 20 to 30 times over the 196 hour experiment. The substantial increase and magnitude of these concentrations suggests colloids are formed as secondary precipitates in leachate solutions produced by MK2 over time, both in the presence of phosphate and in deionized water. MK2 has substantial oxide particles and alteration products sericite

and smectite, which may dissolve to form colloidal particles which release As into solution.

Tuff above Willamette Flora

The tuff above Willamette Flora unit, WF and WFw, is a small ash fall tuff exposed within a marine sedimentary sequence. The tuffs are incipiently devitrified, with axiolitic rims on glass particles still retained and visible in thin section. Both tuffs contain mordenite as a major component. The Willamette Flora tuffs are substantially oxidized, with large amorphous oxides and fine-grained oxides occurring in veins and groundmass. WFw is more oxidized and weathered, with more frequent and larger oxides.

During the pH experiments, both tuffs mobilize steadily increasing amounts of As into solution (Figure 10b). Leachate produced by the Willamette Flora tuffs appear clouded in the solution column even after centrifugation, and concentrations of As in solution correlate with several elements, including Si, Al, Fe, Mn, Mg, Pb, V, Zn, and Cr, which are measured in solution at exceptionally elevated concentrations (Appendix D). WFw produces solutions with greater concentrations of As compared with WF. The elevated concentrations of aluminosilicate-forming elements, which increase concurrent with As, suggests that the Willamette Flora tuffs mobilize As through the formation of colloids, potentially dissolved from mordenite, which was identified by XRD.

In the phosphate experiments, WF and WFw release increasing concentrations of As into solutions with the addition of 10 µM P and 1 mM P. At the highest concentration of phosphate examined, 100 mM P, As concentrations in solution decreases (Figure 11). Although the small number of experiments limits interpretation of correlation statistics,

59

several other elements experience a significant decrease in concentration along with As, including Cu, Fe, Al, Mg, Pb, V, Zn, and Si, in the 100 mM P experiment. This suggests that the Willamette Flora Tuff hosts As associated with colloidal particles, and extremely elevated concentrations of P produce secondary precipitates. WFw is more altered, as evidenced by the alteration index (Table 3) and may produce more colloids, which would result in the observed higher concentrations of As and associated elements.

Tuff of Foster Dam

The Foster Dam tuffs retain the greatest glass content, and contain significant amounts of heulandite, as well as minor amounts of mordenite and sericite. Generally, FD1 has less sericite observed in thin sections with increasing sericite content from FD1 to FD4. Differences in mineralogy were not quantifiable with XRD. FD4 has an increased alteration index compared to FD1-FD3, which may relate to its greater concentration of bulk As and increased concentrations of As mobilized into solution.

During the pH experiments, FD1, FD2, and FD3 release concentrations of As above the MRL only when buffered near pH 10. FD4 produces 8.4 µg/L of As when mixed with deionized water, and increases to 25.4 µg/L under pH 9 and pH 10 buffers, respectively (

c). Most other elements in leachate solution produced by FD4 do not increase in concentration with increased pH, except for V which forms similar oxyanions. This suggests FD4 mobilizes As into solution as pH increases due to surficial desorption from a host phase, which also releases V as an oxyanion.

Both Foster Dam tuffs examined in the phosphate experiments mobilize more As into solution with moderate to extreme concentrations of phosphate (1 mM and 100 mM P; Figure 7). The concentrations of most other elements do not increase in solution with addition of phosphate, except those of Sr, Mg, and Na which increase ~20 times with increasing phosphate. Concentrations of other elements, e.g. Al, Si, Mn, and Fe, either do not change significantly or decrease; in the case of Fe, concentrations in solution decrease from 2200 µg/L and 1200 µg/L in the water leachate experiment to 23 µg/L and 32 µg/L in the 100 mM P experiment for FD1 and FD4 respectively. This suggests these elements may form secondary precipitates due to increased ionic strength resulting from the addition of phosphate. The predominance of heulandite, which is an aluminosilicate series with Ca, Sr, and Ba as possible end member cations, is a potential source of the elevated concentrations observed for Sr, Mg, Na, and As. Breakdown of heulandite may result from cationic displacement caused by the K_2HPO_4 salt used to create the phosphate solutions. pH increases with the addition of phosphate as well, from pH = 6.6-6.7 when the Foster Dam samples are mixed with deionized water to 7.9-8.1 when mixed with 100 mM P solution, which may also induce dissolution (Cotton, 2008).

Mobilization of As from FD4 was further examined through the time series experiment, performed with deionized water and moderate concentrations of phosphate (0.1 mM as P; Figure 11). Concentrations of As mobilized to solution increase through the time series, particularly in the presence of phosphate: during the 0.1 mM P time series, As increased from 13.0 µg/L after 4 hours to 34.8 µg/L at 194 hours. The concentrations of nearly every other element increase 2-5 times steadily through the time

series in 194 hours, except Sr which increases in concentration in the first 50-72 hours followed by a decrease to nondetect. This suggests that dissolution of zeolites is controlling the mobility of these elements which are released into solution over time. The addition of phosphate increases ionic strength, which may contribute to dissolution over time.

Bond Creek

The Bond Creek tuffs include one volcaniclastic sample and one incipiently devitrified sample. BCg is incipiently devitrified, containing glass particles which retain a glassy interior and are rimmed with axiolitic intergrown fine-grained minerals, along with few spherulites altered to sericite. Clinoptilolite is a primary mineral, with zeolite and smectite identified as trace minerals. BCw is a volcaniclastic sandstone, with rounded grains of quartz and plagioclase, along with few spherulites and pumice fragments indicating proximal diagenesis and minimal alteration of the sediment. Sericite and sulfide phases are common in the groundmass and mineral cracks.

When mixed with buffers of increasing pH, BCg releases gradually increasing concentrations of As, which correlate positively with V and negatively with Mn, Mg, and Ca. The correlation with another oxyanion forming element, V as HVO_4^- or $H_2VO_4^-$, and lack of correlation with other elements suggests desorption from a charged surface as increased pH deprotonates the surface. Concentrations of As released from BCw increase drastically with increased pH, from 107 μg/L in deionized water, to 1100 μg/L when buffered with pH 10 solution. The concentrations of nearly every other element increases in solution along with As, most notably Cr and V, which increased tenfold.

Concentrations of Fe in solution increase from 6 mg/L to 30 mg/L. A sulfide was the most common As-bearing phase in SEM analysis and at pH 10, 30% of total As was released. Sulfide oxidation is a common mobilization method for As, and becomes unstable in oxidized environments (Smedley & Kinniburgh, 2002; Wang & Mulligan, 2008). The rate of dissolution of pyrite, the most commonly studied As-bearing sulfide, is described by the following equation (Williamson & Rimstidt, 1994):

$$R_{Pyrite} = 10^{-10.19}(O_{2(aq)})^{0.5}(H^+)^{-0.11}$$

Decreasing proton concentration would increase the rate of sulfide dissolution, and therefore increase As mobilized into solution, which follows experimental observations. The oxidation of ferrous iron is also implicated in increasing the rate of dissolution, although specific mechanisms remain unclear (Wang & Mulligan, 2008; Williamson & Rimstidt, 1994). The disparate increases in Fe compared to As, where As increases more significantly than Fe, indicates that As is preferentially hosted on surface species which are first to dissolve or release As and/or that some Fe reprecipitates, potentially as an iron oxyhydroxide species but does not remove As from solution (Williamson & Rimstidt, 1994). BCw demonstrates the potential for weakly altered volcanic sediments to produce readily mobilized As associated with sulfides.

Under increasing concentrations of phosphate, As released into solution produced by BCg increases substantially to 33 µg/L. Leachate experiments with increased concentrations of phosphate produce solutions with decreased concentrations of Fe, Si, and Al, and increased concentrations of Mg, Na, and Sr four to five times greater than in deionized water. This suggests P precipitates with other elements, and As mobilization

may be related to dissolution of clinoptilolite. Clinoptilolite is similar to heulandite, although clinoptilolite is observed to dissolve at higher pH compared with heulandite (Cotton, 2008). The correlation with Sr, Mg, and Na released into solution supports the role of dissolution of clinoptilolite. The decrease of Si and Al may be due to secondary precipitation of these elements due to increased ionic strength with the addition of phosphate or incongruent dissolution of clinoptilolite. Since clinoptilolite appears to dissolve at higher pH, As released during the pH experiments does not demonstrate the same pattern of increased element concentration.

During the time series, BCg mobilizes low amounts of As, ranging from 1.6 µg/L to a maximum value of 9.6 µg/L with 0.1 mM P after 72 hours. No other elements are released or increase in substantial amounts (i.e., greater than a twofold increase or decrease) except for Zn, which increases from 25 µg/L to 490 µg/L after 194 hours with 0.1 mM P, and Pb which increases from 4.72 to 15.92 after 72 hours with 0.1 mM P then decreases to 12.5 mM P in the subsequent analysis at 194 hours. Concentrations of Zn are typically controlled by adsorption onto clay minerals, Fe, Mn, or Al hydroxides, and organic matter (Smedley & Kinniburgh, 2002). This indicates that circumstances required to dissolve clinoptilolite or surficially desorb As were not achieved during the time series.

Low-As tuffs

Some tuffs did not mobilize significant amounts of As under any conditions presented in the study. These include both lithophysae samples, GHw and LDN, and two devitrified samples, SP and GHg. All four samples have bulk As concentrations similar to other tuffs, which mobilize As into solution (Table 5). SP and LDN contain trace

amounts of alteration products, smectite, sericite, and zeolite. GHg contains primary amounts of heulandite and no alteration products were identified in GHw. It initially appears that the lack of these alteration products may be related to the low mobilization of As. However, GHg does not release significant amounts of As, despite evidence of significant amounts of heulandite. Solutions produced by GHg which were buffered at elevated pH released 142 µg/L of V in the water leachate experiment and increased to 220 µg/L of V when buffered with pH 10 solution. It may be that vanadate anions occupy sites that are occupied by As in other tuffs. Minor differences in zeolite composition have been observed to result in significant changes in sorption behavior (Sheppard & Hay, 2001).

In summary, samples which exhibit surficial desorptive control on As mobility are FHb$_1$ and BCg under more extreme leachate conditions. Samples which exhibit dissolution control on As mobility include MK2, FD4, BCw, WF, and WFw. Of these, WF and WFw produce colloids under all leachate conditions examined, and MK2 appeared to produce colloids during the time series experiment.

Mineral control on As mobility

Alteration products, e.g. zeolites and clays, may serve as host phases for As. At increased pH or phosphate concentrations, these alteration products may dissolve or desorb As, producing concentrations which pose human health risks. Results of this study suggest that desorption tends to control As mobility in samples with primarily clay alteration products, and dissolution tends to control As mobility in samples with primarily zeolite alterations products.

Sorption activities to/from a charged surface are potentially operating in FHb$_1$, BCg, MK1, and MK2 under certain leachate conditions. Although specific sorption phases could not be identified, the most probable sorption sites are aluminosilicates or Fe and Mn oxyhydroxides (Dixit & Hering, 2003; Wilkie & Hering, 1996). Increased pH will desorb As through deprotonation and subsequent surface charge reversal, which is shown on a modeled desorption of As from hydrous ferric oxide surface as pH increases from 6-11 (Figure 16). The presence of 10 mM phosphate decreases the initial amount of sorbed As. Depending on the water chemistry conditions, host phases in BCg, MK1, and MK2 dissolve to produce elevated As in solution. WF and WFw produced As-bearing colloids under most experimental conditions examined, possibly dissolved from mordenite.

Arsenic anions are capable of sorbing to clay and zeolite surfaces which are altered by surface complexation, as demonstrated in the following equations, following Li, Beachner, McManama, & Hanlie (2007):

$$Z\text{-}X^- + H_2AsO_4^- = Z - H_2AsO_4 + X^-$$

$$2Z\text{-}X^- + HAsO_4^{2-} = Z_2 - HAsO_4 + 2X^-$$
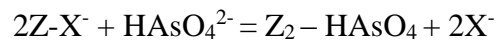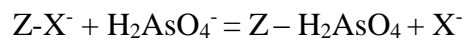
Where X represents a surficially bound anion, and Z represents a host phase, e.g. clay or zeolite. Natural zeolites have been experimentally determined to sorb As at circumneutral pH, owing to protonation of the surface creating positively charged sites onto which anionic As species can sorb (Šiljeg, Foglar, & Gudelj, 2012). Increased pH has varying effects on As mobilization due to minor differences in zeolite composition and surface complexes. Experimental sorption studies demonstrate that As desorbed from some clinoptilolites at increased pH, while others did not release As, which was

attributed to oxidation and subsequent resorption onto the zeolite surface (Elizalde-

González, Mattusch, Einicke, & Wennrich, 2001).
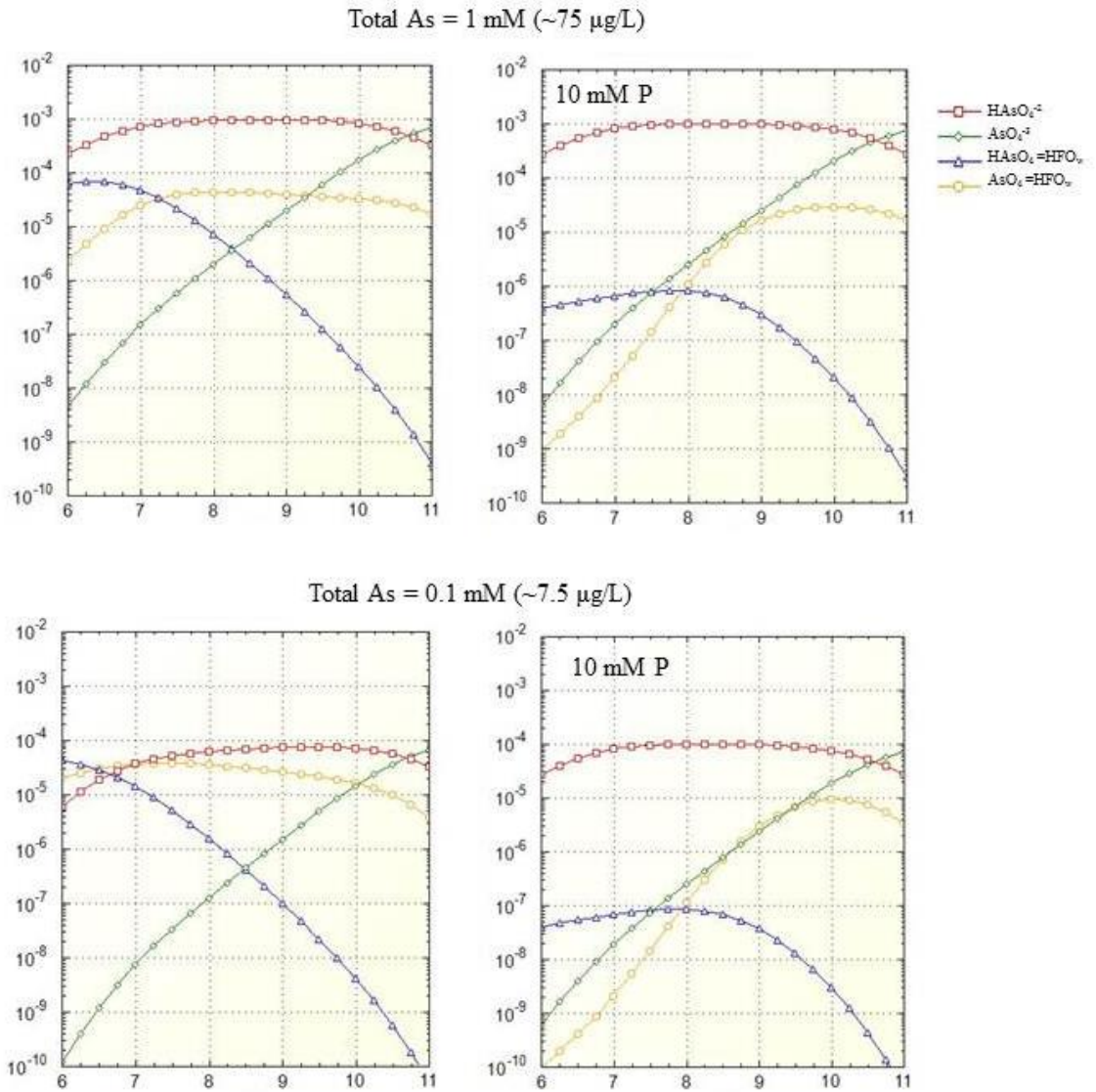
Figure 16: Concentrations of 1 mM and 0.1 mM As from hydrous ferric oxide under increasing pH and in the presence of 10 mM P modeled with PHREEQCi (Parkhurst & Appelo, 1999).

Colloidal behavior was observed in WF, WFw, and MK2. Many studies demonstrate the importance of colloids in transporting contaminants (de Jonge, Kjaergaard, & Moldrup, 2004; McCarthy & Zachara, 1989; Ryan & Elimelech, 1996; Schemel, Kimball, & Bencala, 2000) and potential for colloidal-transport of As anions (Puls & Powell, 1992). Colloid mobilization may occur as a result of increased pH, particularly when pH is raised above the point of zero charge of a surface, such that surface forces repel any colloidal particles attached (Ryan & Elimelech, 1996). The pH range examined in this study (7-10) coincides with the PZC of common oxyhydroxides and silicate minerals (Kosmulski, 2009). A combination of both the increased oxidation of As(V) above pH = 7-8 (Figure 1) and change in surface charges may release colloids capable of transporting surficially bound or incorporated As. Colloids may also form secondarily, following dissolution of alteration host phase of As.

A spike in As after 72 hours is observed in FD4 and MK2 which may be a result of diffusion controlled release of arsenic and increased ionic strength necessary to catalyze zeolite release or dissolution (Elizalde-González et al., 2001).

The production of zeolites and clays can occur during diagenetic or hydrothermal alteration. It is evident that if any hydrothermal alteration has occurred within these units, it is limited in extent given that glass morphology and volcanic particles are relatively preserved (De' Gennaro et al., 1999; Gifkins & Allen, 2001). The alteration indices calculated for samples in this study also suggest weak alteration, ranging from 17-43; alteration indices from 50-100 are indicative of hydrothermal alteration (Large et al., 2001). Sericite alteration, observed in several tuffs in this study, is interpreted to

represent early alteration of volcanic glass synchronous with regional burial and

compaction (e.g. Gifkins & Allen, 2001). The alteration represented is characterized by

locally complex distribution of alteration on a small scale (millimeters to centimeters)

which may have significant implications for As mobilization, as demonstrated by FHb_1,

FHb_2, and FHr. Between pairs of samples within units, the sample which mobilizes

greater As concentrations in solutions is consistently the more altered sample, evidenced

by mineralogy and alteration indices (Table 3; Table 5). Alteration type may also control

As mobilization behavior: samples which displayed surficial desorption behavior (FHb,

BCg) were composed of clay alteration products, and samples which displayed

dissolution and/or formation of colloids (WF, WFw, FD4) were more likely composed of

zeolite alteration products. MK2 and BCw are exceptions: MK2 contains significant

oxide particles, which may host As and dissolve under elevated pH and P conditions,

rather than the clay alteration products present. BCw contains detectable As in sulfide

phases (Figure 9), which preferentially host As, released upon oxidative dissolution.

Samples with no or trace alteration products, e.g. SP, LDN, and GHw do not release

significant As, even at elevated pH values (pH > 10). These mechanisms are summarized

in Figure 17. The geospatial analysis suggests that tuffs are influential in developing high

As groundwater in the Willamette Valley. The average As concentration for data points

located within surficial tuffs was 19 ppb, nearly double the regulatory limit, despite

comprising a small percentage of values examined (Figure 15). The overall distribution

of groundwater As values occurring within surficially mapped tuff lithologies was also

substantially greater than observed for other lithologies.
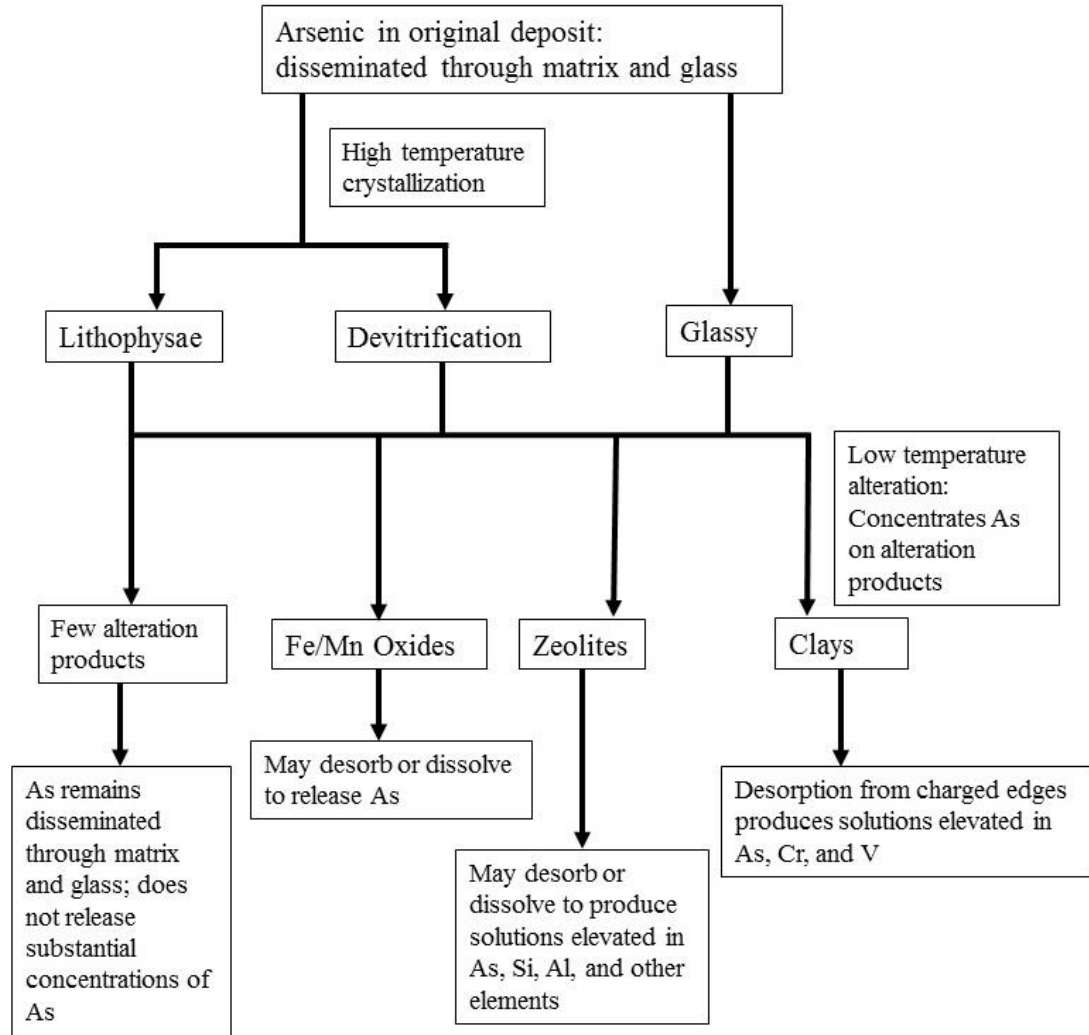
Figure 17: Summary diagram illustrating primary processes controlling As

Future Work

Collection of additional tuff samples, primarily from locations that displayed high variability, would allow for better definition of factors controlling As mobility. Future leachate studies should consider the possibility of colloids and filter leachate columns at different sizes to determine the size and mobility of colloids generate, and potentially analyze filtrate using WDS/EDS if resolution permits. Although groundwater analysis of

70

arsenic and distribution exists in the region, complete groundwater chemistry could be analyzed and modeled to determine how experimental leachate may serve as an example of groundwater conditions. The addition of a leachate experiment controlling redox state may also shed light on oxidative conditions which control As mobility.

Conclusions

This study demonstrates that silicic volcanic tuffs are capable of mobilizing As at concentrations above regulatory limits at pH conditions produced naturally by the tuffs (pH 8-9) and with moderate concentrations of P (10-100 μM). Alteration products, e.g. zeolites and clays, are interpreted to influence mobilization of As with significant implications for human health. Samples which do not contain these alteration products tend to produce concentrations of As below detection limit. Within a natural pH range produced by tuffs (pH 8-9), incipiently devitrified and devitrified tuffs are more likely to produce concentrations of As in leachate solutions above the regulatory limit. The process of devitrification allows for subsequent alteration to host phases, e.g. clays, zeolites, and amorphous oxides, which are susceptible to mobilization of As through dissolution and desorption processes. The type of alteration may influence As mobilization, in that tuffs containing more clays tend to mobilize As through surficial desorption, and tuffs containing more zeolites tend to mobilize As by dissolution or colloids. Additionally, one volcaniclastic sample (BCw) demonstrates how minor alteration to sediment and subsequent formation of As-bearing sulfide phases is capable of producing extremely elevated concentrations of As, up to 1000 μg/L, as a result of oxidative dissolution of the sulfides.

71

Geospatial analysis suggests the connection of mapped tuff units and elevated As in groundwater in the Willamette Valley. The results of this study suggest that this may relate to the capacity for tuffs to alter to host phases which mobilize As by alkaline pH and introduction of phosphate. Therefore, diagenetically altered tuffs within volcanic aquifers contain moderate concentrations of As likely associated with alteration products, clays and zeolites which are available to solution through surficial desorption, dissolution, and formation of colloids.

References

Aiuppa, A., D'Alessandro, W., Federico, C., Palumbo, B., & Valenza, M. (2003). The aquatic geochemistry of arsenic in volcanic groundwaters from southern Italy. *Applied Geochemistry*, *18*(9), 1283–1296. http://doi.org/10.1016/S0883-2927(03)00051-9

Bowell, R. J., Alpers, C. N., Jamieson, H. E., Nordstrom, D. K., & Majzlan, J. (2014). The Environmental Geochemistry of Arsenic: An Overview. In *Reviews in Mineralogy & Geochemistry, 79* (pp. 1–13).

Breitkreuz, C. (2013). Spherulites and lithophysae-200 years of investigation on high-temperature crystallization domains in silica-rich volcanic rocks. *Bulletin of Volcanology*, *75*, 1–16. http://doi.org/10.1007/s00445-013-0705-6

Camp, Vic. (2004). *How volcanoes work*. Project ALERT, [http://www.geology.sdsu.edu/how_volcanoes_work/]

Campbell, K. M., & Nordstrom, D. K. (2014). Arsenic speciation and sorption in natural environments. In *Reviews in Mineralogy & Geochemistry, 79* (pp. 185–216).

Casentini, B., Pettine, M., & Millero, F. J. (2010). Release of arsenic from volcanic rocks through interactions with inorganic anions and organic ligands. *Aquatic Geochemistry*, *16*(3), 373–393. http://doi.org/10.1007/s10498-010-9090-3

Cotton, A. (2008). Dissolution kinetics of clinoptilolite and heulandite in alkaline conditions. *Bioscience Horizons*, *1*(1), 38–43. http://doi.org/10.1093/biohorizons/hzn003

De Jonge, L. W., Kjaergaard, C., & Moldrup, P. (2004). Colloids and colloid-facilitated transport of contaminants in soils. *Vadose Zone J.*, *3*, 321–325. http://doi.org/10.2136/vzj2004.0321

De la Fuente, S., Cuadros, J., & Linares, J. (2002). Early stages of volcanic tuff alteration in hydrothermal experiments: Formation of mixed-layer illite-smectite. *Clays and Clay Minerals*, *50*(2), 578–590.

De' Gennaro, M., Incoronato, a., Mastrolorenzo, G., Adabbo, M., & Spina, G. (1999). Depositional mechanisms and alteration processes in different types of pyroclastic deposits from Campi Flegrei volcanic field (Southern Italy). *Journal of Volcanology and Geothermal Research*, *91*(2-4), 303–320.

Department of Environmental Quality, P. N. W. E. (2015). Real Estate Transaction 2003 Database. Retrieved January 1, 2015, from http://deq12.deq.state.or.us/pnwTest

Dixit, S., & Hering, J. (2003). Comparison of arsenic (V) and arsenic (III) sorption onto iron oxide minerals: Implications for arsenic mobility. *Environmental Science & Technology*, *37*(18), 4182–4189. Retrieved from http://pubs.acs.org/doi/abs/10.1021/es030309t

Elizalde-González, M. P., Mattusch, J., Einicke, W.-D., & Wennrich, R. (2001). Sorption on natural solids for arsenic removal. *Chemical Engineering Journal*, *81*, 187–195. http://doi.org/10.1016/S1385-8947(00)00201-1

Fuente, S. de la, Cuadros, J., Fiore, S., & Linares, J. (2000). Electron Microscopy Study of Volcanic Tuff Alteration to Illite-Smectite under Hydrothermal Conditions. *Clays and Clay Minerals*, *48*(3), 339–350.

Gifkins, C., & Allen, R. L. (2001). Textural and Chemical Characteristics of Diagenetic and Hydrothermal Alteration in Glassy Volcanic Rocks : Examples from the Mount Read Volcanics , Tasmania. *Economic Geology*, *96*, 973–1002 pp. http://doi.org/10.2113/gsecongeo.96.5.973

Goldblatt, E. L., Van Denburgh, A. S., & Marsland, R. A. (1963). The unusual and widespread occurrence of arsenic in well waters of Lane County, Oregon. *Lane County Health Department Monograph, Eugene, Oregon*.

Hawkins, D. B. (1981). Kinetics of Glass Dissolution and Zeolite Formation under Hydrothermal Conditions. *Clays and Clay Minerals, 29*(5), 331–340. http://doi.org/10.1346/CCMN.1981.0290503

Hering, J. G., & Kneebone, P. E. (2002). Biogeochemical controls on arsenic occurrence and mobility in water supplies. In *Environmental chemistry of arsenic* (pp. 183–215).

Hinkle, S., & Polette, D. (1999). *Arsenic in ground water of the Willamette Basin, Oregon*. Retrieved from http://ir.library.oregonstate.edu/jspui/handle/1957/5064

Inskeep, W. P., McDermott, T. R., & Fendorf, S. (2002). Arsenic(V)/(III) cycling in soils and natural waters: Chemical and microbiological processes. In *Environmental chemistry of arsenic* (pp. 183–215).

Ishikawa, Y., Sawahuchi, T., Iwaya, S., & Horiuchi, M. (1976). Delineation of prospecting targets for Kuroko deposits based on modes of volcanism of underlying dacite and alteration halos. *Mining Geology*, *26*, 105–117.

Janoušek, V., Farrow, C. M., & Erban, V. (2006). Interpretation of whole-rock geochemical data in igneous geochemistry: Introducing Geochemical Data Toolkit (GCDkit). *Journal of Petrology*, *47*(6), 1255–1259. http://doi.org/10.1093/petrology/egl013

Johannesson, K. H., & Tang, J. (2009). Conservative behavior of arsenic and other oxyanion-forming trace elements in an oxic groundwater flow system. *Journal of Hydrology*, *378*(1-2), 13–28. http://doi.org/10.1016/j.jhydrol.2009.09.003

Kocar, B. D., & Fendorf, S. (2009). Thermodynamic Constraints on Reductive Reactions Influencing the Biogeochemistry of Arsenic in Soils and Sediments. *Environmental Science & Technology*, *43*(13), 4871–4877.

Kosmulski, M. (2009). The pH dependent surface charging and points of zero charge. VI. Update. *Journal of Colloid and Interface Science*, *439-448*, 209–212. http://doi.org/10.1016/j.jcis.2014.02.036

Kreidie, N., Armiento, G., Cibin, G., Cinque, G., Crovato, C., Nardi, E., … Mottana, A. (2011). An integrated geochemical and mineralogical approach for the evaluation of arsenic mobility in mining soils. *Journal of Soils and Sediments*, *11*(1), 37–52. http://doi.org/10.1007/s11368-010-0274-7

Large, R. R., Gemmell, J. B., Paulick, H., & Huston, D. L. (2001). The alteration box plot—A simple approach to understanding the relationship between alteration mineralogy and lithogeochemistry associated with volcanic-hosted massive sulfide deposits. *Economic Geology*, *96*(2), 957–971.

Li, Z., Beachner, R., McManama, Z., & Hanlie, H. (2007). Sorption of arsenic by surfactant-modified zeolite and kaolinite. *Microporous and Mesoporous Materials*, *105*, 291–297. http://doi.org/10.1016/j.micromeso.2007.03.038

Lin, R., & Puls, R. W. (2000). Adsorption, desorption and oxidation of arsenic affected by clay minerals and aging process: RN - Environ. Geology, v. 39, p. 753-759., *39*(May).

Mahlknecht, J., Steinich, B., & Navarro de Leon, I. (2004). Groundwater chemistry and mass transfers in the Independence aquifer, central Mexico, by using multivariate statistics and mass-balance models. *Environmental Geology*, *45*(6), 781–795. http://doi.org/10.1007/s00254-003-0938-3

Majzlan, J., Drahota, P., & Filippi, M. (2014). Parageneses and crystal chemistry of arsenic minerals. In *Reviews in Mineralogy & Geochemistry, 79* (pp. 17–184).

Mambo, V. S., & Yoshida, M. (1993). Behavior of arsenic in volcanic gases. *Geochemical Journal*, *27*, 351–359. http://doi.org/10.2343/geochemj.27.351

Manning, B. A., & Goldberg, S. (1997). Adsorption and Stability of Arsenic (III) at the Clay Mineral - Water Interface. *Environmental Science & Technology*, *31*(7), 2005–2011.

Mazziotti-Tagliani, S., Angelone, M., Armiento, G., Pacifico, R., Cremisini, C., & Gianfagna, a. (2011). Arsenic and fluorine in the Etnean volcanics from Biancavilla, Sicily, Italy: environmental implications. *Environmental Earth Sciences*, *66*(2), 561–572. http://doi.org/10.1007/s12665-011-1265-8

McCarthy, J., & Zachara, J. (1989). Subsurface transport of contaminants. *Environmental Science & Technology*, *23*, 496–502. http://doi.org/10.1021/es00063a001

McClaughry, J. D., Wiley, T. J., Ferns, M. L., & Madin, I. P. (2010). Digital Geologic Map of the Southern Willamette Valley, Benton, Lane, Linn, Marion, and Polk Counties, Oregon. *DOGAMI Open-File Report O-10-03*.

Morton, W., Starr, G., Pohl, D., & Stoner, J. (1976). Skin cancer and water arsenic in Lane County, Oregon. *Cancer*, *37*(5), 2523–2532. Retrieved from http://onlinelibrary.wiley.com/doi/10.1002/1097-0142(197605)37:5%3C2523::AID-CNCR2820370545%3E3.0.CO;2-B/abstract

Nadakavukaren, J. J., Ingermann, R. L., Jeddeloh, G., & Falkowski, S. J. (1984). Seasonal Variation of Arsenic Concentration in Well Water in Lane County, Oregon. *Bulletin of Environmental Contamination & Toxicology*, *33*, 264–269.

Neupane, G., Donahoe, R. J., & Arai, Y. (2014). Kinetics of competitive adsorption/desorption of arsenate and phosphate at the ferrihydrite–water interface. *Chemical Geology*, *368*, 31–38. http://doi.org/10.1016/j.chemgeo.2013.12.020

Nicolli, H. B., Suriano, J. M., Gomez Peral, M. a., Ferpozzi, L. H., & Baleani, O. a. (1989). Groundwater contamination with arsenic and other trace elements in an area of the pampa, province of Cordoba, Argentina. *Environmental Geology and Water Sciences*, *14*(1), 3–16.

Nicolli, H., Bundschuh, J., & García, J. (2010). Sources and controls for the mobility of arsenic in oxidizing groundwaters from loess-type sediments in arid/semi-arid dry climates – Evidence from the Chaco–Pampean plain (Argentina). *Water Research*, *44*(19), 5589–5604. http://doi.org/10.1016/j.watres.2010.09.029

Noble, D. (1970). Loss of sodium from crystallized comendite welded tuffs of the Miocene Grouse Canyon Member of the Belted Range Tuff, Nevada. *Geological Society of America Bulletin*, (September), 2677–2688. Retrieved from http://gsabulletin.gsapubs.org/content/81/9/2677.short

Onishi, H. and E. B. S. (1955). Geochemistry of arsenic. *Geochimica et Cosmochimica Acta*, *7*, 1–33.

Oregon Water Science Center (OWSC), U. S. G. S. (2013). Oregon Water Use Program. Retrieved from http://or.water.usgs.gov/projs_dir/or007/or007.html

Pearce, J. a. (1983). Role of the sub-continental lithosphere in magma genesis at active continental margin. In C. J. Hawkesworth & M. J. Norry (Eds.), *Continental basalts and mantle senoliths* (pp. 230–249). Shiva.

Pedersen, H. D., Postma, D., & Jakobsen, R. (2006). Release of arsenic associated with the reduction and transformation of iron oxides. *Geochimica et Cosmochimica Acta*, *70*(16), 4116–4129. http://doi.org/10.1016/j.gca.2006.06.1370

Pokrovski, G. S., Zakirov, I. V., Roux, J., Testemale, D., Hazemann, J. L., Bychkov, A. Y., & Golikova, G. V. (2002). Experimental study of arsenic speciation in vapor phase to 500C: Implications for As transport and fractionation in low-density crustal fluids and volcanic gases. *Geochimica et Cosmochimica Acta*, *66*(19), 3453–3480. http://doi.org/10.1016/S0016-7037(02)00946-8

Population Research Center, P. S. U. C. of U. & P. A. (2013). Population estimates. Retrieved from http://www.pdx.edu/prc/population-estimates

Puls, R. W., & Powell, R. M. (1992). Transport of inorganic colloids through natural aquifer material: implications for contaminant transport. *Environmental Science & Technology*, *26*, 614–621. http://doi.org/10.1021/es00027a027

Rango, T., Vengosh, A., Dwyer, G., & Bianchini, G. (2013). Mobilization of arsenic and other naturally occurring contaminants in groundwater of the main ethiopian rift aquifers. *Water Research*, *47*(15), 5801–5818. http://doi.org/10.1016/j.watres.2013.07.002

Raymahashay, B. C., & Khare, A. S. (2003). The arsenic cycle in Late Quaternary fluvial sediments : Mineralogical considerations. *Current Science*, *84*(8), 8–10.

Retallack, G. J., Orr, W. N., Prothero, D. R., Duncan, R. a., Kester, P. R., & Ambers, C. P. (2004). Eocene-Oligocene extinction and paleoclimatic change near Eugene, Oregon. *Bulletin of the Geological Society of America*, *116*(7-8), 817–839. http://doi.org/10.1130/B25281.1

Ross, C. S., & Smith, R. L. (1960). Ash-flow tuffs: their origin, geologic relations and identification. *Geological Survey Professional Paper*, *366*, 1–50. Retrieved from http://scholar.google.com/scholar?hl=en&btnG=Search&q=intitle:Ash-Flow+Tuffs+:+Their+Origin+Geologic+Relations+and+Identification#0

Rowe, M. C., Ellis, B. S., & Lindeberg, a. (2012). Quantifying crystallization and devitrification of rhyolites by means of X-ray diffraction and electron microprobe analysis. *American Mineralogist*, *97*, 1685–1699. http://doi.org/10.2138/am.2012.4006

Rudnick, R. L., & Gao, S. (2003). The composition of the continental crust. *Treatise on Geochemistry*, *3*, 1–64.

Ryan, J. N., & Elimelech, M. (1996). Colloid mobilization and transport in groundwater. *Colloids and Surfaces A: Physicochemical and Engineering Aspects*, *107*(November 2015), 1–56. http://doi.org/10.1016/0927-7757(95)03384-X

Savoie, C. (2013). *Arsenic Mobility and Compositional Variability in High-Silica Ash Flow Tuffs*. Portland State University.

Schemel, L. E., Kimball, B. a, & Bencala, K. E. (2000). Colloid formation and metal transport through two mixing zones affected by acid mine drainage near Silverton, Colorado. *Applied Geochemistry*, *15*, 1003–1018. http://doi.org/10.1016/S0883-2927(99)00104-3

Scott, R. B. (1971). Alkali Exchange during Devitrification and Hydration of Glasses in Ignimbrite Cooling Units. *The Journal of Geology*, *79*(1), 100–110. http://doi.org/10.1086/627591

Sheppard, R. a., & Hay, R. L. (2001). Formation of Zeolites in Open Hydrologic Systems. *Reviews in Mineralogy and Geochemistry*, *45*, 261–275. http://doi.org/10.2138/rmg.2001.45.8

Shuichi, T., Ito, Y., & Hashimoto, S. (2005). The leaching characteristic of heavy metals from altered volcanic rocks of several grain sizes in Hokkaido, northern Japano. In *Geoline* (pp. 23–26). Retrieved from http://www.geotech-fr.org/sites/default/files/congres/geoline/GEOLINE2005 S12 pp 1-4 Tamoto.pdf

Šiljeg, M., Foglar, L., & Gudelj, I. (2012). The removal of arsenic from water with natural and modified clinoptilolite. *Chemistry and Ecology*, *28*(November), 75–87. http://doi.org/10.1080/02757540.2011.619531

Smedley, P., & Kinniburgh, D. (2002). A review of the source, behaviour and distribution of arsenic in natural waters. *Applied Geochemistry*, *17*(5), 517–568. Retrieved from http://www.sciencedirect.com/science/article/pii/S0883292702000185

Smith, R. L. (1980). Zones and Zonal Variations in Welded Ash Flows Zones and Zonal Variations in Welded Ash Flows. *USGS Professional Paper*.

Stimac, J., Hickmott, D., Abell, R., Larocque, A. C. L., Broxton, D., Gardner, J., … Gauerke, E. (1996). Redistribution of Pb and other volatile trace metals during eruption, devitrification, and vapor-phase crystallization of the Bandelier Tuff, New Mexico. *Journal of Volcanology and Geothermal Research*, *73*(3-4), 245–266.

Streck, M. J. (1994). *Volcanology and Petrology of the Rattlesnake Ash-Flow Tuff, Eastern Oregon*. Oregon State University.

Symonds, R. B., Reed, M. H., & Rose, W. I. (1992). Origin, speciation, and fluxes of trace-element gases at Augustine volcano, Alaska: Insights into magma degassing and fumarolic processes. *Geochimica et Cosmochimica Acta*, *56*(2), 633–657. http://doi.org/10.1016/0016-7037(92)90087-Y

Tabelin, C. B., Hashimoto, A., Igarashi, T., & Yoneda, T. (2014). Leaching of boron, arsenic and selenium from sedimentary rocks: I. Effects of contact time, mixing speed and liquid-to-solid ratio. *Science of the Total Environment*, *472*, 620–629. http://doi.org/10.1016/j.scitotenv.2013.11.006

Tang, J., & Johannesson, K. H. (2010). Ligand extraction of rare earth elements from aquifer sediments: Implications for rare earth element complexation with organic matter in natural waters. *Geochimica et Cosmochimica Acta*, *74*(23), 6690–6705. http://doi.org/10.1016/j.gca.2010.08.028

Twarakavi, N. K. C., & Kaluarachchi, J. J. (2006). Arsenic in the shallow ground waters of conterminous United States: Assessment, health risks, and costs for MCL compliance. *Journal of the American Water Resources Association*, *42*(2), 275–294.

Vaniman, D. T., Chipera, S. J., Bish, D. L., Carey, J. W., & Levy, S. S. (2001). Quantification of unsaturated-zone alteration and cation exchange in zeolitized tuffs at Yucca Mountain, Nevada, USA. *Geochimica et Cosmochimica Acta*, *65*(20), 3409–3433. http://doi.org/10.1016/S0016-7037(01)00682-2

Vinson, D. S., Mcintosh, J. C., Dwyer, G. S., & Vengosh, A. (2011). Arsenic and other oxyanion-forming trace elements in an alluvial basin aquifer: Evaluating sources and mobilization by isotopic tracers (Sr, B, S, O, H, Ra). *Applied Geochemistry*, *26*(8), 1364–1376. http://doi.org/10.1016/j.apgeochem.2011.05.010

Wang, S., & Mulligan, C. N. (2006). Occurrence of arsenic contamination in Canada: Sources, behavior and distribution. *Science of the Total Environment*, *366*(2-3), 701–721. http://doi.org/10.1016/j.scitotenv.2005.09.005

Wang, S., & Mulligan, C. N. (2008, August). Speciation and surface structure of inorganic arsenic in solid phases: A review. *Environment International*. http://doi.org/10.1016/j.envint.2007.11.005

Welch, A. H., Lico, M. S., & Hughes, J. L. (1988). Arsenic in Ground Water of the Western United States. *Ground Water*, *23*(3), 333–347.

Welch, A. H., Westjohn, D. B., Helsel, D. R., & Wanty, R. B. (2000). Arsenic in Ground Water of the United States: Occurrence and Geochemistry. *Ground Water*, *38*(4), 589–604.

Whanger, P. D., Weswig, P. H., & Stoner, J. C. (1977). Arsenic levels in Oregon waters. *Environmental Health Perspectives*, *Vol.19*(August), 139–143.

Wilkie, J. a., & Hering, J. G. (1996). Adsorption of arsenic onto hydrous ferric oxide: Effects of adsorbate/adsorbent ratios and co-occurring solutes. *Colloids and Surfaces A: Physicochemical and Engineering Aspects*, *107*, 97–110. http://doi.org/10.1016/0927-7757(95)03368-8

Williamson, M. a., & Rimstidt, J. D. (1994). The kinetics and electrochemical rate-determining step of aqueous pyrite oxidation. *Geochimica et Cosmochimica Acta*, *58*(24), 5443–5454. http://doi.org/10.1016/0016-7037(94)90241-0

Wolfsberg, K., Bayhurst, B. P., Crowe, B. M., Daniels, W. R., Erdal, B. R., Lawrence, F. O., … Smyth, J. R. (1979). *Sorption-Desorption Studies on Tuff: I. Initial studies with samples from J-13 Drill Site, Jackass Flats, Nevada* (pp. 1–54).

Xu, W., Wang, H., Wu, K., Liu, R., Wenxin, G., & Qu, J. (2012). Arsenic Desorption from Ferric and Manganese Binary Oxide by Competitive Anions: Significance of pH. *Water Environment Research*, *84*(6), 521–528.

Appendix A: ICP Operating conditions

Operating Condition	Date of Analysis								
	11/24/2014	9/24/2014	8/11/2015	7/23/2014	7/18/2014	6/5/2015	4/23/2015	7/9/2015	6/19/2015
Power (kW)	1.3	1.3	1.35	1.3	1.25	1.25	1.3	1.35	1.35
Replicate read time	45	45	45	40	45	45	40	45	45
Instrument stabilization delay	20	20	20	20	20	20	20	20	20
Sample uptake delay	25	25	25	25	25	25	25	25	25
Max rinse	60	60	60	60	60	60	60	60	60
Number of replicates	3	3	3	3	3	3	3	3	3
PolyBoost	On	On	On	On	On	On	On	On	On
Plasma	15 L/min								
Auxillary	1.5 L/min								
Nebulizer	0.75 L/min								

Appendix C: Quality control/quality assurance data

Date of analysis: 5/30/2014

	IDL1	IDL2	IDL3	IDL4	IDL5	IDL6	IDL7	Standard Deviation	IDL	MRL
Al 236.705	6.0	5.5	8.4	4.1	5.5	7.1	6.2	1.4	4.1	13.7
Al 237.312	7.2	6.8	7.2	6.2	6.6	7.3	6.5	0.4	1.3	4.2
As 188.980	7.3	7.5	9.3	7.9	7.1	7.2	8.4	0.8	2.4	8.1
As 193.696	8.2	7.2	7.1	7.1	7.8	7.6	6.9	0.5	1.4	4.8
Ba 233.527	6.3	6.1	6.1	6.1	6.1	6.1	6.1	0.1	0.2	0.6
Ba 455.403	7.3	7.0	7.0	7.1	7.1	7.0	7.1	0.1	0.3	0.9
Be 249.473	7.3	8.0	7.5	7.2	7.2	7.1	7.1	0.3	1.0	3.3
Be 313.042	7.1	7.0	6.9	7.0	7.1	7.0	7.0	0.1	0.2	0.5
Ca 317.933	6.0	9.6	5.4	5.2	5.2	5.3	5.1	1.6	4.9	16
Ca 396.847	2.3	6.2	1.5	1.4	1.3	1.5	1.2	1.8	5.4	18
Co 228.615	6.6	6.5	6.4	6.5	6.5	6.5	6.4	0.1	0.3	0.9
Cr 267.716	6.9	6.9	6.8	6.7	6.8	6.7	6.7	0.1	0.3	1.0
Cu 327.395	6.8	6.6	6.7	6.7	6.8	6.8	6.7	0.1	0.2	0.6
Fe 238.204	5.4	6.0	5.4	5.6	5.4	5.5	5.0	0.3	1.0	3.2
Fe 258.588	6.5	7.1	6.2	6.0	6.3	6.2	5.6	0.5	1.4	4.5
Fe 259.940	6.1	6.3	6.2	6.1	6.2	6.2	5.7	0.2	0.6	2.0
K 766.491	44	44	42	42	45	41	41	1.5	4.4	15
Mg 279.078	5.8	5.9	5.7	5.0	6.4	5.2	5.4	0.5	1.4	4.5
Mn 260.568	6.5	6.4	6.3	6.4	6.5	6.4	6.4	0.1	0.2	0.7
Ni 231.604	6.4	6.5	6.2	6.4	6.2	6.1	6.4	0.2	0.5	1.6
P 177.434	53	52	52	52	52	52	51	0.6	1.9	6.4
Pb 220.353	5.9	6.0	5.7	6.3	5.8	5.3	5.6	0.3	0.9	3.0
Si 185.005	36	41	38	37	72	42	40	13	38	125
Si 250.690	41	43	41	41	72	43	38	12	35	117
Sr 407.771	7.3	7.1	7.0	7.1	7.2	7.1	7.1	0.1	0.2	0.7
V 311.837	6.2	6.2	6.1	6.1	6.1	6.1	6.0	0.1	0.2	0.7
Zn 202.548	4.9	4.5	4.2	4.2	4.2	4.1	4.0	0.3	0.9	3.1
Zn 206.200	4.1	3.7	3.5	3.7	3.4	3.4	3.3	0.3	0.9	2.8

Date of analysis: 6/6/2015

	IDL1	IDL2	IDL3	IDL4	IDL5	IDL6	IDL7	IDL8	IDL9	IDL10	Standard Deviation	IDL	MRL
Al 236.705	15	14	13	14	11	14	13	15	13	13	1.1	3.4	11
Al 237.312	4.8	7.5	5.4	6.5	8.3	7.4	6.8	7.8	6.1	6.4	0.8	2.4	8.1
As 188.980	6.4	5.8	5.9	6.6	6.7	6.5	6.2	7.4	6.2	7.0	0.5	1.5	4.9
As 193.696	8.0	7.6	7.8	8.2	8.4	8.6	7.6	8.1	8.2	8.4	0.4	1.1	3.5
Ba 233.527	7.1	7.1	7.0	7.0	7.0	7.0	7.0	7.0	7.0	7.0	0.0	0.1	0.3
Ba 455.403	7.3	7.3	7.3	7.3	7.3	7.3	7.3	7.3	7.3	7.3	0.0	0.1	0.2
Be 249.473	7.0	6.8	7.0	6.7	6.9	7.1	7.2	6.7	6.7	6.9	0.2	0.6	1.8
Be 313.042	7.0	7.0	7.0	7.0	7.0	7.0	7.0	7.0	7.0	7.0	0.0	0.1	0.2
Ca 317.933	7.9	7.7	7.8	7.7	8.5	8.0	11	8.6	8.4	7.7	0.9	2.7	9.0
Co 228.615	7.0	7.0	7.0	6.9	7.0	6.9	6.9	7.0	7.0	7.0	0.0	0.1	0.4
Co 237.863	6.9	7.0	7.0	6.9	6.9	7.2	6.9	6.9	7.2	7.1	0.1	0.4	1.3
Cr 267.716	7.2	7.2	7.3	7.1	7.3	7.2	7.2	7.2	7.3	7.3	0.1	0.2	0.5
Cu 327.395	7.2	7.2	7.4	7.2	7.3	7.1	7.2	7.4	7.3	7.2	0.1	0.3	0.9
Fe 238.204	8.8	8.7	8.7	8.8	9.6	9.1	8.8	9.0	9.4	9.1	0.3	0.9	3.2
Fe 258.588	9.5	9.5	9.6	9.5	11	9.8	9.6	10.0	9.9	9.7	0.3	0.9	3.1
Fe 259.940	7.5	7.4	7.4	7.5	8.5	7.8	7.4	7.7	7.8	7.7	0.3	1.0	3.4
Mg 279.078	32	32	32	32	32	32	33	33	33	32	0.4	1.3	4.4
Mg 383.829	5.3	6.0	6.3	6.0	6.8	6.1	6.2	6.0	5.4	6.7	0.5	1.4	4.7
Mn 260.568	6.8	6.7	6.8	6.8	6.8	6.7	6.8	6.8	6.8	6.7	0.0	0.1	0.3
Mn 261.020	9.9	10	10	8.9	9.7	9.5	9.9	9.6	10	11	0.6	1.9	6.4
Na 588.995	21	21	20	22	22	20	21	21	22	21	0.6	1.7	5.5
Na 589.592	17	17	17	17	17	17	17	17	17	17	0.2	0.5	1.6
Ni 231.604	6.9	6.9	6.9	7.1	6.9	7.0	7.0	7.0	6.8	7.1	0.1	0.2	0.7
Pb 220.353	7.6	7.4	6.9	7.4	7.5	7.5	7.1	7.4	7.3	7.4	0.2	0.6	2.1
Si 185.005	7.0	7.3	7.8	7.8	6.9	7.6	7.2	7.8	7.6	7.5	0.3	1.0	3.4
Si 250.690	37	36	35	32	36	33	31	34	50	34	5.2	16	52
Sr 407.771	7.5	7.3	7.3	7.2	7.6	7.8	7.3	7.0	7.3	7.2	0.2	0.7	2.4
Sr 460.733	6.7	6.6	6.7	6.8	6.6	6.7	6.6	6.6	6.7	6.7	0.1	0.2	0.6
V 311.837	7.4	7.9	7.1	7.3	7.1	7.7	7.7	7.4	7.5	7.2	0.3	0.8	2.8
Zn 202.548	6.8	6.7	6.8	6.8	7.0	6.8	6.7	6.8	6.7	6.7	0.1	0.3	1.0
Zn 206.200	6.6	6.7	6.7	6.6	7.0	6.8	6.6	6.8	6.6	6.6	0.1	0.4	1.3

Date of analysis		Al 237.312	As 193.696	Ca 317.933	Cr 267.716	Cu 327.395	Fe 238.204	K 766.491	Mg 279.078	Mn 260.568	Na 589.592	Ni 231.604	Pb 220.353	Si 185.005	Sr 407.771	V 311.837	Zn 202.548
5/30/2014	QC blank	1.5	0.7	2.6	0.3	ND	0.2	2.0	ND	ND	--	0.1	ND	7.5	0.0	ND	ND
	QC1a	38.5	39.9	42.5	40.5	40.5	39.0	162.8	38.6	39.9	--	40.0	39.6	203.7	41.0	39.4	38.2
	QC2a	205.0	208.5	202.8	205.9	209.3	205.7	911.9	203.7	204.8	--	204.9	206.0	1041.3	206.2	207.0	212.2
	QC1b	42.5	44.7	44.4	42.5	44.2	41.3	180.3	41.0	42.0	--	41.9	42.3	223.4	44.2	42.4	39.6
	QC2b	216.6	222.7	204.3	205.8	219.3	207.5	954.8	203.9	207.4	--	206.9	209.4	1108.8	214.2	212.3	204.5
	QC1c	46.7	48.6	42.4	43.8	47.0	42.2	224.0	42.1	42.6	--	43.2	42.3	243.3	46.8	44.0	41.9
	QC2c	229.2	238.5	212.8	215.5	235.9	215.8	1017.7	211.2	212.7	--	213.1	217.5	1196.1	228.8	223.8	212.1
	QC1 = 40 µg/L (K, Si = 200 µg/L); QC2 = 200 µg/L (K, Si = 1000 µg/L)																
7/23/2014	QC blank	1.0	ND	ND	0.0	0.6	0.2	10.9	ND	0.2	17.6	0.0	ND	71.8	0.0	2.3	1.3
	QC1a	19.4	18.1	19.7	18.9	19.2	18.8	93.9	13.1	18.7	33.4	18.9	19.4	145.7	17.9	19.6	19.4
	QC2a	203.1	199.5	202.8	198.1	201.5	203.1	1025.1	203.1	197.5	188.5	206.6	201.6	987.8	188.6	199.1	202.1
	QC2b	204.4	203.7	207.0	202.9	208.7	205.1	1054.7	205.1	198.8	194.3	206.5	203.9	998.7	194.4	203.8	202.6
	QC1 = 20 µg/L (K, Si = 100 µg/L); QC2 = 200 µg/L (K, Si = 1000 µg/L)																
9/24/2014	QC blank	ND	ND	ND	0.4	ND	ND	43.4	ND	ND	4.3	0.0	1.0	ND	ND	0.0	0.6
	QC1a	--	15.7	13.8	18.6	20.0	--	115.0	6.8	18.5	21.3	19.7	19.0	38.4	18.7	17.1	18.3
	QC2a	193.9	200.9	202.7	201.5	220.4	207.8	1004.9	210.6	207.4	200.0	223.2	199.3	1044.1	203.9	194.4	202.5
	QC1b	--	16.1	15.0	18.7	19.6	--	116.9	8.3	18.2	20.2	19.6	19.0	74.1	18.6	17.1	18.3
	QC2b	200.0	201.4	205.5	204.6	219.6	212.4	996.6	214.0	206.4	199.3	223.2	200.7	1109.9	201.6	194.3	205.7
	QC1c	--	15.7	14.2	18.8	20.1	--	119.6	8.1	18.5	20.5	19.8	19.0	47.5	18.8	17.1	18.5
	QC2c	196.7	203.1	206.0	203.0	221.1	211.5	1002.6	212.3	204.9	196.0	221.9	198.7	1090.4	202.8	194.0	204.0
	QC1 = 20 µg/L (K, Si = 100 µg/L); QC2 = 200 µg/L (K, Si = 1000 µg/L)																

Date of analysis		Al 237.312	As 193.696	Ca 317.933	Cr 267.716	Cu 327.395	Fe 238.204	K 766.491	Mg 279.078	Mn 260.568	Na 589.592	Ni 231.604	Pb 220.353	Si 185.005	Sr 407.771	V 311.837	Zn 202.548
11/29/2014	QC blank	ND	0.1	ND	ND	0.0	ND	30.1	ND	ND	196.6	ND	ND	8.2	0.0	ND	ND
	QC1a	20.2	17.7	--	19.4	19.4	19.0	106.3	23.0	19.1	231.8	19.0	18.9	102.4	20.4	18.3	22.3
	QC2a	427.0	360.9	--	382.0	384.5	377.2	1694.9	439.1	373.9	924.5	376.0	367.7	1880.1	389.6	378.2	380.4
	QC1b	19.3	17.4	--	19.3	19.9	19.1	109.1	21.6	19.1	232.6	19.0	19.2	96.0	20.6	18.1	22.5
	QC2b	421.7	358.0	--	379.7	384.4	374.4	1700.5	437.9	370.5	916.4	373.4	366.9	1832.7	389.4	378.3	376.0
	QC1c	19.6	16.9	--	18.9	19.7	18.5	127.3	21.6	18.7	250.5	18.5	18.5	96.5	20.6	17.8	21.4
	QC2c	423.1	358.6	--	376.1	390.0	371.8	1704.5	432.3	366.8	916.2	367.9	361.3	1839.1	393.3	378.6	366.6
	QC1 = 20 µg/L (K, Si = 100 µg/L); QC2 = 400 µg/L (K, Si = 2000 µg/L)																
4/29/2015	QC1a	32.5	36.0	28.5	36.5	40.5	36.6	43.8	38.5	37.1	--	--	37.4	33.4	35.8	36.5	35.6
	QC2a	410.2	394.6	394.0	395.3	428.2	410.7	1802.3	418.7	405.0	--	--	404.7	412.9	406.3	398.2	388.3
	QC3a	50.0	48.8	42.9	50.1	54.5	51.3	57.5	54.0	50.9	--	--	50.8	47.4	48.6	49.6	49.1
	QC1b	34.7	35.9	29.2	37.1	41.3	41.4	45.5	38.5	37.4	--	--	37.9	33.9	36.3	37.3	38.6
	QC1c	33.4	37.4	30.4	36.5	40.8	36.4	50.3	37.8	36.8	--	--	37.0	31.9	35.4	36.9	35.6
	QC2c	413.7	404.7	398.3	393.6	430.0	408.4	1829.3	417.5	401.1	--	--	401.6	421.4	405.0	401.2	393.4
	QC1d	31.0	35.1	27.9	34.8	38.8	35.0	46.4	37.0	36.8	--	--	36.9	29.3	34.3	35.4	35.2
	QC2d	418.3	404.4	390.5	391.4	420.5	406.9	1809.1	414.9	412.3	--	--	412.6	420.6	400.0	394.0	399.3
	QC1e	38.5	35.6	74.4	101.8	44.7	363.5	158.6	39.0	58.2	--	--	155.4	37.0	35.7	37.2	--
	QC2e	418.9	432.4	396.4	395.3	449.1	405.6	379.2	414.4	417.2	--	--	412.2	395.6	402.3	416.8	695.2
	QC1f	39.3	34.4	29.2	34.6	40.4	46.8	50.0	36.1	36.3	--	--	36.2	30.4	34.3	36.0	33.9
	QC2f	422.2	419.3	388.7	391.2	450.7	404.5	382.3	405.6	411.5	--	--	403.5	389.9	398.1	416.4	661.2
	QC1 = 35 µg/L; QC2 = 400 µg/L; QC3 = 50 µg/L																
6/5/2015	QC blank	2.1	1.8	1.6	0.1	ND	2.0	ND	0.4	ND	10.5	ND	0.7	23.6	0.0	0.0	0.1
	QC1a	18.5	20.2	20.8	20.1	20.4	20.7	16.5	20.2	19.5	28.0	19.6	21.0	--	20.4	19.1	19.5
	QC2a	98.7	102.7	102.8	104.7	104.8	100.5	110.4	102.8	102.5	104.4	102.7	106.6	--	105.0	104.4	102.6
	QC1b	20.1	21.5	26.4	20.6	21.1	22.4	17.7	20.3	19.9	38.0	19.9	20.6	--	21.3	20.0	20.1
	QC2b	104.7	107.2	107.4	108.8	110.9	105.0	114.8	105.8	106.0	110.5	106.4	110.1	--	110.6	110.0	104.3
	QC1 = 20 µg/L; QC2 = 200 µg/L																

Date of analysis		Al 237.312	As 193.696	Ca 317.933	Cr 267.716	Cu 327.395	Fe 238.204	K 766.491	Mg 279.078	Mn 260.568	Na 589.592	Ni 231.604	Pb 220.353	Si 185.005	Sr 407.771	V 311.837	Zn 202.548
6/6/2015	QC blank	2.1	1.8	1.6	0.1	0.0	2.0	0.0	0.4	0.0	10.5	0.0	0.7	23.6	0.0	0.0	0.1
	QC1a	18.7	20.2	20.8	20.1	20.4	20.7	16.5	20.2	19.5	28.0	19.6	21.0	--	20.4	19.1	19.6
	QC2a	99.2	102.7	102.8	104.7	104.8	100.5	110.4	102.8	102.5	104.4	102.7	106.6	--	105.0	104.4	102.6
	QC1b	20.2	21.5	26.4	20.6	21.1	22.4	17.8	20.3	19.9	38.0	19.9	20.6	--	21.3	20.0	20.1
	QC2b	105.0	107.2	107.4	108.8	110.9	105.0	114.8	105.8	106.0	110.5	106.4	110.1	--	110.6	110.0	104.3
									QC1 = 20 µg/L; QC2 = 100 µg/L								
6/19/2015	QC blank	2.6	1.1	4.7	0.2	ND	1.6	169.5	ND	0.0	3.9	0.0	0.6	37.5	0.0	0.1	0.1
	QC1a	20.7	20.5	25.6	20.3	20.2	25.5	--	18.6	20.6	22.4	20.1	21.3	--	20.8	20.6	20.8
	QC2a	102.8	102.2	109.2	101.8	101.7	106.5	--	103.7	104.9	101.8	102.4	106.2	--	104.2	108.2	106.2
	QC1b	22.5	20.0	25.0	19.5	19.3	24.3	--	18.0	19.6	22.2	19.1	19.8	--	20.2	19.7	19.6
	QC2b	101.7	100.6	106.3	99.2	100.1	103.6	--	99.5	101.8	99.9	99.3	102.9	--	102.8	106.4	102.5
	QC1c	18.9	19.3	23.0	18.8	19.2	20.1	--	16.8	18.6	27.3	18.3	18.0	--	19.8	19.4	18.2
									QC1 = 20 µg/L; QC2 = 200 µg/L								
7/9/2015	QC blank	1.3	ND	1.3	0.2	0.1	0.5	--	ND	ND	ND	0.1	0.6	--	0.0	0.1	ND
	QC1a	20.6	20.5	21.5	20.9	20.7	20.7	--	20.2	20.9	19.9	20.3	20.8	--	21.2	20.3	20.6
	QC2a	19.8	19.1	21.0	19.8	19.5	19.8	--	19.6	19.8	18.7	19.3	19.8	--	20.1	19.2	19.7
	QC1b	105.6	103.0	107.6	104.8	104.8	104.5	--	104.5	106.1	105.5	103.4	106.9	--	106.0	105.6	106.6
	QC2b	24.6	20.2	22.7	21.1	21.3	23.8	--	21.0	20.9	20.3	20.2	21.1	--	21.8	20.8	20.7
	QC1c	22.5	18.8	21.1	19.5	19.8	21.1	--	18.8	19.3	19.0	18.8	19.8	--	20.1	18.7	19.0
	QC2c	107.0	104.1	107.1	103.8	105.6	104.0	--	103.2	104.4	107.0	101.4	104.2	--	107.1	106.1	103.5
							QC1 = 20 µg/L (K, Si = 100 µg/L); QC2 = 200 µg/L (K, Si = 1000 µg/L)										

Date of analysis		Al 237.312	As 193.696	Ca 317.933	Cr 267.716	Cu 327.395	Fe 238.204	K 766.491	Mg 279.078	Mn 260.568	Na 589.592	Ni 231.604	Pb 220.353	Si 185.005	Sr 407.771	V 311.837	Zn 202.548
8/11/2015	QC blank	3.9	0.0	0.5	0.0	0.3	0.6	212.1	ND	0.0	0.1	0.0	1.9	81.8	0.0	0.1	0.6
	QC1a	20.0	18.8	16.3	19.3	19.4	18.9	--	17.8	19.5	18.4	19.0	20.0	--	19.9	18.6	17.5
	QC2a	103.1	102.2	100.8	100.6	100.1	103.9	--	101.2	102.4	99.1	100.5	101.7	--	102.5	101.0	99.7
	QC3a	206.0	202.4	202.6	199.9	199.0	209.4	--	201.8	202.2	199.8	200.7	197.7	--	201.7	202.3	197.9
	QC1b	22.2	20.6	16.4	20.5	20.5	21.5	--	18.3	20.4	19.3	19.9	20.3	--	21.5	20.1	17.1
	QC2b	107.6	105.9	102.8	102.9	103.6	106.2	--	103.6	103.3	100.5	101.3	101.2	--	107.6	105.5	97.8
	QC1c	22.7	21.4	19.1	21.5	21.6	22.5	--	18.9	21.1	20.2	20.6	21.2	--	22.7	21.2	17.8
	QC2c	111.3	108.6	114.0	106.3	106.5	110.1	--	107.9	105.5	102.8	103.7	103.3	--	111.4	108.7	100.4
	QC1d	22.8	21.1	17.0	20.4	20.9	22.7	--	17.3	19.9	19.4	19.4	19.5	--	21.9	20.4	16.3
	QC2d	108.9	107.0	104.9	103.2	105.1	107.4	--	101.4	101.6	101.8	99.5	99.9	--	109.7	106.0	95.4
	QC1e	26.2	21.3	17.4	20.9	21.2	23.5	--	17.7	20.3	19.8	19.7	20.4	--	22.4	20.8	16.7
	QC2e	109.4	106.1	104.8	103.9	104.8	106.7	--	102.2	101.8	100.9	99.4	100.3	--	109.9	106.2	97.9
	QC1f	27.8	21.1	20.1	21.5	21.7	30.2	--	20.0	20.7	20.7	20.2	20.7	--	22.8	21.3	17.5
	QC2f	113.0	106.2	107.3	105.0	104.9	109.5	--	104.0	102.1	133.6	100.4	101.7	--	110.9	107.8	97.1
	QC3f	247.2	215.7	215.6	213.7	215.0	225.6	--	212.2	206.6	209.0	205.5	205.4	--	223.6	220.4	199.2

QC1 = 20 µg/L; QC2 = 100 µg/L; QC3 = 200 µg/L

Appendix D: Leachate Data

Table notes: All values in µg/L except where otherwise noted. Values less than the method detection limit (MDL) are represented by ND. Values exceeding the detection limit but less than the method reporting limit (MRL) are italicized to indicate quantitation is estimated.

Leachate condition	Sample ID	pH	Al (mg/L)	As	Ca (mg/L)	Co	Cr	Cu	Fe (mg/L)	K (mg/L)	Mg (mg/L)	Mn	Na (mg/L)	Ni	P	Pb	Si (mg/L)	V	Zn
	MDL (µg/L)		2.42	1.43	4.93	0.26	0.31	0.27	0.96	4.42	1.35	0.20	0.47	0.47	1.92	0.90	34.98	0.35	0.30
	MRL (µg/L)		8	4.77	16.43	0.87	1.04	0.89	3.19	14.75	4.49	0.68	1.58	1.55	6.39	2.98	116.61	1.16	1.00
Deionized Water	DX	7.4	13	ND	5.47	13.2	4.99	20.4	26.5	0.775	6.9	257	4.13	1.93	690	4.49	79.5	106	31.9
Deionized Water	Fine SS		19.4	3.7	7.45	9.33	3.16	20.7	22.6	1.61	6.02	324	18.5	1.41	187	6.96	105	327	42.8
Deionized Water	WF	9.0	210	10.7	30	101	9.39	49.9	143	3.18	49.7	1330	20.4	13.6	513	62.3	1210	233	608
Deionized Water	WFw	9.3	261	18	41.3	85.3	15.2	76.4	184	4.34	56.4	1600	29.3	21.4	438	55.3	1380	365	452
Deionized Water	OC Shale	9.4	5.71	12.8	3.01	7.09	5.43	24.5	9.02	0.799	2.61	94.3	16.5	3.25	225	1.62	45	572	21.1
Deionized Water	OC Shale 2	7.5	0.533	1.9	18.6	0.76	0.531	5.57	1.09	0.574	2.07	54.4	22.4	ND	138	1.02	12.9	16.3	1.56
Deionized Water	Basal SS		6.34	5.76	5.19	7.74	2.19	12.1	12.8	1.49	3.97	132	16.2	1.99	753	1.51	50.9	250	9.78
Deionized Water	Cong SS	7.4	5.96	ND	5.93	7.56	3.2	56.3	10.1	2	3.53	73.6	8.52	3.31	211	1.11	40.9	25.3	9.86
Deionized Water	Mica SS	7.9	13.4	ND	1.21	35.6	15.8	5.81	22.3	0.919	2.13	541	1.19	28.8	548	3.03	42.7	51.8	14.6
Deionized Water	Peb Cong	7.5	2.85	ND	6.84	3.55	0.946	9.71	6.1	0.225	2.71	108	3.77	0.576	143	ND	20.4	23.8	5.83
Deionized Water	FHr	8.5	4.72	2.18	6.06	5.56	1.17	2.04	1.66	2.2	0.748	27.1	3.04	ND	29.7	1.25	27.9	8.17	15.4
Deionized Water	FHb	8.7	4.87	13.3	4.82	18.2	1.55	21.2	1.02	3.42	2.53	20	3.02	ND	31.3	ND	27.9	8.57	4.22
Deionized Water	LDNss	6.4	17.8	2.13	2.55	9.62	22.2	17.7	18.8	1.55	3.84	70.3	2.22	20.6	401	3.77	64.7	27.8	45.7
Deionized Water	Mica SS	7.0	3.12	ND	8.14	3.01	10.4	0.619	4.72	0.957	5.74	48.7	0.594	2.64	21	1.53	17.1	20.8	8.16
Deionized Water	LDN	8.9	12	3.5	10.7	20.7	16.5	26.7	25	0.883	20.6	203	2.87	36.2	376	1.63	94.7	374	15.2
Deionized Water	WS3	7.3	5.28	2.43	0.0143	4.63	2.58	1.44	1.21	1.03	0.104	2.45	0.195	1.98	16	1.68	18.6	4.12	8.17
Deionized Water	GHg	8.8	6.08	5.06	8.62	12.1	3.15	61.2	12.5	0.316	5.13	180	2.58	2.07	392	1.24	44.5	142	8.91
Deionized Water	GHw	7.7	16	2.88	1.17	11.7	2.06	11	2.73	3.46	0.675	7.77	1.29	0.851	58.9	1.86	67.7	13.4	12.5
Deionized Water	BCg	7.2	8.72	6.64	13	4.39	8.03	2.33	6.79	1.68	4.42	137	10.9	3.75	67.6	3.56	67	17	19.7
Deionized Water	BCw	6.9	7.25	107	1.61	30.7	23.5	4.19	6.54	2.67	1.14	16.8	1.04	1.11	110	2.48	59.8	35.4	11.1
Deionized Water	SP	6.7	12.2	1.73	2.78	23	1.64	52.5	18.4	1.2	4.43	167	0.825	2.41	330	2.12	84.5	3.52	47
Deionized Water	FD1	6.7	2	ND	1.64	1.61	ND	1.4	2.17	0.286	ND	21.3	2.74	ND		1.29	22.1	3.92	9.53
Deionized Water	FD2	6.8	1.47	2.46	0.891	2.78	ND	0.939	1.38	0.471	0.113	18.3	3.5	ND		1.15	22	4.57	8.09
Deionized Water	FD3	6.7	1.78	3.14	1.17	1.79	38.7	2.87	1.6	0.378	0.151	38.6	2.9	59.4		1.41	23.6	1.7	491
Deionized Water	FD4	6.6	1.48	8.4	1.33	1.68	ND	1.89	1.2	1.23	0.465	12.1	2.42	ND		ND	24.1	4.73	5.77
Deionized Water	MK1	8.4	0.834	4.8	3.16	6.89	ND	1.32	0.994	2.78	1.44	21.5	7.09	ND		ND	18.9	7.25	1.91
Deionized Water	MK2	6.9	2.25	10.7	0.775	35.3	0.433	1.67	1.94	0.901	0.406	3.56	3.44	1.26		ND	26.3	12.6	6.57
Deionized Water	TW1	6.9	2.66	2.48	1.17	14.9	1.42	2.64	1.59	2.36	0.401	139	3.66	1.18		ND	23.4	12.3	7.49
Deionized Water	TW2	8.5	1.01	1.71	1.59	2.05	ND	8.94	1.76	0.15	0.473	17.8	12.9	0.251		ND	13.3	43.4	1.52
pH 7 + P	WF	6.9	130	10.7	22.1	72.7	57.2	37.7	85.5	499	33.2	788	1760	8.23	1040000	33.5	1080	175	379
pH 7 + P	WFw	7.0	120	19.2	18.1	47.4	57.9	45.6	79.7	574	27.1	560	1760	8.95	1040000	15.5	949	214	175
pH 7 + P	OC Shale		0.573	33.8	11.5	11.3	56.1	74.6	0.793	764	7.78	67.8	1790	4.29	1060000	ND	60.1	595	1.74
pH 7 + P	Mica SS		3.37	2.82	7.42	49.7	68.1	15.3	3.77	1470	10.7	300	1720	9.54	1070000	ND	27.3	69.1	2.35
pH 7 + P	FHr	7.1	6.1	13.9	12.4	71	62.2	14.2	1.38	1960	4.06	111	1710	1.72	1070000	ND	75.5	22	1.38
pH 7 + P	FHb	7.1	6.88	60.6	13	124	63.6	99.8	1.06	1970	10.5	114	1720	3.1	1060000	ND	60.3	18.2	1.48
pH 7 + P	LDN ss	7.0	0.339	17.9	7.22	33.3	60.7	22.9	0.306	473	21.4	119	83.2	12.1	134000	ND	18.9	18.2	3.68
pH 7 + P	LDN	7.1	0.354	12	11	6.21	56.9	59.9	0.427	473	22.7	68.8	86	3.06	137000	ND	52.7	332	1.94
pH 7 + P	WS3	7.1	0.382	14.4	ND	58.6	63	7.32	0.047	497	0.414	3.05	83.1	1.32	135000	ND	8.23	5.16	8.86
pH 7 + P	GHg	7.1	0.186	17.5	10.6	5.04	57.6	67.8	0.18	464	13.8	79.1	83.4	1.17	136000	ND	44.1	211	61.6
pH 7 + P	GHw	7.1	0.923	10.1	10	62	61.4	12.2	0.161	497	7.79	24	84.4	2.49	135000	ND	30	21.7	3.75
pH 7 + P	BCg	6.9	3.82	47	18.1	24.7	54.5	11.4	3.28	389	38.8	303	84.2	10.4	136000	1.39	59.6	30.8	14.2
pH 7 + P	BCw	7.1	0.475	904	13.2	104	62.8	8.19	0.239	495	5.49	29.1	83.3	2.81	135000	ND	29.1	18	4.61
pH 7 + P	SP	7.1	1.77	ND	11.8	50.9	62.3	20.3	2.35	497	11.6	148	83.2	3.36	134000	ND	23.9	3.83	14.7

88

Leachate condition	Sample ID	pH	Al (mg/L)	As	Ca (mg/L)	Co	Cr	Cu	Fe (mg/L)	K (mg/L)	Mg (mg/L)	Mn	Na (mg/L)	Ni	P	Pb	Si (mg/L)	V	Zn
MOPS7	Buffer blank	7.0	ND	ND	0.00766	ND	ND	0.761	ND	0.183	ND	ND	77.1	ND		ND	ND	ND	ND
	BCg	7.1	0.162	ND	41.9	ND	ND	1.73	0.095	3.98	7.19	188	74.4	0.488		ND	12.1	1.06	1.7
	BCw	6.9	3.71	163	5.33	43.2	13.7	6.13	4.19	7.06	1.74	19.9	75.3	1.56		3.84	36	22.6	14.6
	DX	7.1	2.39	ND	9.11	2.7	0.732	4.97	4.85	1.02	2	64.3	76.6	0.477		ND	24.2	17.9	6.09
	FD1	7.1	0.0196	ND	39.8	ND	ND	1.31	0.0111	0.974	4.02	21.7	71.9	ND		ND	16	ND	0.67
	FD2	7.2	0.0336	ND	40.8	1.1	ND	1.16	0.0114	1.61	1.33	21.4	72.5	ND		ND	16.5	ND	ND
	FD3	7.0	0.0776	ND	41.8	ND	ND	1.36	0.0203	1.65	2.54	45.4	71.9	ND		ND	16.9	ND	0.852
	FD4	7.0	0.0958	ND	34.4	1.2	ND	1.9	0.0306	11	7.65	27.7	71	ND		ND	16.9	0.388	0.597
	FHb	7.5	0.178	ND	38.4	1.29	ND	4.18	0.165	7.03	16.7	168	76.1	ND		1.66	7.5	0.458	1.38
	FHr	7.5	0.136	ND	48.2	0.542	ND	2.06	0.0621	7.14	2.86	167	76	ND		7.23	9.15	0.408	3.47
	GHg	7.2	0.0842	ND	67.6	ND	ND	3.44	0.108	3.8	9.12	237	76.2	ND		ND	9.89	8.07	0.933
	GHw	6.9	0.303	ND	3.37	4.74	0.36	1.47	0.0679	9.44	1.4	9.63	75.8	0.814		ND	11	1.23	0.444
	LDN	7.4	0.146	ND	50.6	ND	ND	2.57	0.172	5.39	6.34	9.84	76.1	ND		1.4	10.4	83.8	1.09
	LDNss	6.8	0.0759	ND	8.94	ND	ND	1.87	0.082	1.61	3.36	38.7	74.8	0.9		ND	5.33	ND	1.14
	MK1	7.3	0.0153	ND	21.5	12	ND	1.53	0.0137	7.78	7.62	193	76.5	0.801		ND	9.5	ND	ND
	MK2	7.1	0.0978	ND	7.17	12	ND	1.1	0.0842	8.01	2.25	0.477	74.9	0.799		ND	15.6	1.67	0.982
	SP	7.0	0.356	ND	6.27	2.68	ND	2.36	0.403	4.99	2.37	37.4	75.2	ND		ND	8.53	ND	1.83
	WS1	7.1	0.856	ND	5.74	4.06	0.338	1.63	0.505	14	1.38	43.8	75.6	0.516		ND	16.4	1.99	1.38
	WS2	7.3	0.0282	ND	24	ND	ND	2.08	0.0248	0.771	2.06	3.5	76.8	ND		ND	8.87	1.59	0.52
	WF	7.3	47.2	5.01	16.7	25.5	2.56	13.4	35.7	2.79	11.3	324	138	3.04		12.9	452	77.2	175
	WFw	7.2	98.6	3.35	19.7	16	2.07	17.6	37.8	2.87	11.4	334	121	3.51		13	450	73	133
	WS3	6.8	0.251	ND	0.0289	ND	ND	1.23	0.0711	3.3	0.0358	0.6	75	ND		ND	2.4	1.14	0.71
Tris8	Buffer blank	8.2	ND	ND	ND	ND	ND	ND	ND	0.0187	ND	ND	ND	ND		ND	0.163	ND	ND
	WF	8.2	228	11.7	24.5	106	10	59.3	153	3.5	53.4	1410	43.4	14	469	56.3	1270	247	649
	WFw	8.0	175	15.2	24.8	52.2	9.21	46.9	121	3.07	36.4	969	45.1	12.1	308	30.8	1010	233	279
	FHr	8.0	0.409	1.51	31	0.462	0.327	4.16	0.0587	3.16	2.45	54.4	3.57	ND	9.63	ND	12.1	1.12	0.304
	FHb	8.0	0.193	6.1	27.7	2.1	0.591	147	0.0986	4.5	7.88	54.7	3.6	ND	23.1	1.28	8.66	1.16	1.67
	LDN	8.2	0.672	2.97	35.7	0.617	1.85	50.3	0.827	0.654	5.88	10.5	4.03	ND	9.14	ND	15.1	140	2.38
	GHg	8.1	0.335	1.87	31.7	ND	0.338	22.2	0.154	0.334	3.73	14.7	4.05	ND	15.6	ND	10.4	20.3	0.766
	GHw	7.7	2.44	3.32	2.43	2.63	0.663	2.68	0.488	4.42	1.11	4.15	1.62	ND	27.6	ND	21.7	6.89	1.69
	BCg	7.9	2.93	7.35	16.9	1.34	2.94	2.28	1.89	1.08	4.37	76.7	11.1	0.954	22.3	1.36	33.3	7.54	3.6
	BCw	7.7	7.74	379	2.36	52.8	28.7	8.92	8.76	2.45	1.62	23.2	0.905	2.09	293	2.46	59.1	45.8	20.9
	SP	7.8	2.98	1.48	5.81	6.35	0.579	12.8	3.71	1.91	3.01	56.7	1.12	ND	141	1.17	25.8	1.4	10
Tris9	Buffer blank	8.7	ND	ND	ND	ND	ND	ND	ND	0.0176	ND	ND	ND	ND		ND	ND	ND	ND
	BCg	8.4	7.59	13.7	7.69	3.92	7.51	5.21	6.05	1.44	3.04	113	15.9	3.59		2.48	64.8	24.7	14.4
	BCw	8.3	37.5	737	2.15	75.8	217	16.6	25	6.78	5.51	54	2.94	4.72		ND	256	287	156
	DX	8.8	10.1	ND	5.03	12.2	4.21	22.9	23.4	0.762	6.41	261	20.2	2.26		4.61	69.8	97.2	28.1
	FD2	8.6	4.2	ND	2.11	ND	ND	1350	3.5	0.638	0.217	43.4	6.9	ND		3.36	38.8	9.16	39.7
	FD3	8.7	6.16	2.52	2.93	0.871	0.366	6.05	6.5	0.759	0.611	89.3	5.09	0.851		3.51	46.4	5.46	35.8
	FD4	8.6	4.15	11.2	2.1	0.476	ND	11.3	4.19	1.38	0.806	31.8	1.67	0.562		3.19	35	7.5	22.8
	FHb	8.6	1.63	ND	5.71	1.5	0.553	134	0.377	2.23	5.79	9.67	4.77	ND		4.61	16.6	3.67	4.72
	FHr	8.5	10.1	1.8	7.75	10.1	2.6	7.23	4.43	2.44	1.13	62.1	5.67	1.01		1.94	46.1	13.7	27.8
	GHg	8.6	2.79	2.75	7.98	5.64	0.934	78.3	5.95	0.474	3.03	92.8	6.57	1.03		3.37	24.8	95.1	5.03
	GHw	8.4	32.6	6.4	1.93	24.5	5.89	26.3	9.22	4.23	1.72	12.2	2.23	2.69		0.946	129	62.4	43.1
	LDN	8.6	6.2	2.64	9.89	9.49	7.75	132	10.8	1.08	9.99	107	7.02	16.5		1.77	56.7	313	12.3
	LDNss	8.2	11.6	ND	2.39	9.2	16.4	16.3	12.4	0.988	3.1	64.3	ND	16.2		1.86	42.3	22.8	42.5
	MK1	8.7	1.78	ND	4.48	ND	ND	87.2	1.67	1.99	2.3	43.6	9.44	ND		1.81	19	4.59	6.51
	MK2	8.6	17.1	3.96	2.8	2.04	0.47	15.3	15.8	1.41	2.16	19.9	2.3	0.997		ND	100	23.9	33.8
	SP	8.5	4.62	ND	2.23	17.3	1.02	36.1	8.7	1.44	2.74	103	0.826	1.38		ND	45.2	2.71	34
	WS1	8.7	3.64	ND	1.59	0.538	1.35	4.66	2.64	2.57	0.625	130	6.98	0.895		1.39	30.1	13.5	12
	WS2	8.8	2.09	ND	3.96	2.18	0.357	6510	4.53	0.241	1.13	42.4	18.3	1.23		3.81	17.3	30.8	80.7
	WF	9.0	216	10	33.4	122	12.2	67.7	158	3.32	55.7	1640	60.8	15.5		73.5	1450	329	946
	WFw	8.9	224	15	37.1	79.7	12.7	77.9	167	3.88	51.4	1590	59.4	18.5		53.4	1470	382	618
	WS3	8.3	14.4	8.23	0.0427	11.2	7.21	5.81	3.85	0.816	0.358	6.82	0.75	1.62		1.88	40	16.6	18.8

Leachate condition	Sample ID	pH	Al (mg/L)	As	Ca (mg/L)	Co	Cr	Cu	Fe (mg/L)	K (mg/L)	Mg (mg/L)	Mn	Na (mg/L)	Ni	P	Pb	Si (mg/L)	V	Zn
pH 9	WF	8.8	0.364	2.32	229	ND	1.32	9.96	0.0723	528	2.07	3.7	611	ND	67.8	ND	29.5	20.4	ND
pH 9	WFw	8.8	0.326	8.99	214	ND	1.19	10.1	0.112	590	1.92	4.75	582	ND	62.1	ND	31.2	53.8	ND
pH 9	OC Shale		0.0708	7.92	214	ND	1.09	9.62	0.0404	765	6.23	9.4	488	ND	26.6	ND	12.3	204	8.1
pH 9	FHr	8.9	0.616	4.71	31.3	0.946	1.33	9.05	0.115	2010	3.1	7.21	308	ND	182	ND	10.6	6.04	ND
pH 9	FHb	8.9	1.54	16.1	22.2	4.35	1.94	16.8	0.996	2000	9.16	47.7	310	ND	165	ND	14.4	6.78	ND
pH 9	TF477B		0.249	2.42	3.64	181	2.42	49.2	0.0983	1930	0.268	14.4	309	1.31	2260	ND	12.7	1.21	ND
pH 10	WF	10.0	189	14.2	4.47	108	11.4	46.8	135	9.78	50.4	1350	72.2	15	665	67.7	1120	274	666
pH 10	WFw	10.0	204	17.7	5.26	89.8	17.6	67.8	160	11.7	52.2	1630	71.2	22.3	937	69	1110	388	522
pH 10	OC Shale		2.91	20.1	1.09	4.53	3.88	17.6	5.98	3.77	2.06	52.3	70	2.17	133	ND	27.7	612	18.2
pH 10	Mica SS (5)		1.16	1.74	1.05	2.36	2.27	3.56	1.42	3.97	0.889	24.8	63.9	1.44	1600	ND	13.7	53.6	6.28
pH 10	FHr	10.4	3.64	6.82	0.887	3.61	1.18	4.74	1.02	12.9	0.672	10.9	62.3	0.523	74.9	ND	24.9	18.1	6.35
pH 10	FHb	10.3	2.32	32	1.32	6.91	0.973	16.4	0.518	19	1.35	12.8	62.5	0.713	90.6	ND	24.5	15.1	4.9
CAPS10	Buffer blank (BP)	10.0	ND	2.42	ND	ND	ND	0.81	ND	0.0886	ND	ND	74.1	ND		ND	ND	ND	ND
CAPS10	Buffer blank (GF)	10.0	ND	4.54	ND	ND	ND	0.575	ND	0.03	ND	ND	70.7	ND		ND	ND	ND	0.547
CAPS10	BCg	9.4	1.23	23.6	9.9	0.348	0.603	2.18	0.895	1.99	0.994	16.7	62.2	0.648		ND	23.2	36.6	2.79
CAPS10	BCw	9.4	47.2	1060	3.96	114	273	26.8	29.7	12.2	6.89	69.7	287	5.68		ND	379	373	61
CAPS10	DX	9.6	8.87	1.46	7.52	11	3.45	19	20.8	1.16	6.14	238	65.9	1.95		2.61	54.2	106	24.8
CAPS10	FD1	9.4	0.947	7.02	11.8	0.574	ND	1.45	0.741	0.546	0.572	5.35	57.5	ND	386	ND	40.1	17.4	2.26
CAPS10	FD2	9.3	1	6.01	13	0.847	ND	1.64	0.667	1.03	0.213	6.48	59.6	ND		ND	45.3	12.5	3.65
CAPS10	FD3	9.4	0.509	13	13.9	ND	ND	1.31	0.32	0.853	0.36	3.67	58.6	ND	321	ND	44	6.21	2.98
CAPS10	FD4	9.3	0.729	25.4	9.33	0.285	ND	3.13	0.323	4.77	1.14	2.83	56	ND		ND	29.7	17.5	1.52
CAPS10	FHb	9.7	12.9	8.02	1.92	10.2	4.92	19	3.52	4.21	2.3	29	101	1.95	86	ND	78.7	25.7	19.6
CAPS10	FHr	9.7	14.4	3.4	3.38	16.1	18.1	6.32	6.35	4.25	0.97	64	98.1	26.9		1.17	68.9	23	41.50
CAPS10	GHg	9.7	1.49	7.78	4.36	1.8	ND	19.8	2.82	1.27	1.19	37.4	63.9	ND		3.37	18	221	4.94
CAPS10	GHw	9.6	4.12	11.3	1.72	15	0.581	7.88	0.934	5.56	0.651	7.25	65.2	0.629		ND	28.5	33.3	9.99
CAPS10	LDN	9.7	6.67	5.63	6.34	13.9	12.4	19.3	15.3	2.1	12.2	133	64.5	23.3		ND	58.8	451	12.2
CAPS10	LDN ss	9.3	13.4	7.32	3.4	11.2	21.2	16.7	12.8	1.59	3.39	75.5	62.9	15.9		2.42	71.1	37.9	54.4
CAPS10	MK1	9.7	1.92	10.9	1.69	8.09	ND	1.75	1.98	3.5	0.81	29.7	68.7	ND	103	ND	32.6	12.1	1.28
CAPS10	MK2	9.5	27.5	28.8	3.88	101	2.3	8.92	27.2	4.32	3.49	36.2	92	5.18	542	ND	205	59.3	44.1
CAPS10	SP	9.7	2.28	3.06	3.22	15.9	0.474	13.9	2.54	2.95	1.46	65.4	66.4	1.03		ND	25.2	4.43	25.1
CAPS10	WS1	9.6	16.8	2.55	4.85	59.8	8.88	10.9	9.92	9.78	2.81	417	91.7	5.92		ND	151	74.9	39.8
CAPS10	WS2	9.7	0.644	2.4	3.51	ND	ND	5.03	0.405	0.293	0.17	3.67	66	ND		ND	18.3	61	5.52
CAPS10	WF	9.6	208	18.4	40.1	113	12.2	57.5	161	4.68	50.8	1530	126	15	571	80.2	1580	361	1360
CAPS10	WFw	9.5	247	24.7	45.6	79.2	13.2	74.8	193	6.31	53	1690	122	18.6	844	60.7	1740	420	633
CAPS10	WS3	9.9	1.6	8.61	10.3	0.516	0.689	13.3	0.74	3.69	0.386	5.51	198	ND		ND	54.1	183	1.62
pH 11 + P	WF	10.4	1.25	11	1.87	0.625	17.5	6.2	0.813	12.7	0.28	10	1790	0.549	731000	ND	71.3	38	3.45
pH 11 + P	WFw	10.4	1.43	13.3	1.9	0.343	16.4	9.15	0.956	12.7	0.284	13.9	1720	0.489	688000	ND	68	97	2.37
pH 11 + P	OC Shale		0.962	25.3	1.79	0.438	19	8.21	0.755	9.57	0.317	8.22	1910	3.64	765000	ND	30.2	666	ND
pH 11 + P	Mica SS		4.52	4.99	1.53	4.16	28.6	7.17	4	9.37	2.09	52.4	2120	0.543	804000	ND	33.1	82.1	1.41
pH 11 + P	FHr	10.9	10.3	14.3	1.71	3.84	22.8	9.53	1.71	18.7	0.7	14.8	2040	ND	783000	ND	61.4	34.1	2.03
pH 11 + P	FHb	10.9	8.14	43.7	1.29	16.2	24.5	32.7	1.41	24.5	3.1	13.4	2160	ND	795000	ND	57.9	20.5	3.03
10 uM P	10 uM P Blank		1.2	ND	ND	0.274	ND	ND	0.189	0.0633	0.229	2	0.00112	ND	358	ND	9.18	1.22	1.06
10 uM P	FD1	7.21	4.42	ND	2.18	3.72	0.76	3.37	4.91	0.468	0.502	42.4	1.98	0.476	278	2.29	37.7	7.79	21.2
10 uM P	FD4	7.07	3.58	10.4	1.56	2.74	0.626	2.89	3.21	1.66	0.656	27.3	1.89	0.61	277	1.55	43.3	7.6	15.1
10 uM P	MK1	8.9	1.22	4.49	3.01	6.2	0.383	1.66	1.34	2.11	1.33	29.5	5.65	0.474	291	1.48	23.2	9.18	4.49
10 uM P	MK2	7.8	4.12	12	0.953	36.3	0.825	2.36	3.78	0.801	0.647	7.03	2.66	1.69	375	ND	42.5	17	10.4
10 uM P	BCg	7.16	6.33	5.79	8.27	4.42	7.09	2.07	5.55	1.21	2.97	124	9.84	3.21	105	2.43	45.8	17	15.1
10 uM P	FHb	8.75	3.92	1.56	3.93	3.61	1.47	8.56	1	2.27	4.06	13.7	2.48	0.621	166	ND	25.5	8.58	6.71
10 uM P	FHr	8.45	5.95	1.67	6.59	10.7	1.81	3.27	2.39	2.51	0.846	47	3.52	0.562	349	ND	35.3	11.4	11.5
10 uM P	WF	9.08	188	25.5	31.2	103	11.1	51.1	102	2.74	47.1	1320	24	12.9	591	62.3	1450	329	750
10 uM P	WFw	8.64	195	29.6	30.7	60.3	10.2	58.1	107	3.91	43.4	1250	19.6	13.4	772	42.4	1460	338	493

Leachate condition	Sample ID	pH	Al (mg/L)	As	Ca (mg/L)	Co	Cr	Cu	Fe (mg/L)	K (mg/L)	Mg (mg/L)	Mn	Na (mg/L)	Ni	P	Pb	Si (mg/L)	V	Zn
1 mM P	1 mM P Blank		2.04	ND	0.0127	ND	0.689	ND	1.28	60.2	0.368	4.82	0.025	ND	33200	ND	17.9	2.32	ND
1 mM P	FD1	7.5	1.47	5.86	9.98	0.927	0.507	0.797	1.07	0.91	1.23	16.6	11	ND	22800	ND	28.9	8.95	5.49
1 mM P	FD4	7.3	2.09	24.2	9.56	2.01	0.638	1.49	1.8	3.91	2.65	26.9	9.32	ND	22700	ND	36	10.4	6.79
1 mM P	MK1	8.3	0.882	6.95	4.15	6.81	0.556	0.57	0.924	30.5	2.42	22.9	8.12	ND	27000	ND	17.8	9.71	2.76
1 mM P	MK2	7.5	2.77	14.9	2.81	39.7	1.24	1.99	2.55	24.9	1.07	6.96	8.7	1.9	24200	ND	34.2	16.6	441
1 mM P	BCg	7.4	2.76	24.6	11	1.04	3.31	1.04	1.93	1.96	2.67	76	18.8	1.19	22200	ND	30.4	22.7	6.15
1 mM P	FHb	8.5	2.44	3.61	3.31	5.34	1.86	9.51	0.723	39	4.81	17.3	3.74	1.11	26400	ND	16.5	10	280
1 mM P	FHr	8.1	3.72	3.19	6.75	11.4	1.6	1.56	1.5	38.7	0.982	35.7	5.12	0.473	27600	ND	22.3	10.9	7.49
1 mM P	WF	8.9	179	19.4	31.4	76.4	10.7	45.6	107	3.8	43.5	1200	41.1	11.6	28600	52.9	1070	324	702
1 mM P	WFw	8.3	187	27.4	30.7	37.2	9.77	52.7	113	5.21	40.9	1130	36.8	12.3	28200	38.7	1060	333	460
100 mM P	100 mM P Blank		0.022	3.95	0.0384	ND	69.2	1.62	0.0271	500	0.00498	2.8	1.67	1.37	223000	ND	0.377	ND	0.32
100 mM P	FD1	7.9	0.0304	13.6	7.35	ND	52.9	1.12	0.023	527	7.62	4.84	50	ND	374000	ND	33.3	13.8	1.25
100 mM P	FD4	8.1	0.0371	34.7	7.85	0.775	54.2	1.93	0.0321	470	11.7	7.62	46.3	0.476	372000	ND	27.5	9.68	1.68
100 mM P	MK1	8.6	0.0616	11.7	4.12	11	61.7	0.969	0.0766	456	9.68	11.4	11.4	1.54	374000	ND	14	9.39	9.87
100 mM P	MK2	8.6	0.0302	18.6	5.5	18.5	60.1	0.388	0.0205	471	6.89	4.56	12.7	1.48	377000	ND	20.6	15.2	1.42
100 mM P	BCg	8.1	0.0666	33.3	8.78	ND	51.5	1.52	0.0659	520	19	31.9	51.6	1.13	373000	ND	19.8	18.9	1.26
100 mM P	FHb	8.8	0.0942	8.13	3.23	1.31	60.9	4.69	0.0681	496	12.4	11.1	5.75	0.518	376000	ND	8.65	8.77	2.56
100 mM P	FHr	8.7	0.0607	8.14	3.8	1.48	60.4	0.964	0.0256	486	1.94	6.41	6.71	ND	383000	ND	9.93	8.73	2.6
100 mM P	WF	7.9	0.107	12.6	3.94	ND	59.8	1.43	0.0736	523	1.26	2.47	51.2	ND	314000	ND	31.2	27.5	2.98
100 mM P	WFw	7.9	0.234	21.8	4.67	ND	53.4	2.26	0.17	525	1.22	3.17	53.2	ND	308000	ND	35.7	43.4	2.34
water 4h	BCg	7.3	11.4	1.6	6.76	3.46	9.85	2.13	7.38	1.84	3.21	126	6.32	2.74	53.2	3.78	72.3	17.9	17.7
water 4h	FD4	6.5	12.1	10.5	3.39	5.33	0.921	5.46	9.19	4.53	1.45	79.8	1.26	0.796	224	3	82.3	10.9	28.9
water 4h	FHb	8.8	7.81	ND	3.6	7.36	2.19	12.4	1.69	2.81	3.57	22.5	2.31	0.835	20.6	0.9	40.4	9.99	6.34
water 4h	FHr	8.6	14.3	ND	5.11	14.9	3.14	4.69	4.79	2.54	0.957	69.9	2.87	0.907	39	0.932	59.8	15.3	13.1
water 4h	MK2	6.5	5.98	6.77	1.41	29.3	0.655	3.07	4.77	0.847	0.745	7.88	1.21	1.38	164	ND	39.5	12	10.2
water 10h	BCg		12.1	2.16	8.56	5.13	9.31	2.85	9.31	1.72	3.75	168	6.74	3.95	83.4	6.65	54	17.7	29.4
water 10h	FD4		11.9	10.1	4.8	6.7	0.74	6.58	7.2	3.49	1.45	65.7	1.54	0.778	256	4.23	57.8	10.1	27.3
water 10h	FHb		5.49	1.62	4.38	10.4	2.76	19	1.48	2.78	3.95	30.3	2.61	1.94	42.3	8.13	30.5	8.44	21.4
water 10h	FHr		7.85	ND	5.83	18.6	1.81	3.23	2.29	2.49	0.975	63.5	2.81	0.678	38.9	1.96	38.2	11	11.8
water 10h	MK2		8.94	9.37	3.75	86.3	0.857	6.15	6.81	1.3	1.52	15.4	1.66	4.32	219	ND	54.3	14.9	20.2
water 50h	BCg	6.8	20.7	5.64	14.4	11.1	20.3	6.25	20.9	2.27	7.17	353	7.56	9.8	185	12.3	85	38.5	75.9
water 50h	FD4	6.8	11.4	9.26	5.86	9.05	0.824	8.29	7.69	3.27	1.74	71.3	1.94	1.09	278	5.15	59	10.9	147
water 50h	FHb	8.2	3.95	1.97	5.29	12	1.2	20.1	1.27	2.72	4.65	32.7	2.47	0.726	31.1	ND	25.1	8.26	16.6
water 50h	FHr	8.4	9.93	ND	8.09	36.2	2.42	4.27	2.6	3.13	1.49	116	3.27	1.03	57.1	2.75	47.1	14.8	68
water 50h	MK2	7.2	12.4	13.5	6.52	145	1.26	10.5	10.6	1.64	2.49	23.3	2.22	7.22	268	1.22	77.1	20.7	210
water 72h	BCg		31.2	6.48	21.1	17.5	28	9.14	31	2.87	10.6	541	8.46	14.7	275	19.2	101	54.5	120
water 72h	FD4		16.3	7.74	9.04	14.1	0.936	11.2	9.84	4.28	2.59	98.8	2.57	1.47	319	7.76	68	13.5	51
water 72h	FHb		3.48	1.77	5.82	10.5	1.11	17.3	1.13	2.68	5.02	28.5	2.49	0.68	33.7	1.14	23.2	7.79	7.71
water 72h	FHr		11.2	ND	9.21	42.8	2.88	4.75	3.16	3.34	1.69	138	3.4	1.21	43.1	2.93	51.1	16.6	20.1
water 72h	MK2		16.6	14.2	8.2	187	1.86	13.2	23.8	1.98	3.55	33.1	2.82	9.39	244	1.58	165	27.8	58.4
water 194h	BCg		7.25	2.29	13	4.94	6.16	3.48	7.56	1.22	4.09	192	9.29	4.13	123	6.04	39.8	11.8	33.7
water 194h	FD4		17	11.4	13.9	20.2	0.855	11.6	8.02	4.65	3.74	112	3.33	1.87	427	10.8	60.3	15.6	55.7
water 194h	FHb		2.75	1.74	10.2	16.3	1.04	3.49	0.699	2.8	4.99	53.4	3.12	ND	31.6	1.86	21.1	8.05	4.08
water 194h	FHr		2.98	ND	9.88	16.3	1.14	3.96	0.765	2.8	4.73	52.4	3.12	ND	38	1.3	21.7	8.63	4.8
water 194h	MK2		187	52.8	18.5	461	13.5	59.3	132	6.12	20.8	225	5.68	28.6	445	7.41	1110	226	350

Leachate condition	Sample ID	pH	Al (mg/L)	As	Ca (mg/L)	Co	Cr	Cu	Fe (mg/L)	K (mg/L)	Mg (mg/L)	Mn	Na (mg/L)	Ni	P	Pb	Si (mg/L)	V	Zn
0.1 mM P 4h	BCg	7.2	10.9	3.82	7.42	4.45	8.71	2.75	8.22	1.67	3.32	144	6.66	3.42	488	4.72	53.2	17.6	25.4
	FD4	6.5	9.18	12.9	3.52	3.78	0.692	4.75	6.29	3.41	1.24	56.1	1.83	0.543	2060	2.77	54.7	9.05	21.7
	FHb	8.8	6.79	2.08	3.66	9.66	1.93	16.1	1.55	3	3.78	25.9	2.36	1.01	2190	0.929	33	9.33	9.17
	FHr	8.6	8.11	ND	5.93	16.2	1.8	3.07	2.45	2.64	0.993	60.2	2.78	0.529	2650	ND	36.2	10.2	9.36
	MK2	6.5	4.76	7.38	1.33	26.2	0.548	2.84	3.69	1.22	0.631	6.58	2.05	1.23	2220	ND	33	10.5	18.4
0.1 mM P 10h	BCg		14.1	4.47	9.49	6.31	11.8	3.55	11.9	1.88	4.44	203	6.98	5.06	482	7.14	61.7	23.6	35.5
	FD4		9.1	15.4	4.15	4.76	0.644	5.57	5.74	2.96	1.27	52.5	1.86	0.703	1910	3.57	47.9	9.57	23.6
	FHb		4.29	3.12	3.93	10.1	1.27	16.5	1.17	2.83	3.93	26.4	2.28	0.625	2070	ND	23.8	7.94	4.94
	FHr		9.24	ND	7.31	26.3	2.18	3.61	2.54	3.13	1.31	90.4	3.1	0.814	2610	1.09	42.5	12	16.5
	MK2		8.79	11.2	3.73	85.2	0.959	6.26	6.76	1.7	1.5	15.7	2.49	4.17	2190	1.09	54.4	15.1	21.4
0.1 mM P 24h	BCg	7	16.9	5.6	11.7	8.19	15	4.86	15.2	2.05	5.52	260	7.33	6.98	479	11.2	72.1	29.3	52.7
	FD4	6.8	6.98	8.78	3.34	4.24	0.619	4.96	4.56	2.12	1.02	42.7	1.1	ND	1670	3.17	30.6	6.85	28.6
	FHb	8.6	4.46	4.27	4.6	12.3	1.35	20.5	1.36	2.98	4.44	33.4	2.49	0.913	1930	ND	25.8	9.38	6.65
	FHr	7.7	9.2	2.12	8.16	30.7	2.29	3.96	2.63	3.24	1.44	104	3.23	0.916	2520	1.84	43.9	13.9	16.3
	MK2	6.5	10.2	13.5	4.84	109	1.05	8.06	8.25	1.78	1.94	18.8	2.67	5.37	2120	2.37	65.6	17.8	30.4
0.1 mM P 72h	BCg		25.6	9.56	17.7	13.6	23.9	8.03	25.1	2.62	8.63	431	8.16	12	612	15.9	96	46.9	88.8
	FD4		13.3	17.2	7.68	9.51	0.967	10.5	9.61	3.79	2.35	82	2.53	1.31	1240	6.92	69	14.5	46.2
	FHb		3.3	5.71	5.33	11.4	1.1	18.1	1.05	2.9	4.95	26.3	2.61	0.934	1570	ND	22.4	10.1	6.12
	FHr		10.8	3.7	10	41.2	2.91	5.17	3.24	3.6	1.76	138	3.52	1.18	2290	3.42	50.1	18.1	26.2
	MK2		23.3	20.3	8.68	194	2.67	14.1	31.2	2.58	4.22	40.1	3.73	10.2	1740	2.3	240	38.5	77.6
0.1 mM P 194h	BCg		14.4	6.49	16.6	9.88	12.1	6.14	14.8	1.7	5.97	298	9.54	7.94	423	12.5	53	23.6	487
	FD4		52.5	34.8	15.3	19.9	3.11	14.8	39.6	9.86	5.33	175	3.62	3.67	1320	14	327	34.2	206
	FHb		2.2	6.13	7.94	4.98	0.694	5.17	0.494	3.46	7.02	11.4	3.52	ND	932	ND	21.9	9.5	65
	FHr		2.87	6.95	10.2	20.5	1.24	2.21	0.732	2.87	1.06	59.7	3.37	ND	1810	ND	23.1	14.1	31.5
	MK2		198	58.5	19.2	480	13.8	61.6	138	6.67	21.7	234	5.85	29.5	1900	8.26	1190	240	320

Appendix E: Lithologic Groups

Lithologic group	Unit	Lithologic description
Alluvium	Qg1	Sand and gravel that postdates Missoula Floods
	Qls	Landslide deposits
	Qa	Fine grained alluvium
	Qal	Alluvium
	Qau	Alluvium, undifferentiated
	Qt	Alluvium on terraces
	Qns	Nonmarine sedimentary deposits
	Qoa	Older alluvium
	Qfd	Fan-delta Alluvium
	Qal	Meander-belt Alluvium
	Qc	Colluvium
	Qls	Landslide debris
	Qda	Debris avalanche deposits
	Qg2	Sand and gravel that predates Missoula Floods
	Qbf	Fine-grained alluvium
	QTal	Older alluvium
	Qoam	Older alluvium
	Qf	Braided-fan alluvium
	Qoal	Older alluvium
	Qa	Recent alluvium
	Qf	Alluvial fan
	Qal	Alluvium and beach deposits
	Qls	Landslide
	Qpal	Older alluvium
	Qyal	Recent alluvium
	Qral	Recent alluvium
	Qms	Youngest till deposits
	Qys	Young sand and silt
Basalt and andesite	Tb	Basalt and basaltic andesite
	Tb	Basalt flows and volcaniclastic sedimentary rocks
	Ta	Andesite, basalt, gabbro, and norite; plugs and dikes
	Tlb	Little Butte Volcanic Series; basaltic andesite and olivine basalt flows
	Tb	Basalt flows
	Tbf	Basalt flows
	Ttb	Basaltic andesite flows
	Ti	Intrusive basalt
	Ti	Intrusive rocks
	Tsr	Siletz River volcanic series
	Tsr	Submarine basalt flows
	Jrs	Serpentinized ultramafic rock
	Taf	Andesite flows
	Tla	`
	Tbm	Basalt of Mohawk
	Tib	Basaltic intrusive rocks
	Tlbb	Little Butte Volcanics, basalt and basaltic andesite
	Tpb	Pyroxene Basalt
	Tl	Tholeiitic lavas
	Tub	Umpqua Formation, basalt member
	Tiba	Basaltic andesite intrusive rocks
	Tgr	Granitic intrusions
	KJi	Intrusive rocks
	Tub	Basalt and basaltic andesite flows and flow breccias
	Ts	Calc-alkaline lavas
	Ti2	Intrusive rocks, undivided
	Jri	Mafic intrusive unit
	Tsr	Siletz River Volcanics
	Tbah	Basalt and andesite of Coburg Hills
	Tf	Basalt flows

Lithologic group	Unit	Lithologic description
Conglomerate	KJr	Riddle Formation
	KJrc	Riddle Formation, conglomerate
	Tbr	Bushnell Rock Formation, conglomerate
Fisher	Tf	Fisher Formation
Fluvial	Qf	Fluvial deposits
	Qalc	Floodplain deposits of the Willamette River and major tributaries
	Qft	Fluvial terrace deposits
	Qws	Willamette Silt
Glacial and glaciofluvial	Qgf1	Glacial and glaciofluvial deposits
LBV	Tlb	Little Butte Volcanics, undivided
Marine	Tte	Tyee Formation; Elkton Siltstone member
	Te	Eugene Formation
	Tms1	Marine sedimentary rocks
	Tl	Lorane Shale
	Tcv	Umpqua Group, Camas Valley Formation
Missoula Flood deposits	Qff2	Main body of fine-grained Missoula Flood deposits
Mudstone	Tmm	Tenmile Formation, Basin plain mudstone
	Tus	Umpqua Formation, siltstone member
	KJdm	Dothan Formation, mudstone matrix melange
	Twrm	White Tail Ridge Formation, mudstone
Sandstone	Ts	Spencer Formation
	Ts	Spencer Foramtion
	Ttbs	Tyee Formation, Baughman member
	Twc	White Tail Ridge Formation, Coquille River member
	Twr	White Tail Ridge Formation, Remote member
	Dp	Deflation plain
	Tbsc	Bushnell Rock Formation, Slater Creek member
	Tem	Eugene Formation, micaceous, quartz sandstone
Terrace	Qtg	Terrace gravel
	QTg	Weathered terrace gravel
	Qal	Terrace gravel
	Qt	High terrace gravels
	Qoft	Older fluvial terrace deposits
	Qtl	Quaternary lower terrace
	Qt	Terrace and fan deposits
	QTtg	Terrace gravel
Tuffs and volcaniclastics	Tlt	Little Butte Volcanic Series; tuff
	Tu	Tuffaceous sedimentary rocks, basalt flows, and tuffs, undivided
	Tv	Volcanic Group, undifferentiated volcanic rocks
	Tlt	Little Butte Volcanics, tuffaceous volcaniclastic rocks
	Tt	Tuff, lapilli tuff, agglomerate, and volcanic sandstone
	Te	Eugene Formation, volcanic sandstone and tuff
	Tp1	Pyroclastic deposits and associated sediments
	Tvs	Volcanolithic sandstone, conglomerate, and laharic breccia
	Tov	Oligocene volcanic rocks
	Ttw	Tuff of South Willamette Street
	Ttf	Tuff of Fox Hollow
Turbidite	Tt	Tyee Formation
	Tty	Tyee Formation
	Tmss	Tenmile Formation, turbidite sandstone
	Tmsm	Tenmile Formation, turbidite sandstone and mudstone
	KJdd	Dothan Formation, phyllitic siltstone and metagraywacke
	KJda	Dothan Formation, turbidite sandstone broken formation
	Trs	Roseburg member, turbidite sandstone and mudstone
	Tmms	Tenmile Formation, mudstone and turbidite sandstone
	Tm	Tenmile Formation, undivided
	Tet3	Tyee Formation, Baughman Lookout member
	Ttts	Tyee Mountain member